8-2001

Reversible melting and crystallization of short and long flexible chain molecules by Temperature-modulated calorimetry

Jeongihm Pak
University of Tennessee - Knoxville

To the Graduate Council:

I am submitting herewith a dissertation written by Jeongihm Pak entitled "Reversible melting and crystallization of short and long flexible chain molecules by Temperature-modulated calorimetry." I have examined the final electronic copy of this dissertation for form and content and recommend that it be accepted in partial fulfillment of the requirements for the degree of Doctor of Philosophy, with a major in Chemistry.

Dr. Bernhard Wunderlich, Major Professor

We have read this dissertation and recommend its acceptance:

Dr. Alexander van Hook, Dr. Mark Dadmun, Dr. Paul Phillips

Accepted for the Council:
Dixie L. Thompson

Vice Provost and Dean of the Graduate School

(Original signatures are on file with official student records.)

To the Graduate Council:

I am submitting herewith a dissertation written by Jeongihm Pak entitled "Reversible melting and crystallization of short and long flexible chain molecules by Temperature-modulated calorimetry." I have examined the final copy of this dissertation for form and content and recommend that it be accepted in partial fulfillment of the requirements for the degree of Doctor of Philosophy, with a major in Chemistry.

Dr. Bernhard Wunderlich
Major Professor

We have read this dissertation
and recommend its acceptance:

Dr. Alexander van Hook

Dr. Mark Dadmun

Dr. Paul Phillips

Accepted for the Council:

Dr. Anne Mavhew
Interim Vice Provost and
Dean of The Graduate School

(Original Signatures are on file in the Graduate Student Services Office.)

Reversible Melting and Crystallization of Short and Long Flexible Chain Molecules by Temperature-Modulated Calorimetry

A Dissertation

Submitted for the

Doctor of Philosophy

Degree

The University of Tennessee, Knoxville

Jeongihm Pak

August 2001

DEDICATION

To my teacher

Professor Bernhard Wunderlich

in the celebrate of his 70th birthday.

ACKNOWLEDGMENTS

I am very thankful to my research adviser, Prof. Bernhard Wunderlich, for his endless support, guidance and encouragement. His help has been a constant source of knowledge and motivations. I would also like to thank all the other members of my committee, Dr. Alexander van Hook, Dr. Mark Dadmun and Dr. Paul Phillips for their comments and patience.

I would like to thank Drs. Marek Pyda, Wei Chen, Rene Androsch, Yong-ku Kwon, Il-kwon Moon, Alexander Buzin and Wenbing Hu for their unlimited help and cooperation. My thanks extend to all the former members and visiting scholars in the *ATHAS* research group for their long discussions and suggestions. It has been both honor and pleasure to work in the *ATHAS* Laboratory. I deeply appreciate the financial support from the National Science Foundation, Grant # DMR-9703692 and U.S. Department of Energy, under Contract DOE-AC05-00OR22725 with UT-Battelle.

Last, but not least, I would like to express my sincere appreciation to my beloved husband, Youngsun Kim for his encouragement and his sacrificial decision to leave my country and to study in UT with me. Without his support, this dissertation might never be finished. My thank also goes to my parents (Mr. Chong-ok Pak and Mrs. Song-ja Oh) and my brothers (Seongchoon and Seongsoo Pak) in Nashville, and to my family-in-laws in South Korea, for their patient, understanding support and absolute love.

ABSTRACT

Melting and crystallization of linear, flexible molecules of different lengths was studied by temperature-modulated differential scanning calorimetry, TMDSC. Various techniques for TMDSC with single and multifrequency modulations have been analyzed to optimize the conditions for the present study. The finally chosen method involved a quasi-isothermal mode with a temperature amplitude of 0.5 K and a period of 60 s (frequency = 0.167 Hz). The interpretation of the reversible and irreversible melting was developed by comparison of a variety of different modes of analysis (sinusoidal, sawtooth, and complex sawtooth). The analyzed molecules ranged from n-paraffins, oligomeric fractions of polyethylene and poly(oxyethylene) to macromolecules of polyethylene. The most important discovery was that there is a critical chain length for reversible melting and crystallization of small, flexible molecules at 10 nm or about 75 backbone chain atoms. Below this chain length, melting and crystallization is reversible under the given conditions of analysis and in the presence of primary crystal nuclei. Above this chain length, the crystallization requires a degree of supercooling which becomes constant for 200 chain atoms or more at a value of 6.0 ! 10 K. This critical chain length sets a lower limit for the need of supercooling, a characteristic property of flexible polymers. This result was then applied to resolving the problem of the existence of a small amount of reversible melting in polymers, discovered about five years ago. The following was shown: chain segments with melting temperatures equal to oligomers of less than the critical chain length can crystallize and melt reversibly, even when contained within the metastable structure of semicrystalline polymers. Above this chain length, longer segments can only

show reversible melting when a molecular nucleus remains on the crystal surface after partial melting. The short-chain segments have been seen in linear-low-density polyethylene. The longer segments in the main melting peak of polyethylene. These observations are combined with the knowledge derived from the *ATHAS* data bank to propose three reversible and three irreversible calorimetric contributions to the heat capacity of flexible macromolecules.

TABLE OF CONTENTS

CONTENTS **PAGE**

CHAPTER 1 INTRODUCTION..... 1

1.1 Melting and Crystallization..... 4

1.1.1 Melting..... 4

1.1.2 Crystallization..... 7

1.1.3 Melting and crystallization of flexible linear macromolecule..... 11

1.1.4 Heat capacities in the melting/crystallization range..... 16

1.1.5 Crystallinity calculations..... 19

1.2 n-paraffins and polyethylene..... 21

1.2.1 Similarity..... 21

1.2.2 Differences..... 22

1.3 Temperature-Modulated Differential Scanning Calorimetry (TMDSC)..... 23

1.3.1 Calorimetry..... 23

1.3.2 DSC..... 24

1.3.3 TMDSC..... 27

1.3.3.1 Quasi-isothermal TMDSC..... 30

CHAPTER 2 EXPERIMENTAL..... 35

2.1 Instrumentation..... 35

2.1.1 Mettler-Toledo DSC 820 and its New Sensor..... 35

2.1.2 Thermal Analyst 2920..... 40

2.2 Calibration..... 40

2.3 Evaluation of reversing heat capacity..... 44

2.4 Samples..... 47

CHAPTER 3 RESULTS..... 53

3.1 n-Hexacontane, n-$C_{60}H_{122}$..... 53

3.1.1 Standard DSC of n-$C_{60}H_{122}$..... 54

3.1.2 TMDSC of n-$C_{60}H_{122}$..... 55

3.1.3 Eutectic study, 50:50 mixture of n-$C_{50}H_{102}$ and n-$C_{60}H_{122}$..... 56

3.2 Polyethylene-Extended Chain Crystals..... 58

3.2.1 Melting temperatures as a function of scanning rates..... 59

3.2.2 TMDSC of PE560..... 60

3.2.3 TMDSC of PE1150..... 65

3.2.4 TMDSC of PE2150..... 68

3.3 Polyethylene-Folded Chain Crystal..... 72

3.3.1 Melting temperatures as a function of scanning rates..... 72

3.3.2 TMDSC of PE15520..... 73

3.4 Poly(oxyethylene)-Extended Chain Crystal..... 77

3.4.1 Melting temperatures as a function of scanning rates..... 77

3.4.2 Standard DSC of POE1500..... 79

3.4.3 TMDSC of POE1500..... 80

3.4.4 TMDSC of POE1960..... 81

3.4.5 TMDSC of POE3060..... 84

3.5 Effect of seeding on degree of supercooling 88

CHAPTER 4 DISCUSSION..... 92

4.1 Melting and Crystallization of PE Observed by Quasi-isothermal TMDSC 92

4.1.1 Comparison of PE560 with n-Paraffins 92

4.1.2 Comparison of PE2150 to PE560 and PE15520..... 99

4.2 Kinetics of the Processes Seen by TMDSC..... 102

4.3 Melting and Crystallization of POE Observed by Quasi-isothermal TMDSC..... 112

4.4 Critical length for nucleation 116

4.4.1 Degree of Supercooling vs. Number of Carbons..... 116

4.4.2 Entropic work of extension..... 121

4.5 Contributions to apparent heat capacities..... 124

4.6 Degree of reversibility..... 128

4.6.1 Reversibility in n-paraffins 128

CHAPTER 5 CONCLUSIONS..... 131

LIST OF REFERENCES..... 135

VITA..... 149

LIST OF FIGURES

FIGURE **PAGE**

1.1. Illustration of difference on heterogeneous nucleation between small molecule and polymer molecule crystallization..... 1

1.2. Gibbs free energy *versus* temperature..... 5

1.3. Illustrations of the specific volume and enthalpy as a function of temperature..... 7

1.4. Schematic representation of the change in free enthalpy as a function of size illustrating the nucleation process..... 8

1.5. Nucleation rate as a function of temperature..... 9

1.6. Types of crystal nuclei..... 10

1.7. Fraction of polyethylene as a function of supercooling..... 12

1.8. A schematic of molecular nucleation of linear macromolecules..... 14

1.9. Deviation of the heat capacity of crystalline polyethylene from the computed vibrational heat capacity..... 17

1.10. Schematic drawing of the Thermal Analyst 2920..... 25

1.11. Typical start of a heating scan of a standard DSC..... 26

1.12. A typical heating scan of a TMDSC..... 28

2.1. Schematic of the Mettler-Toledo DSC 820..... 36

2.2. Top view of a FRS5 sensor plate..... 37

2.3. Difference in T_m of indium between standard DSC and quasi-isothermal TMDSC measurements when A_T is 0.05 K..... 42

2.4. Difference in T_m of indium between standard DSC and quasi-isothermal TMDSC measurements when A_T is 0.5 K..... 43

2.5. An example of the preliminary, reversing heat capacity from quasi-isothermal TMDSC measurements..... 45

3.1. Onset temperatures of the phase transitions of *n*-paraffins..... 53

3.2. Heat capacity of n-$C_{60}H_{122}$..... 55

3.3. Heat capacities of mixture of n-$C_{60}H_{122}$ and n-$C_{50}H_{102}$ 57

3.4. Peak temperatures of the phase transitions of polyethylene oligomers..... 59

3.5. Heat capacity of PE560 by standard DSC and TMDSC..... 61

3.6. Eutectic phase diagrams..... 63

3.7. Heat capacity of PE560 on first heating and cooling by TMDSC..... 64

3.8. Heat capacity of PE560 on second heating and cooling by TMDSC..... 65

3.9. Heat capacity of PE1150 by standard DSC and TMDSC..... 66

3.10. Heat capacity of PE1150 on first heating and cooling by TMDSC..... 67

3.11. Heat capacity of PE1150 on second heating and cooling by TMDSC..... 68

3.12. Heat capacity of PE2150 by standard DSC and TMDSC..... 69

3.13. Heat capacity of PE2150 on first heating and cooling by TMDSC..... 70

3.14. Heat capacity of PE2150 on second heating and cooling by TMDSC..... 71

3.15. Phase transition temperatures of polyethylene and its oligomers..... 73

3.16. Heat capacity of PE15520 by standard DSC and TMDSC..... 74

3.17. Heat capacity of PE15520 on first heating and cooling by TMDSC..... 75

3.18. Heat capacity of PE15520 on second heating and cooling by TMDSC..... 76

3.19. Phase transition temperatures of poly(oxyethylene) oligomers..... 78

3.20. *HF*(*t*) of POE1500 *versus* sample temperature..... 79

3.21. Heat capacity of POE1500 by TMDSC..... 80

3.22. Heat capacity of POE1960 by standard DSC and TMDSC..... 82

3.23. Heat capacity of POE1960 on first heating and cooling by TMDSC..... 83

3.24. Heat capacity of POE1960 on second heating and cooling by TMDSC..... 84

3.25. Heat capacity of POE3060 by standard DSC and TMDSC..... 85

3.26. C_p of POE3060 before and after the quasi-isothermal TMDSC..... 86

3.27. Heat capacity of POE3060 on first heating and cooling by TMDSC..... 87

3.28. Heat capacity of POE3060 on second heating and cooling by TMDSC..... 88

3.29. *HF*(*t*) of PE15520 with seeds *versus* time..... 90

3.30. *HF*(*t*) of PE15520 with seeds *versus* sample temperature..... 90

4.1. Heat capacity of n-$C_{50}H_{102}$..... 92

4.2. Heat capacity of n-$C_{26}H_{54}$..... 93

4.3. Heat capacity of n-$C_{44}H_{90}$..... 96

4.4. Modulated heat-flow rate and sample temperature of modulation set D in Figure 4.1..... 97

4.5. Apparent reversing heat capacity during cooling and subsequent heating of PE560..... 98

4.6. Free enthalpy diagram illustrating the zero entropy production melting..... 100

4.7. Apparent reversing heat capacity during cooling and subsequent heating of PE2150..... 102

4.8. Apparent reversing heat capacity, total heat-flow rate <Φ>, and sample temperature $T_s(t)$ during cooling and subsequent heating of PE560..... 103

4.9. Raw heat-flow rate data $\Phi(t)$ as a function of time for PE560..... 104

4.10. Apparent reversing heat capacity, total heat-flow rate <Φ>, and sample temperature $T_s(t)$ during cooling and subsequent heating of PE2150..... 106

4.11. Raw heat-flow rate data $\Phi(t)$ as a function of time for PE2150..... 108

4.12. Apparent reversing heat capacity, total heat-flow rate <Φ>, and sample temperature $T_s(t)$ during cooling and subsequent heating of PE15520..... 109

4.13. Apparent reversing heat capacity during cooling and subsequent heating of PE15520..... 110

4.14. Plot of the change in apparent, reversing heat capacity as a function of annealing time for PE15520..... 110

4.15. Raw heat-flow rate data $\Phi(t)$ as a function of time for PE15520..... 111

4.16. Heat capacity measured by standard DSC and quasi-isothermal TMDSC for POE1500 113

4.17. Quasi-isothermal TMDSC of POE5000..... 114

4.18. Change of the apparent heat capacity at 315.7 K of POE1500..... 115

4.19. Degree of supercooling as a function of the number of chain atoms in the backbone 117

4.20. Illustration of the extension from a random coil to a fully extended chain of n-paraffin..... 121

4.21. The work *versus* the number of carbon atoms..... 124

4.22. Apparent reversing heat capacity of PET..... 125

4.23. Heat capacities of PE15520 on heating by standard DSC and TMDSC.... 126

4.24. Δw_c(rev) as a function of time for n-$C_{50}H_{102}$..... 129

LIST OF TABLES

TABLE **PAGE**

2.1 Thermal properties of paraffins..... 48

2.2 Thermal properties of equilibrium polyethylene and poly(oxyethylene)..... 49

2.3 Crystal properties of polyethylene and poly(oxyethylene)..... 49

2.4 Melting temperature and heat of fusion of poly(oxyethylene) and polyethylene fractions calculated depending on their molar mass..... 52

4.1 Molar masses, chain-lengths, and melting temperatures of paraffins, polyethylenes and poly(oxyethylene)..... 118

4.2 The parameters and resulting work for random coils to be stretched with comparison to the thermodynamic entropic term on crystallization..... 123

CHAPTER 1

INTRODUCTION

It is well known that crystallization does not occur under equilibrium conditions, but at lower than the melting temperature, i.e., crystallization occurs with supercooling. The reason is that to initiate the crystallization, primary nucleation is necessary due to a free energy barrier to crystallization. For small molecules the supercooling can be avoided by self-nucleation or heterogeneous nucleation. In the presence of primary nuclei, small molecules can easily add on the pre-existing crystal surface and crystallization does not need supercooling, as illustrated on the left of Figure 1.1. For polymer molecules, however, there is always a supercooling needed to crystallize, even in the presence of crystals. A polymer molecule is not a compact small particle, but a flexible, long chain. In the melt it is a random

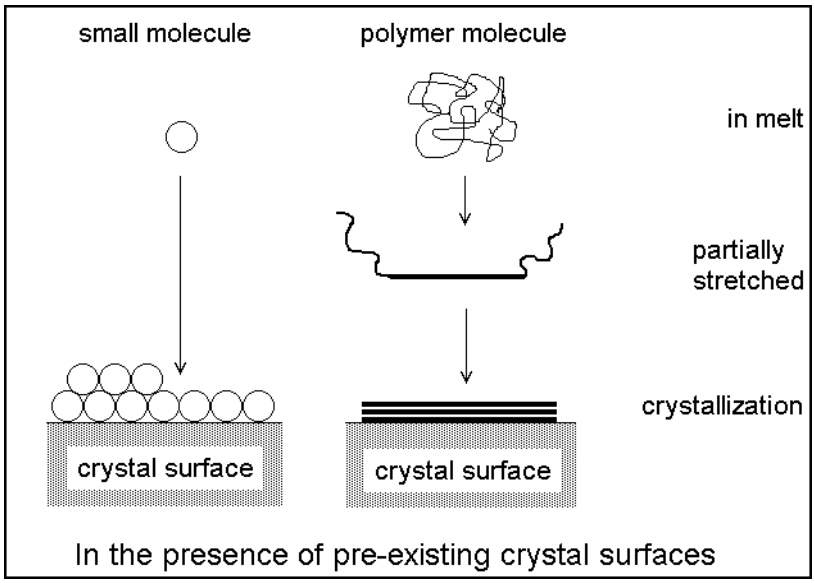

Figure 1.1. Illustration of difference on heterogeneous nucleation between small molecule and polymer molecule crystallization.

coil. The polymer molecule as a random coil cannot add to the pre-existing crystal surface. It first must be stretched to some degree as shown in Figure 1.1. A more extended chain can then more easily add to the crystal surface. The stretching process decreases the entropy of the molecule and, thus, increases the free enthalpy, so that polymers supercool even in the presence of primary nuclei or crystals. To rationalize the supercooling of polymers on crystallization even in the presence of nuclei, a second barrier to crystallization was assumed in addition to the free energy barrier for primary nucleation, and the term 'molecular nucleation' was coined by Wunderlich [1].

To study the detail of the molecular nucleation process, the n-paraffins $C_{50}H_{102}$, $C_{44}H_{90}$ and $C_{26}H_{54}$ were chosen in my MS thesis as simple model compounds for polyethylene, a flexible polymer. The earlier study on the n-paraffins showed unexpectedly no supercooling on crystallization from the melt [2]. It seems that the n-paraffins, which are flexible chain molecules and obviously need some chain extension, require only a short time to overcome this barrier for the molecular nucleation. In a recent study of the heterogeneous and homogeneous nucleation of n-alkanes by Sirota *et al.* [3–5] similar results were reported for n-paraffins with $21 \leq n \leq 37$ carbon atoms.

A question, thus, arises from this surprising observation. What if the chain lengths increase beyond n-$C_{50}H_{102}$? In the other direction, what if the chain lengths of polymers decrease gradually from the lengths showing a large amount of supercooling? Would the supercooling decrease gradually or abruptly with the chain lengths? What is the limit of chain length where a polymer behaves like a small molecule on crystallization or how long must a molecule be before a noticeable nucleation barrier exists for crystallization? To answer these

questions the study described in this thesis is designed to analyze very flexible polymers like polyethylene, poly(oxyethylene), and poly(oxytetramethylene). The molecular nucleation will be addressed in section 1.1.3 with a general description of melting and crystallization. The other two major points studied in this thesis are the development of the method of analysis in form of temperature-modulated calorimetry of sufficient precision, and the description of the change of reversible melting as one increases the chain length from paraffins to polyethylene.

In this study eliminating any instrumental effect is very important to see the intrinsic characteristics of crystallization of linear molecules. The recently developed temperature-modulated differential scanning calorimetry (TMDSC), specially in the quasi-isothermal mode, which is main tool used in the research described in this thesis, can meet this requirement. The quasi-isothermal mode permits the measurement of heat effects with a zero underlying heating rate, i.e., by modulation about a fixed temperature, T_o. In this way the supercooling studied in this thesis is due only to the sample itself, without major instrument effects. Using TMDSC, a total apparent heat capacity is measured similarly as by standard DSC, but this total apparent heat capacity can be separated into a reversing and a non-reversing part. An apparent heat capacity may have a latent heat effect [$C_p^* = (\partial H/\partial w_c)_{p,\,T}$] besides the true thermodynamic heat capacity [$C_p = (\partial H/\partial T)_{p,\,w_c}$] where p designates the constant pressure and w_c the constant crystallinity. The reversing heat capacity is the heat capacity that reverses on modulation. It may still contain contributions from slow irreversible processes, such as annealing or melting, as well as errors due to incomplete description of the reversing contribution, as will be discussed in section 2.3. After all these nonreversible effects and

errors have been excluded, the remaining apparent heat capacity is called reversible in the thermodynamic sense. The apparent reversible heat capacity, in turn, must be separated into its true thermodynamic heat capacity and the latent heat contribution arising from reversible melting and crystallization over the temperature range of one modulation cycle.

The reversing heat capacity is measured to study the degree of supercooling of the chain molecules and the detail of the reversing heat capacity will be given with the description of the TMDSC in section 1.3.3. The understanding of the reversible heat capacity measurement is basic to the thermal analysis of flexible linear macromolecules. Recently we identified six different contributions to the apparent heat capacity which will be described in section 1.1.4 and form the basis of the discussion of the TMDSC measurements displayed in this thesis.

1.1 Melting and Crystallization

1.1.1 Melting

The equilibrium state of a system of two phases at constant temperature is characterized by zero in the change of Gibbs free energy when going from one phase to the other:

$$\Delta G = \Delta H - T \Delta S \tag{1.1}$$

where ΔG is the change in free enthalpy, ΔH in enthalpy, and ΔS in entropy. The most stable state of a given system is reached at the minimum of G [6].

Traditionally, condensed phases are classified as crystals, glasses, or liquids. In the vicinity of the melting temperature, or in contact with its crystals liquid phases are also called

melts. At sufficiently low temperature, the solid phases (glasses and crystals) have vibrations as their only thermal motion. The ideal crystals are fully ordered, i.e., their entropy is zero, and glasses have a degree of order similar to the liquid. The liquid phase shows in addition to their vibrations, all possible types of large-amplitude motion for the given molecule. Large amplitude motions are translation, rotation, and internal rotation (conformational motion). The transition from crystals to melts is characterized by the loss of order and the attainment of this large-amplitude motion. The transition from glasses to liquids, in contrast is characterized by no change in order but also the attainment of large-amplitude motion.

In a plot of Gibbs free energy *versus* temperature as shown in Figure 1.2, the slope for the melt is greater than that for the crystal. From the equilibrium conditions as expressed by eq (1.1) it follows that below the point of intersection only the crystal is stable and at temperature higher than the point of intersection only the melt is stable. The temperature

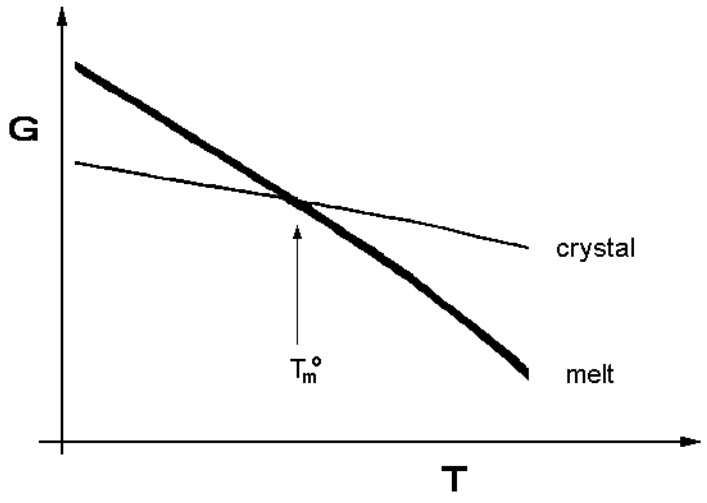

Figure 1.2. Gibbs free energy *versus* temperature. Thin line is for crystal and the thick line is for melt.

where both phases are stable is called the equilibrium temperature (equilibrium melting temperature, $T_m°$). The equilibrium melting transition is characterized thermodynamically by:

$$T_m^o = \frac{\Delta H_f^o}{\Delta S_f^o} \tag{1.2}$$

where T_m^o is the equilibrium melting temperature and ΔH_f^o and ΔS_f^o are the enthalpy and entropy of fusion, respectively [7].

Melting is a first order transition, defined by a discontinuity of the volume (V) and the enthalpy (H) which are the first derivatives of the free energy, G, i.e., $V = dG/dp$ and $H = dG/dT$. Figure1.3 is an illustration of the specific volume (a) and enthalpy (b) as a function of temperature. The temperature of the discontinuity is the melting temperature. The jump in enthalpy at T_m in Figure 1.3 (b) is the latent heat of fusion which is a "hidden" heat, since it does not change the temperature.

Thermodynamically one would write at constant pressure:

$$dH = \left(\frac{\partial H}{\partial T}\right)_{n,p} dT + \left(\frac{\partial H}{\partial n}\right)_{T,p} dn \tag{1.3}$$

where $(\partial H/\partial T)$ is the heat capacity, C_p, $(\partial H/\partial n)$ the latent heat, and n represents the progress in the phase transition as expressed, for example by the crystallinity w_c. So in calorimetric measurement the measured heat capacity, the first derivative of the enthalpy is not just a heat capacity but an apparent heat capacity (the heat capacity + the latent heat).

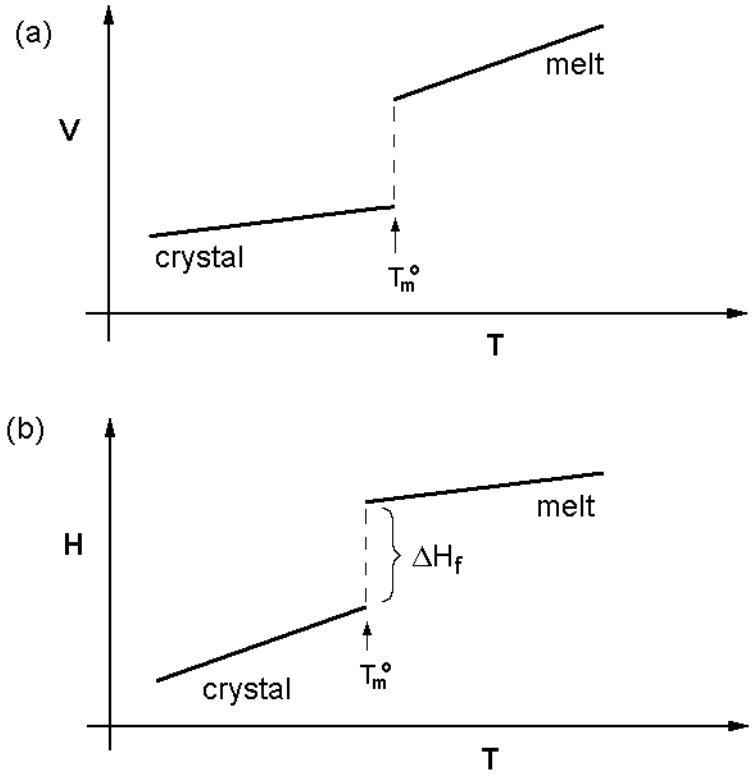

Figure 1.3. Illustrations of the specific volume (a) and enthalpy (b) as a function of temperature. Copied from ref. [8].

1.1.2 Crystallization

The crystallization is the reverse of the melting process, a process where the order with the crystal is produced from the melt or dilute solution. Crystals usually grow from nuclei rather than being generated uniformly throughout the random phase of melt (or solution). As a result melting and crystallization are rarely thermodynamically reversible Two distinctive steps are needed, nucleation and crystal growth.

If the crystallization is fully reversible to melting, crystals grown on cooling would have to be distributed uniformly over the bulk that has reached the melting temperature where ΔG is zero in eq (1.1). In reality, the crystallization does often not occur at the melting

temperature, but at lower temperature, from a supercooled melt or solution. Any crystal must have a nucleus with a small specific surface area (in $cm^2\ g^{-1}$) at the start. The initial step leading to a nucleus is called primary nucleation. Figure 1.4 is a schematic of the primary nucleation. A primary nucleus must be formed via a path of positive ΔG. The maximum in ΔG corresponds to the critical size of the nucleus at the corresponding temperature and is the free energy barrier opposing crystallization. The nuclei to the left of the maximum are called embryos, the nuclei to the right supercritical nuclei. As soon as the nucleus reaches a negative ΔG it becomes a stable crystal. As illustrated in Figure 1.4 when the temperature decreases, the size of the critical nucleus becomes smaller and nucleation is speeded up. But as the temperature is reduced, the viscosity increases, so that the nucleation slows down after a peak in nucleation rate, as shown in experimental data of Figure 1.5. Crystallization occurs normally only between the melting temperature and the glass transition temperature [10].

When small nuclei are generated randomly throughout the melt (or solution) without

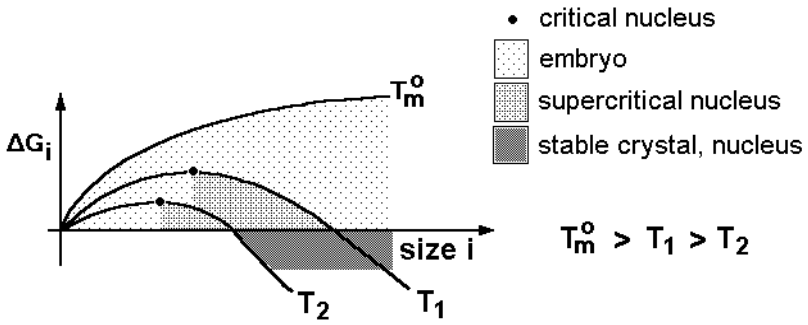

Figure 1.4. Schematic representation of the change in free enthalpy as a function of size illustrating the nucleation process. Copied from ref. [9].

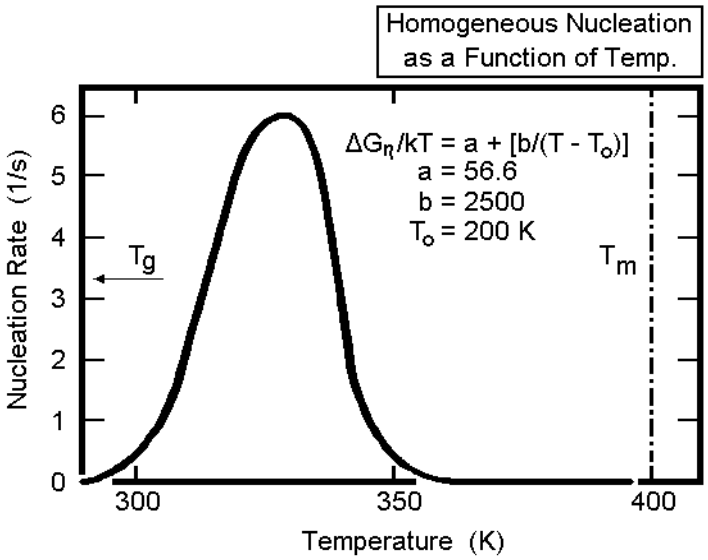

Figure 1.5. Nucleation rate as a function of temperature. Copied from ref. [11].

the help from pre-existing surfaces it is called homogeneous nucleation. The number of nuclei formed homogeneously depends on the temperature and time of crystallization (see Figure 1.5), if all other factors are kept constant. Foreign surfaces such as dust particles or the walls of container of the melt (or solution) reduce the size of nucleus needed for crystal growth because the creation of the interface between the crystal and the surface may be less hindered than the creation of the corresponding free crystal surface. When the previous melting is not complete, crystals are left and act as nuclei (so-called self nucleation). This type of primary nucleation with pre-existing nuclei is called heterogeneous nucleation. The number of nuclei may be constant from the beginning in heterogeneous nucleation and all crystals grow then to the same size at the given crystallization temperature. This heterogenous nucleation is the major case observed in the case of polymer crystallization.

After the initial crystal nuclei are formed further nucleation of crystal growth may be needed. Secondary and tertiary nucleation have been proposed to be involved in the growth of crystals. Because the new interfacial area required by these types of nucleation is smaller than for the primary nucleation, as illustrated in Figure 1.6, the free enthalpy barrier to growth is also smaller than the primary nucleation and the peak in the nucleation rate for secondary nucleation occurs at higher temperature. The crystal growths of most polymers produce sufficiently rough crystal surfaces to obviate secondary nucleation. Tertiary nucleation is almost never necessary.

The kinetics of the overall crystallization is usually described by the Avrami equation, which was originally derived for the crystallization of metals. The following equation is the general Avrami equation.

$$V_c = 1 - \exp(-K t^n) \tag{1.4}$$

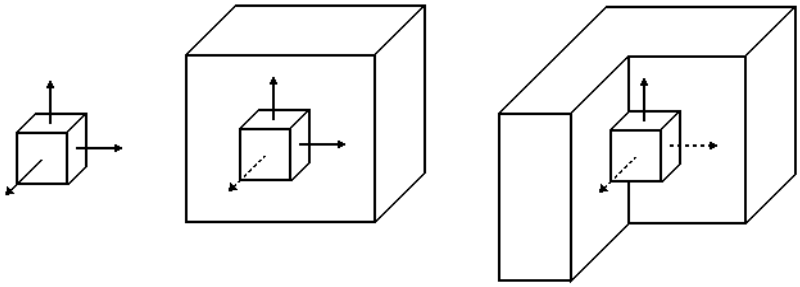

Figure 1.6. Types of crystal nuclei. (a) Primary nucleus, (b) secondary nucleus, (c) tertiary nucleus. Copied from ref. [12].

where V_c is the crystal volume at time *t*, *K* is a geometry and nucleation dependent constant, and n is the Avrami exponent. The constant *K* is a quantity proportional to the number of nuclei per unit volume or the rate of nucleus formation. It is also dependent on the geometry of the growing crystals. The Avrami exponent, n, should always be a whole number and provides information about the nature of the crystal growth theoretically [8].

For polymers this description is incomplete. The crystallization of polymers stops long before a crystallinity of 100% is reached. The resulting semicrystalline polymers must, thus, lose equilibrium at temperature below the equilibrium melting temperature.

1.1.3 Melting and crystallization of flexible linear macromolecule

Melts of small molecules, such as metals or water, supercool before crystallization only because of the need of crystal nucleation. Crystal nucleation is, thus, the first step of any crystallization, but it can be circumvented by either incomplete melting before crystallization (self nucleation) or by adding of foreign nuclei (crystallization by heterogeneous nucleation) [1]. For example, indium shows reversible melting and crystallization on analysis by temperature-modulated differential scanning calorimetry (TMDSC). In this technique the temperature is cycling about a mean value. As long as the melting during the previous heating cycle is incomplete and nuclei are left for re-crystallization during the cooling cycle there is no supercooling [13, 14]. Once, melting is completed; *i.e.*, no nuclei are left, the sample needs to be supercooled by an amount ΔT (= $T_m - T_c$) of 1 − 1.5 K [13, 14].

In contrast to small molecules, it is well known, that flexible linear macromolecules (usually just called polymers) do not crystallize at the temperature where they melt, even if

the melt or solution is nucleated by seeding or self-seeding. Polymers usually need a 5−30 K supercooling to crystallize. Experiments approaching homogeneous nucleation with dispersions of small droplets need even larger supercoolings, of the order of 50−140 K as seen in Figure 1.7 [15]. A polymer molecule is not a small particle, but a long flexible chain which needs a proper conformation to be added to a crystal surface, the polymer molecule must be nucleated itself before the rest of the molecule can add to the growing crystal. Crystallization without supercooling due to molecular nucleation is unlikely since the first segment of the molecule that adds to a crystal restricts the molecule as a whole, *i.e.*, the entropy decrease of the molecule cannot be made up by the small heat of crystallization of the

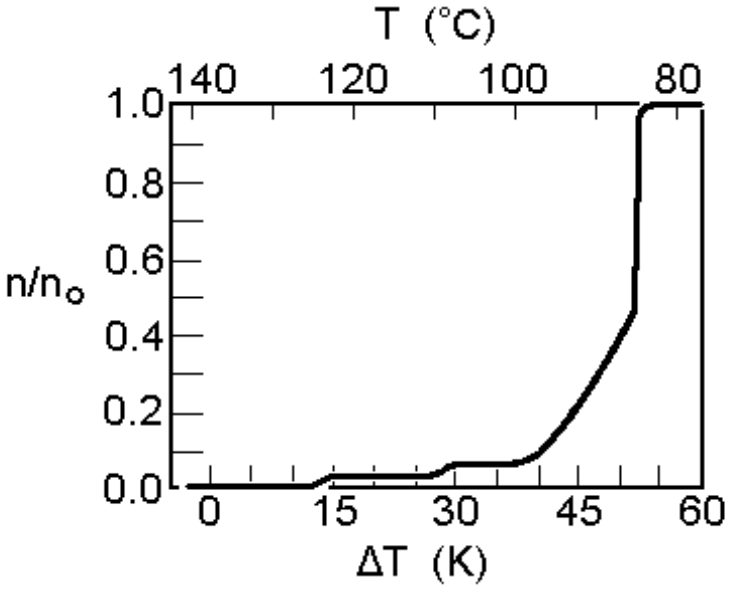

Figure 1.7. Fraction of solidified polyethylene as a function of supercooling. Data by Cormia, *et al*. Cooling rate 0.17 K min^{-1}. Region of no nucleation down to 125°C. Region of heterogeneous nucleation down to 100°C. Region of increasing nucleation with help from heterogeneous nuclei perhaps between 100°C and 85°C. Homogeneous nucleation below 85°C. Copied from ref. [15].

initial chain segment [16]. To rationalize that even in the presence of primary nuclei and crystal surfaces polymer melts and solutions supercool, a second barrier to crystallization is assumed. We expect that each amorphous polymer molecule must traverse many cooperative steps of conformational motion before ordering to the macroconformation that adds to the existing crystal growth face. To describe this initial stage of crystallization of the polymer in the presence of primary nuclei, the term molecular nucleation was coined [1, 17, 18].

Below the equilibrium melting temperature, after crystal nucleation, the second, reversible nucleation process, the molecular nucleation occurs and overcomes the positive barrier in free enthalpy. The process is shown schematically in Figures 1.8 (a) and (b). The completion of the crystallization of the molecule is drawn in Figure 1.8 (c). As soon as the whole molecule is melted, crystallization is not possible until sufficient supercooling has occurred to permit renewed molecular nucleation in the presence of polymer crystals or nuclei [16]. The critical length for molecular nucleation is measurable by a study of the lengths of molecules that get rejected by the growing crystal surface despite the fact that they are below their equilibrium melting temperature.

Only few details of molecular nucleation, however, have emerged over the last 20 years [19–21]. Most important, in addition to the supercooling behavior, is the observation that segregation of molecules of lower masses on crystallization can occur below the equilibrium melting temperature of the rejected species. It was suggested earlier that molecular nucleation is such a process, although the detailed mechanism is not known [22].

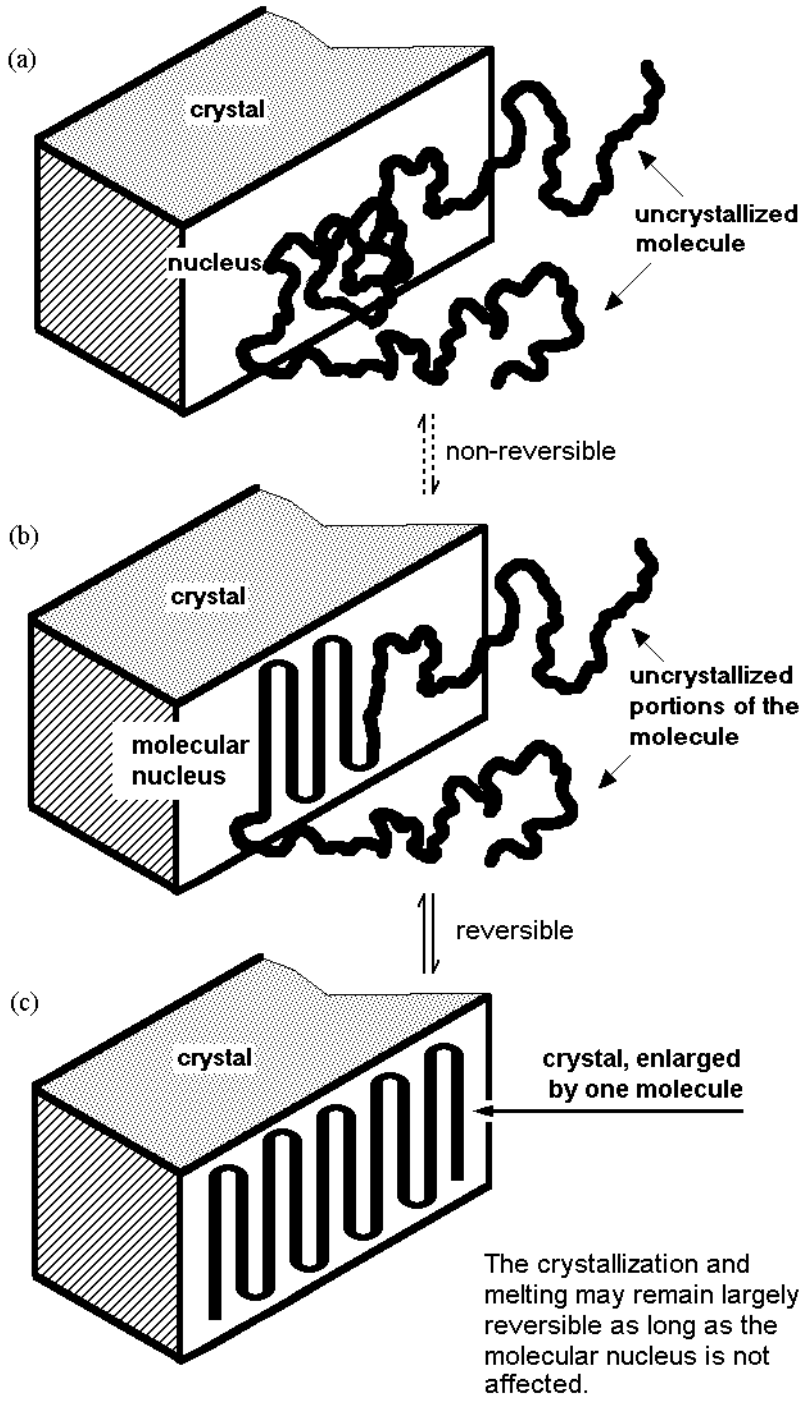

Figure 1.8. A schematic of molecular nucleation of linear macromolecules, (a) to (b) describing molecular nucleation, and (c) the completion of crystallization of the molecule. Copied from ref. [23].

Qualitative evidence for molecular nucleation can be derived from the observation of segregation of molecular weight into different crystals [24]. On crystallization of a mixture of two different molecules (A>B), between the eutectic temperature and the equilibrium temperature of A, the molecules A will crystallize and the molecules B will melt. The final crystal will be formed by only A. Molecules B will be all rejected to the melt. At the equilibrium melting temperature of B, one can predict that both A and B can crystallize. Observations of Mehta gave, however, surprising results [18]. On crystallization even below the equilibrium melting temperature of B, its molecules are still rejected and a crystal is formed with only A molecules. That is, even below the equilibrium temperature the melting of B molecules there must be a reversible process that separates A from B molecules. This process is thought to be the molecular nucleation. Only if a molecule A has sufficient length can it undergo step (a) to (b) in Figure 1.8 at a temperature below its melting temperature. The step (b) to (c) goes then quickly without further nucleation. Knowing that n-paraffins $C_{50}H_{102}$ or shorter do not have a molecular nucleation barrier, but segregate at the equilibrium melting temperature led to the main project of this thesis work, to find the chain length for molecular nucleation and identify molecular nuclei during the melting of polymers.

If secondary nucleation were involved in molecular segregation, only one molecule could be properly selected per crystal layer. Once a secondary nucleus is formed, all molecules of different length can crystallize until completion of the crystal layer. The study of segregation of molecular weights on melt-crystallization shows that the individual molecules need a kind of nucleation process on crystallization. The technique involves fractional dissolution of lower melting crystals and separation by filtration. Only if the

molecules are completely separated from other, such separation of higher melting crystals is possible. As soon as tie molecules exist between crystals of different stability, the lower melting portion of the molecule can be dissolved, but not removed from the sample by filtration. The formation of such tie molecules could be shown to increase with molecular weight and supercooling [25]. This expected increase in tie molecules is an indication of the limits to molecular mobility. As soon as a molecule participates in one or more crystals it cannot be rejected as a molecule [22].

1.1.4 Heat capacities in the melting/crystallization range

In the thermal analysis of flexible linear macromolecules, there are six different contributions to an apparent heat capacity, which is a heat capacity with additional latent heat contributions, in the melting and crystallization region of the analyzed polymer. These are (1) vibrational heat capacity, (2) conformational contribution, (3) reversible melting and crystallization transition, (4) primary crystallization and melting, (5) secondary crystallization, and finally (6) the various annealing and crystal perfection processes [26–30]. The vibrational heat capacity (1) is the true thermodynamic heat capacity of solids with a fast response time (picoseconds) and the others may have additional latent heat contributions. The first three are truly reversible and the second three contributions are irreversible.

(1) the vibrational contribution to the heat capacity has been described for many macromolecules as the sum of the skeletal and group vibration motion, data given in the *ATHAS* Data Bank at the web-site: *http://web.utk.edu/~athas*. It represents the largest contribution to the enthalpy of the macromolecules.

(2) the conformational contribution is a heat capacity arising from large-amplitude molecular motion. As the temperature of a crystal increases, some of the vibrations may change to a large amplitude motion, such as translation, rotation, or internal rotation. In polyethylene, as seen in Figure 1.9, the measured heat capacity of crystalline PE starts to deviate from the vibrational heat capacity (1), far from the melting temperature. This higher heat capacity is due to a larger gauche concentration [31] and contributes a larger amount of potential energy when compared to the corresponding torsional oscillation.

(3) the reversible melting is a phenomenon which cannot be explained with present theories of melting and crystallization of polymers, where the phase transformation from the solid crystalline phase to the melt and vice versa are considered to be irreversible processes. Crystallization should always occur via nucleation with supercooling (i.e., the creation of the

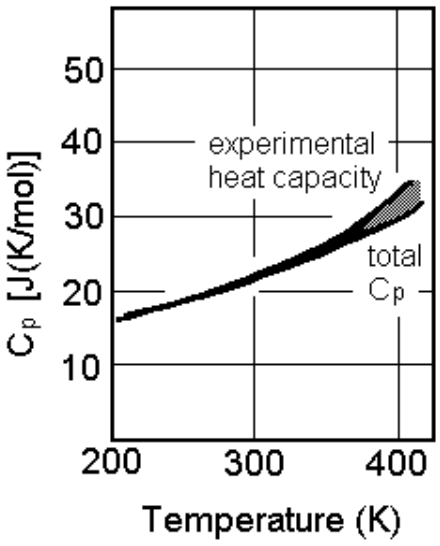

Figure 1.9. Deviation of the heat capacity of crystalline polyethylene from the computed vibrational heat capacity. Copied from ref. [31].

appropriate crystal and molecular nuclei as mentioned in the sections 1.1.2 and 1.1.3), followed by crystal growth and perfection. After crystal growth and perfection are completed, the melting can only occur at a considerably higher temperature. Although crystal nucleation can be avoided by seeding with heterogeneous nuclei or incomplete melting, molecular nucleation cannot be avoided. Parts of the heating and cooling cycles in the poly(ethylene-*co*-octene), however, are fully reversible in the melting range [27]. Accepting the need of molecular nucleation this reversible crystallization and melting must be due to small chain segments arrested on one or both sides on the surface of higher melting crystals which are as short as the paraffins described to melt reversibly in this thesis. It is known, for example, that side-chains of polymers, when they are tied to the main chain with a flexible spacer of four to eight CH_2- groups can crystallize and melt similar to the corresponding small molecule, i.e., crystallize and melt reversibly with a melting temperature not far from the small molecules, severed from the main chain [6]. Paraffins of this length show no supercooling [2]. Two locations offer themselves in the structure of semicrystalline polymers for such chain segments. One is found for chain segments that melt only partially because of their attachment to other, higher melting parts of the crystalline matrix, the other is found for secondary, fringed-micellar crystals, grown within the network of the primary crystals. In both cases, the amount and its low equilibrium melting temperature can be extracted from the TMDSC data [29]. The observed reversible melting at temperatures that exceed the reversible paraffin melting temperatures must have a different explanation. In this case one has a direct measure of the molecular nuclei as they exist on the crystal surface on partial melting. This is the main observation of the research of this thesis that there exists a critical

chain length above which reversible melting is not possible. First experiments which prove that, indeed, the reversible melting (3) of polypropylene occurs on the growth surface were given in ref. [30].

(4) the contribution is the well-studied initial crystallization. It is commonly the biggest latent heat effect and shows large temperature differences between crystal growth and melting, i.e., it is irreversible. The analysis of the thermodynamic stability of both primary and secondary crystals is complicated by crystal perfection, even when its growth occurs isothermally.

The final two contributions (5) and (6) may contribute to annealing peaks [29]. The contribution (5) involves less perfect crystal growth which occurs later than observed for the initial crystals. The contribution (6) involves crystal perfection. Typically the perfected crystals melt 5-20 K above the annealing temperature, as demonstrated by the common annealing peaks [1].

A series of homopolymers analyzed with TMDSC shows that these reversible and irreversible contributions seem to occur universally in flexible linear macromolecules. The homopolymers analyzed in our laboratory were poly(oxyethylene) [32, 33], poly(ethylene terephthalate) [34, 35], poly(trimethylene terephthalate) [36, 37] and polydioxanone [38]. Recently, all six contributions were shown clearly on poly(ethylene-co-octene) [26, 28].

1.1.5 Crystallinity calculations

The crystallinity as a function of time, $w_c(t)$ is calculated by dividing the partial integral of the smoothed heat-flow rate signal by the heat of fusion of PE at the temperature where

the isothermal crystallization experiment is performed. Using these $w_c(t)$ values, the thermodynamic base line heat capacity, $C_p(b)$ is calculated as [39]:

$$C_p(b) = w_c(t)C_p(c) - (1-w_c(t))C_p(a) \quad (1.5)$$

where $C_p(c)$ and $C_p(a)$ are the literature values of the crystalline and amorphous PE, respectively, at the measurement temperature [available in *ATHAS* Data Bank]. The excess heat capacity, $C_p(e)$, due to the reversible melting and crystallization is calculated from the difference between the reversing heat capacity discussed in section 1.3.3 and the baseline heat capacity. The reversibility of the crystalline fraction that follows the temperature modulation, $\Delta w_c(rev)$, can be obtained finally using the equation:

$$\Delta w_c(rev) = \frac{A_T C_p(e)}{\Delta H_f} \quad (1.6)$$

where A_T is the temperature amplitude applied in this modulation. Mathot *et al.* identified 58% of the crystallinity of the PE sample on isothermal crystallization as reversible and the $\Delta w_c(rev)$ is calculated to be 0.01–0.013 [39]. So 1.7-2.2% of total crystalline fractions melt and crystallize reversibly.

Androsch studied the reversible melting/crystallization in poly(ethylene-*co*-octene) [26, 28] and isotactic polypropylene [30]. He measured the degree of reversibility of melting/crystallization with TMDSC. With combination of quantitative standard DSC, TMDSC, X-ray diffraction and AFM he concluded that the reversible melting and crystallization in *i*PP occurs at an active lateral surface [30]. Strobl *et al.*, who believe that the lateral surface melting is irreversible process and disappear upon long-time annealing, get

the conclusion from TMDSC and SAXS experiments that the reversible process occurs at the fold surface [40, 41].

There is no clear evidence for the location where the reversible melting/crystallization in polymer can take place. It might be the lateral surface, the fold surface or both. Even though there are not enough experimental results, still it is obvious, that the locally reversible melting and crystallization exists in polymer. More experimental data will be added to the evidence for the process in this thesis.

1.2 n-Paraffins and Polyethylene

1.2.1 Similarity

Paraffins are saturated hydrocarbons (alkanes) with a chemical formula of C_nH_{2n+2} with straight chains (normal or *n*-paraffins) or branches (isomeric or *iso*-paraffins). As their name indicates in Latin–*parum affinis* they have very little chemical reactivity except for combustion [42]. In general, the odd-numbered *n*-paraffin crystals have an orthorhombic structure and even-numbered ones have a triclinic structure (up to C24) or a monoclinic structure (above C26) at room temperature [43]. At higher temperatures, the more stable structures are the structures with higher symmetry like hexagonal structures (6-fold rotation axis). The *n*-paraffins are long chain molecules and the rotation of the whole molecule in one step is not possible. Instead, the segmental motion along the back bone chains is at the root of the disordering of the chains. These phases with larger mobility within the molecules are not crystals anymore, but are called mesophases. In this particular case they are conformationally disordered crystal, called condis crystals.

In this thesis I would like to study the short and long flexible chain molecules, so when I say polyethylene, it is restricted only to linear polyethylene. The branched or cross-linked polyethylenes are not of interest in this study. Polyethylene, flexible linear macromolecule with chemical structure of $(CH_2\text{-})_X$, is also made up of saturated linear hydrocarbon chains and has similarity in its molecular structure to n-paraffin as can be easily found from their chemical structure. The crystal structure is also similar. PE is common in orthorhombic morphology.

At high pressure PE is known to exhibit an equilibrium hexagonal phase between its low temperature orthorhombic phase and the isotropic liquid phase [44, 45]. This hexagonal phase is a mesophase similar to the one in n-paraffins, but stable only at high pressure.

Their crystallization processes are similar. The crystallization is driven by the free energy of ordering the methylene sequences into the all-trans configuration and packing into an orthorhombic sub-cell structure which is the common structure in PE crystal and in n-paraffin crystal with high molar mass. The n-paraffin forms a lamellar morphology with extended-chain crystals up to $C_{294}H_{590}$, which is the limit for chain folding [46, 47]. Polyethylene is normally know to form chain folding crystals with 10–20 nm lamellar thickness. It is observed to form extended-chain crystals only in its oligomeric size or on crystallization into the hexagonal phase under elevated pressure [48].

1.2.2 Differences

The main difference between n-paraffins and linear polyethylenes is the monodispersity in the paraffin and polydispersity in PE. In n-paraffin crystal the order in crystalline layer

whose spacing corresponds to the molecular length and where the methyl groups lie at the interlamellar planes, and with some case they maybe fully crystallize with 100% crystallinity. Polyethylene, however, forms crystals which are only a fraction of a molecular length and whose surface is populated by chain folds ends, and links into the amorphous phase. Typical polyethylene has only 50–80% crystalline.

As mentioned in the section 1.2.1 polyethylene is similar to n-paraffins in crystal structure, but the chain distribution cannot be neglected in PE crystal. Even with a very small polydispersity index, for example, a low molecular weight PE (M_w = 595) with low polydispersity of 1.11, the chain distribution causes differences in PE crystal structure from n-paraffin with the same molecular weight. The lamellar chain packing in orthorhombic structure is same but the molecular bridges across lamellae are observed in PE sample [49, 50]. Also, a higher chain fractions still exist in polyethylene with polydispersity of 1.11 (in this case the molecular weight was 700) [51].

1.3 Temperature-modulated Differential Scanning Calorimetry (TMDSC)

1.3.1 Calorimetry

Calorimetry is a main thermal analysis method. It involves the measurement of heat, *Q*, in units of joules (J). Since there is no perfect insulator for heat, heat-loss problems are of overriding significance in calorimetry [52]. To better eliminate heat losses, twin calorimeters have been developed that permit measurements in a differential mode. Both calorimeters should then have similar heat losses and eliminate the major loss contribution.

The scanning mode is usually a continuous, linear, temperature change of both calorimeters or their surroundings. These two developments in calorimetry, coupled with a decrease in size to milligrams to increase the measuring speed, are combined in modern differential scanning calorimetry, DSC. The details of the method will be discussed in the next Section. A rather new development in calorimetry is the temperature-modulated DSC (TMDSC) which adds a modulation to the temperature change. By collecting only the response in heat-flow rate to the fixed modulation frequency of temperature, the heat-losses are farther reduced and higher accuracy calorimetry becomes possible. An extensive research was undertaken in this thesis to optimize the modulation method and extend it to multi-frequency experiment. The TMDSC will be introduced in Section 1.3.3 and the experimental details are given in Sections 2.1-2.3.

1.3.2 DSC

There are two types of differential scanning calorimeters, a heat-flux and a power compensation DSC. Of the heat-flux type, a Mettler-Toledo DSC 820 and a TA Instruments Thermal Analyst 2920 system are used for the research described in this thesis. Since the differential mode in calorimetry is coupled with the development of twin calorimeters, the precise name of DSC is scanning isoperibol (equal surrounding) twin calorimetry [53].

Differential measurements are made with a reference and a sample calorimeter within the silver furnace block, as illustrated in Figure 1.10 [54]. There has been some confusion regarding their description. The two “calorimeters” consist of small pans, usually made of aluminum to have high heat conduction. The reference calorimeter consists usually only of

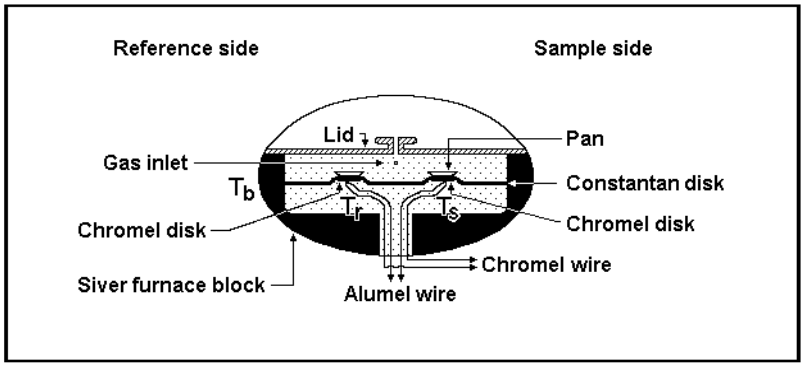

Figure 1.10. Schematic drawing of the Thermal Analyst 2920. Copied from ref. [54].

the empty aluminum pan with a temperature sensor underneath and outside of the calorimeter proper. The sample calorimeter consists of an identical aluminum pan that encloses the sample of interest, again, with the sensor underneath and outside of the calorimeter. Both sides are heated by conduction from a single furnace, governed by the block temperature (Mettler-Toledo DSC 820) or a separate block temperature sensor and the sample sensor (TA Instruments Thermal Analyst 2920) [52, 55]. In contrast, a power compensation DSC, such as the Perkin Elmer DSC 7, has reference and sample sides heated separately as required by their temperatures and temperature difference [52, 56]. The Perkin-Elmer DSC was not used in this research. Only the heat-flux DSC will be discussed in this Chapter.

Sample and heating block (furnace) temperatures are shown in Figure 1.11 [57] for the beginning of a typical heating scan. The block temperature, T_b, increases linearly and is followed, after reaching steady state, by the sample temperature, T_s, with the same heating rate, but lagging in temperature proportional to the heat capacity of the sample and pan which comprise the sample side [58]. A similar graph can be drawn for the reference temperature at the intermediate temperature T_r. For heat capacity measurement only data generated after

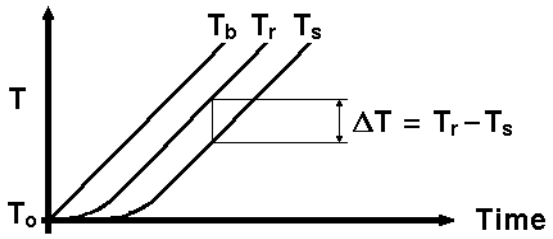

Figure 1.11. Typical start of a heating scan for the block, reference and sample temperatures of a standard DSC, T_b, T_r and T_s, respectively. T_o is initial temperature. Copied from ref. [54].

steady state is reached are used to eliminate the kinetic aspects caused by the scanning operation. Another condition for quantitative measurement is a negligible temperature gradient within the sample. With a negligible temperature gradient the heat-flux into the sample calorimeter is directly dependent on its heat capacity. At steady state, the heat-flow rates of the reference and sample calorimeters are then governed only by the rate of temperature change and their heat capacities. The difference in temperatures between the reference and sample calorimeters ($\Delta T = T_r - T_s$) is directly proportional to this heat-flow rate. Therefore, heat capacity is described by:

$$C_p = K\frac{\Delta T}{q} \tag{1.7}$$

where K is the Newton's law constant (in J $K^{-1}min^{-1}$), which depends mainly on the thermal conductance from the DSC heater to the sample and reference calorimeters, and q is the heating rate (in K min^{-1}). Actually, for an equation for heat capacity of the sample, a minor correction needs to be added the basic equation (1.7) since the sample and reference

calorimeters change their heat capacities with temperature, i.e., T_r and T_s in Figure 1.11 are not strictly parallel to T_b. The heat capacity at steady state is then [59]:

$$mc_p = K\frac{\Delta T}{q} + C_s\left(\frac{d\Delta T}{dT_s}\right) \tag{1.8}$$

where m is the sample mass, c_p is the specific heat capacity of the sample (in J K^{-1} g^{-1}), C_s is the total heat capacity of the sample calorimeter (sample + pan). The second term on the right-hand side is only a small correction term [60]. This correction term can be calculated and does not need any further measurement.

1.3.3 TMDSC

In the more recently developed temperature-modulated DSC (TMDSC) [61–63], a sinusoidal or other periodic change in temperature is superimposed on the underlying heating rate. The heat capacity measurement using TMDSC is easy as long as the condition of steady state and negligible temperature gradients within the sample can be maintained, as required for eq (1.8). The modulation adds, then, a small periodic component to the linear heating ramp $<q>t$, where the $< >$ indicate an average over one full modulation cycle, as depicted in Figure 1.12. The basic temperature-modulation equation for the block temperature can be written as:

$$T_b(t) = T_o + <q>t + A_{T_b}\sin\omega t \tag{1.9}$$

with T_o representing the isotherm at the beginning of the scanning. The modulation frequency ω is equal to $2\pi/p$ in units of rad s^{-1}, with p representing the length of one cycle in seconds.

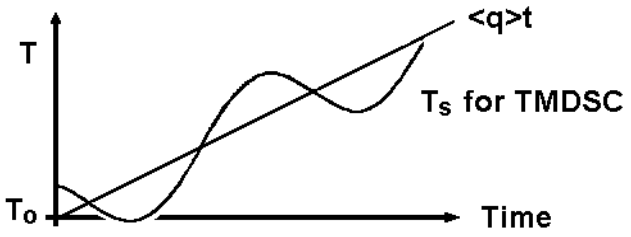

Figure 1.12. A typical heating scan for the sample temperature (T_s) of a TMDSC, the line indicated with <q>t is linear response. T_o is initial temperature. Copied from ref. [54].

Depending an added subscript to T, eq (1.9) can be used to express the sample, or reference temperature (T_s or T_r, respectively) with an additional phase shift added to the sine term. The temperature difference is proportional to the heat-flow rate (Φ) and is used as the response function for the computation of the heat capacity. The heat flow caused by the temperature modulation measures the "reversing" heat capacity, a term introduced in TMDSC to identify a heat effect that appears to be reversed within the temperature range of the modulation amplitude. As long as the heat capacity response is fast and no latent heat contributions exist, the reversing heat capacity is, indeed, the reversible, equilibrium heat capacity. If slow processes or transitions are involved, the reversing heat capacity may be an "apparent" heat capacity and is in need of special interpretation. The reversing heat capacity as calculated by the TMDSC software is solely the first harmonic response to the modulation and is extracted from the time domain data on temperature and heat-flow rate by Fourier transformation into the frequency domain [64].

The basic heat capacity analysis of TMDSC is derived from the well-known alternating-current (AC) calorimetry [65]. The heat capacity of a sample calorimeter, C_s (= $mc_p + C_p'$, where C_p' is the heat capacity of the pan) can be determined from the amplitude

of the heat-flow rate response of the sample, A_Φ, to the amplitude of the sinusoidal sample-temperature modulation, A_{Ts}, and the modulation frequency, ω. The following equation gives the relationship for the case of an AC calorimetry:

$$C_s = \frac{A_\Phi}{A_{Ts}\,\omega} \tag{1.10}$$

Note that $A_{Ts}\,\omega$ is also the amplitude of the modulated heating rate. In the case of the TMDSC, an additional factor should be considered because of it being a twin calorimeter. The sample calorimeter and reference show a phase shift in their response to the modulation [52]. The following equation was proposed for the reversing heat capacity from the heat-flux type TMDSC [64] under the conditions of maintained steady state and negligible temperature gradient within the sample:

$$(C_s - C_r) = \frac{A_{\Delta T}}{A_{Ts}}\sqrt{\left(\frac{K}{\omega}\right)^2 + C_r^{\,2}} \tag{1.11}$$

where C_r is the heat capacity of the reference calorimeter (identical to C_p' when it consists of an identical empty pan as the sample calorimeter), $A_{\Delta T}$ and A_{Ts} are the maximum amplitudes of the modulation found in the temperature difference and sample temperature, respectively, and ω is the modulation frequency. This expression can be modified to the following equation:

$$mc_p = \frac{A_\Phi}{A_{Ts}\omega}\sqrt{1 + \left(\frac{C_r\,\omega}{K}\right)^2} \tag{1.12}$$

where A_Φ is the modulation amplitude of the heat-flow rate. The derivation of equation (1.12) is described in ref. [64] in more detail.

The "total heat capacity," is the quantity determined from a standard DSC by eq (1.8). Under ideal conditions it can also be extracted normal TMDSC with an underlying heating rate $\langle q \rangle \neq 0$. Using $\langle \Delta T \rangle$ and $\langle q \rangle$, the sliding averages over one modulation period in eq (1.8). When there is a difference between the result of the equations (1.12) and (1.8), it is called a nonreversing heat capacity. It is connected to irreversible processes within the sample that cannot be modulated properly, such as a slow chemical reactions (oxidation, curing, evaporation, *etc.*) and non-equilibrium phase transitions (crystallization and reorganization). It may even enable us to separate the complicated simultaneous fusions, glass transitions, and annealing, common in many macromolecules [64].

1.3.3.1 Quasi-isothermal TMDSC

When the underlying heating rate $\langle q \rangle$ equals zero, the experiment is called a quasi-isothermal TMDSC, which is the mode used extensively in this thesis. Such quasi-isothermal experiments involve a modulation about a constant temperature and can be extended over long periods of time, so that slow processes can be eliminated after a given time. The total heat capacity is not available in this case and must be derived from parallel standard DSC experiments or by integration of the quasi-isothermal response over long periods of time. The nonreversing heat capacity, obtained by calculating the difference between the total and reversing heat capacity, must similarly computed indirectly. Among several modes of TMDSC, the quasi-isothermal TMDSC gives the most precise heat capacity measurement. One can await steady state before beginning data collection and extract only the contribution that is sinusoidally modulated with a given frequency. Most of the accidental losses are

eliminated. Since quasi-isothermal TMDSC experiments have no time limit other than the limit of the instrument stability, wide ranges of kinetic studies can be accomplished. Furthermore, details of the kinetics can be extracted by an analysis of the heating and cooling cycles in the time domain.

The right-hand square-root expression in eq (1.12) can be simplified to $K(\omega)$, a dimensionless frequency-dependent constant. One can get a final equation for the reversing heat capacity from TMDSC measurement as:

$$C_p^{rev} = \frac{A_\Phi}{A_{Ts}\omega} K(\omega) \tag{1.13}$$

where C_p^{rev} is the reversing heat capacity of a desired sample in J K^{-1}. For the last several years, the research about the frequency dependent constant $K(\omega)$ was done in our research group using multi-frequency modulation studies carried out with sawtooth-like modulations.

The frequency dependent constant $K(\omega)$ can be determined by quasi-isothermal TMDSC measurements at different frequencies or by one quasi-isothermal TMDSC using sawtooth modulation and analyzing higher harmonics of the Fourier series of the sawtooth modulation. Empirically it can also be rewritten as:

$$K(\omega) = \sqrt{1 + \left(\frac{C_r \omega}{K}\right)^2} = \sqrt{1 + \tau^2 \omega^2} \tag{1.14}$$

where τ is a time constant which can be determined from the response to different frequencies. The correction function $K(\omega)$ was initially derived for a sinusoidally modulated heat-flux calorimeter operating under steady state conditions and with a negligible temperature gradient within the sample [eq (1.12)] [66]. The value for τ in eq (1.14) can then

be obtained by plotting the inverse of the squared, uncorrected heat capacities ($C_p^{uncor.}$) which are computed from eq (1.13) by setting $K(\omega) = 1$ *versus* the square of the frequency [67]. The relationship is:

$$\left(\frac{1}{C_p^{uncor.}}\right)^2 = \left(\frac{1}{C_p^{cor.}}\right)^2 (1 + \tau^2\omega^2) \qquad (1.15)$$

If this procedure yields a linear function, τ is independent of ω and can be determined from the slope of the curve and the corrected heat capacity $C_p^{cor.}$ is given by the intercept.

Initially, τ was determined for a power-compensated, sawtooth modulated TMDSC from the first harmonic of the Fourier series from measurements at different frequencies ω [67]. Later, it was discovered that the higher harmonics of the Fourier series from one measurement at one frequency ω can also be used to determine the correction function [68]. The Fourier series of a centro-symmetric sawtooth contains only odd numbered sinusoidal harmonics, *i.e.*, it represents a sum of sinusoidal modulations of different frequencies (1^{th}, 3^{rd}, 5^{th} … harmonics). In this case, ω in eq (1.15) should be written $\nu\omega$ to describe the different frequencies from the higher harmonics of frequency ω and $\nu = 1, 3, 5, 7$ and 9, the numbers of the harmonics considered. Therefore, the reversing heat capacity equation (1.13) should be changed with $A_\Phi(\nu\omega)$, $A_{Ts}(\nu\omega)$ and $\nu\omega$, instead of A_Φ, A_{Ts} and ω, and then one can get the reversing heat capacity data depending on the frequency from one measurement. This technique is very useful in glass transition studies where the thermal history of the sample is critical [69].

Unfortunately, however, the amplitudes of the higher harmonics decrease quickly with ν, the order of the harmonic. This decrease in amplitude should lead to a diminished

precision of the measurement. Despite the small amplitudes, it was possible to use up to the 11^{th} harmonic to assess the frequency response of the calorimeter and to derive the characteristic relaxation times for the instrument [68].

In order to improve the precision of the analysis, a new, complex sawtooth-modulation was proposed [70]. It is generated by adjusting the 1^{st}, 3^{rd}, 5^{th}, and 7^{th} harmonics of the sawtooth to equal amplitudes. The result was a complex sawtooth with 26 different, linear segments. This complex sawtooth with 26 segments can be simplified without losing much of the similarity of the first amplitudes of the Fourier series by using only 14 segments.

In ref. [71], this simplified complex-sawtooth was tested using a heat-flux DSC, as built by Mettler-Toledo Inc., which is controlled close to the heater. Modulation frequencies, sample mass, and sampling frequency were varied to find a best performance. It was proven that it was possible to reach a 0.1% precision with a temperature-modulated DSC. Similar analyses with a heat-flux DSC controlled close to the sample temperature [72] and with a power-compensation DSC which is controlled at the heater position [73] were also carried out and compared. Each of these differently constructed DSCs gives a different response to the modulation with the complex sawtooth and needs specific analysis and calibration methods to reach peak performance.

The TMDSC in the melting and crystallization region of linear macromolecules is complicated by the need to evaluate the reversible heat capacity in the presence of superimposed, latent-heat effects which are often non-reversing and cause instrument lags and distort the sinusoidal response of the calorimeter and even the temperature modulation. The latent heat may be absorbed or evolved abruptly, causing difficulties in the Fourier analysis

of the apparent heat capacity, so that the data analysis has to be carried out on the raw heat-flow and sample-temperature data in the time domain [$HF(t)$ and $T_s(t)$, respectively, where $HF(t)$ is proportional to the temperature difference $\Delta T = T_r - T_s$] [13]. Despite these difficulties, TMDSC offers the possibility of new insight into the micro-structure of polymers by yielding information on re-crystallization, crystal perfection, melting and crystallization kinetics, and metastability.

CHAPTER 2

EXPERIMENTAL

2.1 Instrumentation

The melting and crystallization of short and long flexible chain molecules were studied using calorimetry in this thesis. The general descriptions of calorimetry including specific descriptions of standard differential scanning calorimetry (DSC) and temperature-modulated differential scanning calorimetry (TMDSC) were given in the Section 1.3.

For the calorimetry two heat-flux differential scanning calorimeters (DSC) were used. The Mettler-Toledo DSC has a temperature control close to the heater, and the TA Instruments DSC is controlled close to the sample. Both calorimeters give a somewhat different response and have used in different modulation modes in addition to a standard DSC.

2.1.1 Mettler-Toledo DSC 820 and its New Sensor

The Mettler-Toledo DSC 820 module was used for all measurements, except for the sinusoidal temperature modulation for quasi-isothermal analyses [66, 74]. These were carried out with the Thermal Analyst 2920 MDSC® from TA Instruments, described in Sect. 2.1.2.

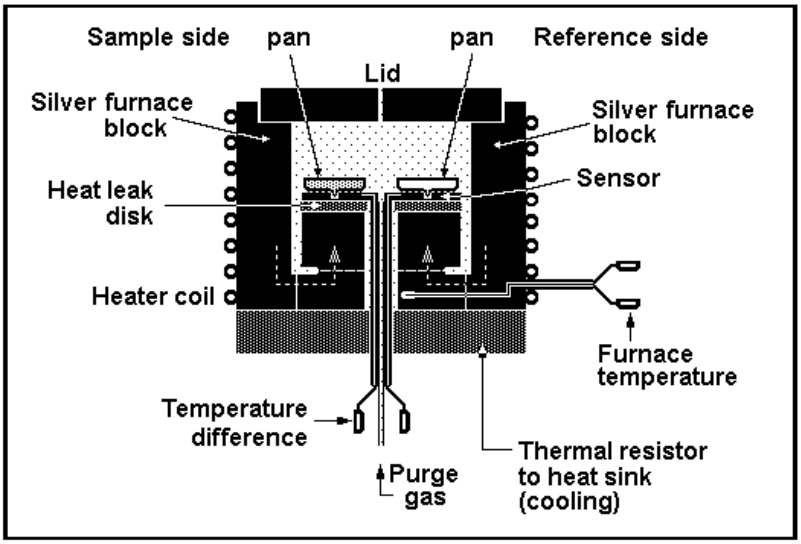

Figure 2.1. Schematic drawing of the Mettler-Toledo DSC 820. The calorimeter is modulated at the furnace temperature. The sensor consists of multiple thermocouples, to give an averaged, sensitive measurement of the temperature difference ΔT. Copied from [TAM 20-11], drawn after Mettler-Toledo instrument descriptions.

In the Mettler-Toledo DSC 820 module, a sample and a reference calorimeters are separated, as shown in Figure 2.1. The heat from the furnace to both calorimeters flows through the heat leak disk. The heating rate is controlled through the furnace temperature sensor, and the temperature of the reference calorimeter, T_r, is calibrated relative to this furnace temperature. The temperature difference between the reference and the sample sides, ΔT, is obtained with the heat-flux meter shown in Figure 2.2, located underneath the calorimeters (see Figure 2.1). In this DSC, temperature is measured close to the furnace body and used to control the modulation and also to establish the reference temperature. In addition, the temperature difference between reference and sample is measured by the heat-flux sensor FRS-5.

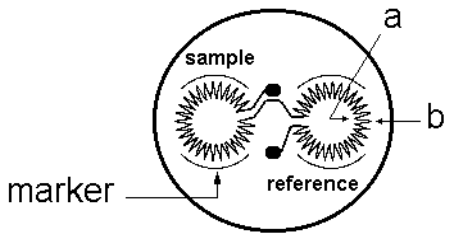

Figure 2.2. Top view of a FRS5 sensor plate with 56 thermocouples for sample and reference. Copied from [TAM 20-11] drawn after a picture in ref. [76]. Note that the thermocouples alternate between inside and outside of the calorimeter, averaging the temperature difference between the sensor plate and the calorimeter placed on the inside thermocouples.

The obtained ΔT signal is proportional to the heat flux, as will be shown below. Both, the reference temperature T_r and the temperature difference, ΔT, are recorded by the computer. The noise level is ±1 μW, sample volumes of 35 and 150 mm^3 can be analyzed with different crucibles, heating rates of up to 250 K min^{-1} can be programmed [75]. The furnace lid is operated automatically. Dry N_2 gas with a flow rate of 20 mL min^{-1} was purged through the furnace chamber. Cooling was accomplished with a liquid-nitrogen cooling-accessory. To avoid condensation of water during operation below room temperature which leads to high damage of the computer chip installed near by the furnace, dry N_2 gas or compressed air with a flow rate of 200 mL min^{-1} was purged through the surroundings of the furnace. Before these limitations were realized, serious errors occurred on fast cooling and low-temperature measurements. The Mettler-Toledo DSC 820 is not suited for cooling rates faster than 15 K min^{-1} with the liquid N_2 accessary because of a faulty design of the connection to the cooling-accessory which was discovered by extended trial and error experimentation.

The Mettler-Toledo DSC 820 was upgraded in 1998 with a new ceramic sensor (FRS5) with 56 vapor-deposited thermocouples, as shown in Figure 2.2, to give an averaged, sensitive measurement of the heat-flux difference, proportional to the temperature difference $T_r - T_s = \Delta T$. The conventional sensors where single thermocouples used to measure the ΔT signal directly and generate a signal of lower magnitude [76] and, thus, yield reduced baseline stability and repeatability. With the new sensor actually the heat-flux between the two thermocouple junctions, indicated with 'a' and 'b' in Figure 2.2, is measured on 28 positions on each side. The heat-flux into the sample is dQ_s/dt, expressed by the difference between the heat-flux to the sample and pan on the sample side and the empty pan on the reference side.

$$\frac{dQ_s}{dt} = \frac{1}{R_{th}} \left(\sum_{i=1}^{28} \Delta T_{s_i} - \sum_{i=1}^{28} \Delta T_{r_i} \right) \tag{2.1}$$

where R_{th} is the thermal resistance between 'a' and 'b', and T_{si} and T_{ri} are the temperature differences of the i^{th} thermocouple on the sample and reference sides, respectively. The heat-flux measured and summed in this manner is proportional to ΔT. The reference and sample sides and thermal amplification of the sensor signal is accomplished by connecting all thermocouples in series [76].

The temperature modulation is controlled using the furnace temperature sensor, at a position far from the sample (see Fig. 2.1) [57]. As a result, the reference side shows the standard modulation and the sample side is influenced by the sample behavior. During melting, for example, the sample temperature will stop changing except for developing temperature gradients until melting is completed.

The heat-flow rate curves are automatically smoothed by the manufacturer's software [77]. Therefore, the heat flow rate curves are not the raw data. An adaptive data smoothing technology is employed, working in the following way: Through all of the data points inside an arbitrary window of time, a smooth function is fitted. The next step is to calculate the square of the deviations of all data points from the fitted function. If the average of this sum is larger then a defined, but not specified limit, the window size is made smaller and the procedure is repeated. Out of this fitted function only the smoothed data point in the center, is computed. This new data point replaces now the old data point. Next, the window is moved by steps of one second until the whole DSC traced is smoothed up to the point where larger changes from the baseline occur.

With the help of Mettler-Toledo we found a way to turn off this automatic smoothing. One must create a module called 'berthAxxx' to see the original data. To do this, one opens the 'Install' window and chooses 'Topic'/ 'Module', then chooses 'File'/ 'Open' and selects the module from the list. After the data are seen, choose 'File'/ 'SaveAs'. When it is prompted for the file name, type 'berthA001'. After saving the module under the new name, go to 'Topic'/ 'Port and Device'. From this window, click on the currently connected module and it will disappear. Then, click on the empty space and connect to the new 'berthA001' module. Any data collected with this module will now be raw, unsmoothed data as needed for the analysis.

2.1.2 Thermal Analyst 2920

A Thermal Analyst 2920 MDSC® from TA Instruments Inc. with modulation control at the sample-temperature sensor was used for all sinusoidal, quasi-isothermal analyses. As the Mettler-Toledo calorimeter it is an isoperibol heat-flux twin calorimeter, but has only a single thermocouple underneath each calorimeter for measurement. Its schematic was already shown in Figure 1.10 (see the Section 1.3.2). The furnace block is programmed to give a linear increase in the sample temperature, and the sample temperature sensor controls the temperature modulation [78]. The temperature range is from 125 to 1000 K [the heating rate, 0.1 to 100 K min^{-1}, noise, ±5 μW, and the sample volume may be 10 mm^3] [58]. The constantan disc provides sufficient thermal resistance to maintain most of the temperature gradient which limits the heat-flow outside the sample calorimeter. The heat from the furnace flows through the disk symmetrically to both calorimeters (see Figure 1.10. in Section 1.3.2.) [54]. Cooling was achieved with a refrigerated cooling system (RCS, cooling capacity to 220 K). Dry N_2 gas with a flow rate of 20 mL min^{-1} was purged through the instrument. Dry N_2 gas with a flow rate of 10 mL min^{-1} flowed through the cell. The recorded data consist of the sample temperature T_s and the temperature difference $\Delta T = T_r - T_s$. The heat-flow rate is proportional to ΔT and available as the uncorrected measurement, in contrast to the Mettler DSC 820.

2.2 Calibration

The sample temperature was first calibrated in the standard DSC mode. The onset-temperatures of the transition peaks were used for this calibration [tin (505.05 K), indium

(429.75 K), H_2O (273.15 K), and n-octane (216.4 K)]. A scanning rate of 10 K min^{-1} was employed. The onset of melting was determined by extrapolating the sample temperature from the linear portion of the melting peak to the baseline [52, 69]. The heat-flow rate was then calibrated approximately with the heat of fusion of indium (28.62 J g^{-1}) [79]. For the Mettler-Toledo DSC 820 calorimeter there was an additional tau-lag calibration with indium prior to both calibrations. It largely eliminates the effect of different heating rates, so that the onset temperatures do not change significantly with heating rates. However, this calibration does not work well for cooling, so that the transition temperatures on cooling change with cooling rates.

Because of the influence of temperature gradients within the sample and thermal conductivity effects the typical accuracy of temperatures measured by DSC is not better than ±0.5 K. The smallest possible temperature-modulation amplitude is 0.05 K with steps of ±0.1 K and this leads to a relative accuracy of perhaps ±0.01 K for temperature differences. For n-paraffins which have narrow transition regions, the 0.05 K amplitude can fix the melting end with accuracy as high as ±0.05 K by covering the complete melting range in steps of 0.1 K. For the polymers, however, it would take 50 times as long to measure with amplitudes of 0.05 K without leaving gaps in the analysis because their transition regions are much broader. Therefore, as a compromise 0.5 K of temperature amplitudes were chosen for the polymer fractions in this thesis work. This matches the accuracy of absolute and relative temperature measurement. The melting temperature of indium was in addition to measurement by standard DSC, also measured in the quasi-isothermal modulation mode using the Thermal Analyst 2920 with 0.05 K and 0.5 K of temperature amplitudes, and a 60 s period to identify

the differences between two modes of measurement (see Section 1.3.3). To carry out this TMDSC, the melting temperature, T_m, of indium was set to be 429.75 K in the standard mode at 10 K min^{-1} and found then to be 429.34 K in the modulation mode with a 0.05 K temperature amplitude, as seen in Figure 2.3 [14]. This difference between the two measurements is not fully explained at present, but rests mainly with a 0.03 K change of onset temperature per K min^{-1} heating rate [14]. It occurs also in the quasi-isothermal sawtooth modulation mode with a 0.05 K temperature amplitude and 60 s period using the Mettler-Toledo DSC 820. In this case 0.44 K were found in an additional experiment. To correct the sample temperatures from quasi-isothermal measurements we added 0.41 K as a calibration constant to all data of quasi-isothermal measurements with a 0.05 K temperature amplitude and 60 s period. This correction is needed for the C60 data in this thesis and was applied

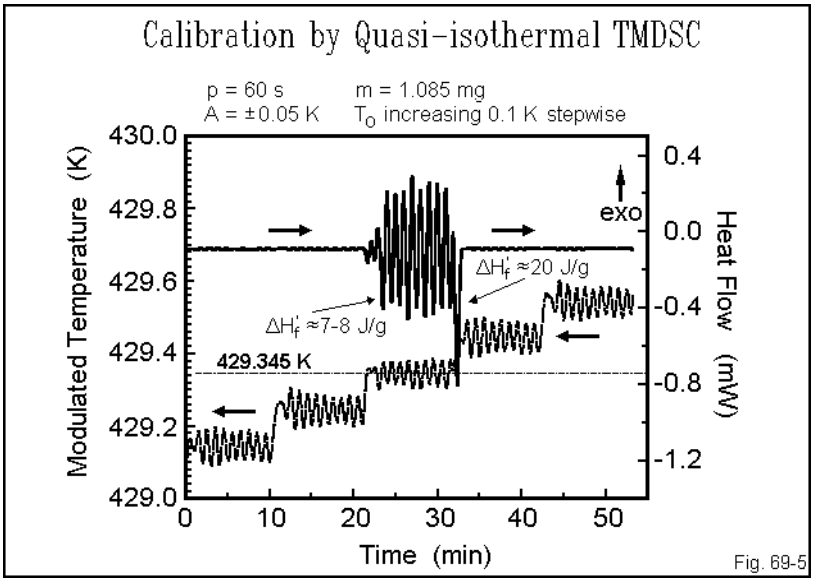

Figure 2.3. Difference between standard DSC and quasi-isothermal TMDSC measurements for melting temperature of indium. Measured by TA Instruments 2920 with 0.05 K temperature amplitude and 60 s modulation period and copied from [14].

earlier to the data for $C_{26}H_{54}$, C44 and C50 [2].

When the temperature amplitude in the modulation mode was changed to 0.5 K, which is the most often used temperature amplitude in this thesis, the melting temperature, T_m, of indium was found to be 428.88 K after it was set to be 429.75 K in the standard mode at 10 K min^{-1}. Figure 2.4 shows the analysis. The difference of 0.87 K was similarly added as a calibration constant for the sample temperature to all data out of quasi-isothermal measurements with a 0.5 K temperature amplitude and a 60 s period.

The relation between the temperature difference and modulation frequency is not established yet. For more information regarding to the differences depending on temperature amplitude a further study is necessary and in progress.

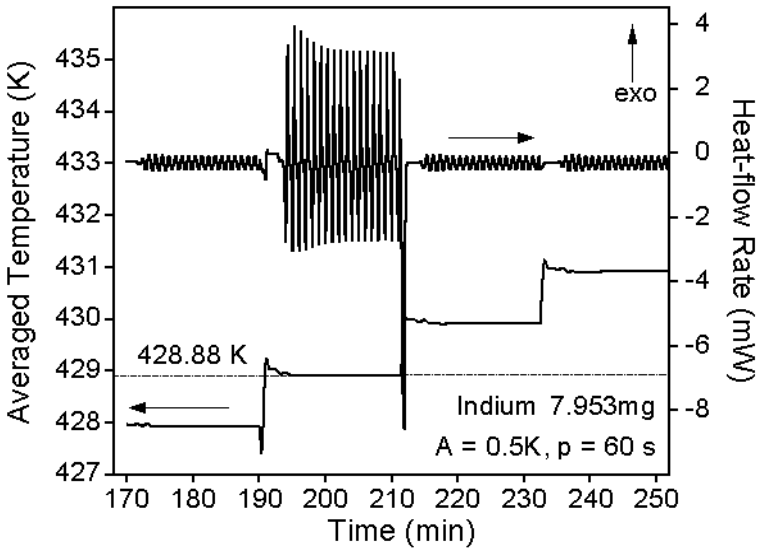

Figure 2.4. Difference in melting temperature of indium between standard DSC and quasi-isothermal TMDSC measurements when the temperature amplitude is 0.5 K.

2.3 Evaluation of reversing heat capacity

To measure the reversing heat capacities, three measurements are necessary, a sample run, an empty run, and a reference run using an identical temperature programing method. The sample run is done with the desired sample in an aluminum pan on the sample side of the calorimeter and an about 1 mg lighter empty aluminum pan than the sample side pan on reference side. The pan on reference side stays on the reference side for all three measurements and the empty pans on the sample side are all similar in their masses, 1 mg heavier than the reference pan. The empty run uses a similar mass empty pan on the sample side calorimeter and the same empty pan on reference side. The reference run is carried out with a reference material in a pan for heat capacity, normally sapphire single crystal, on the sample side calorimeter and the same empty pan on reference side. The sampling intervals are 3 s and 1 s per point for Thermal Analyst 2920 MDSC® and Mettler-Toledo DSC 820, respectively.

After these three measurements, the modulated heat-flow rates are analyzed in the time domain and the amplitudes of the first harmonic of the Fourier series (A_{Φ}) are collected. The modulated sample temperatures are treated in same way and the amplitudes of the first harmonic of the Fourier series (A_{T_S}) are collected. Using eq (1.13) assuming that the frequency-dependent constant $K(\omega)$ equals one, a preliminary apparent, reversing heat capacity is calculated for each temperature in units of mJ K^{-1}. The derivation step of eq (1.13) is described in the Section 1.3.3 briefly and details can be found in ref. [16].

Figure 2.5 shows an example of the resulting preliminary, reversing heat capacity for each measurement in the time domain for 22 consecutive runs of a $C_{60}H_{122}$ mixture with $C_{50}H_{102}$ in the melting range. The software provided by the TA Instruments computes the preliminary, reversing heat capacity (C_p^{pre}) using the following equation [80]:

$$C_p^{pre} = \frac{smoothed \langle A_\Phi \rangle}{smoothed \langle A_{T_s} \rangle \omega} \tag{2.2}$$

and gives the figure after each measurement, but they call it "complex heat capacity" which is an incorrect nomenclature.

The next step in the evaluation was an inspection of the preliminary, reversing heat capacity and sample temperature of each run in the time domain. The sample temperature should be T_o of eq (1.9) (see the Section 1.3.3), which corresponds to the mid-temperature of the modulated temperature. In TA Instruments software they call it "sample temperature".

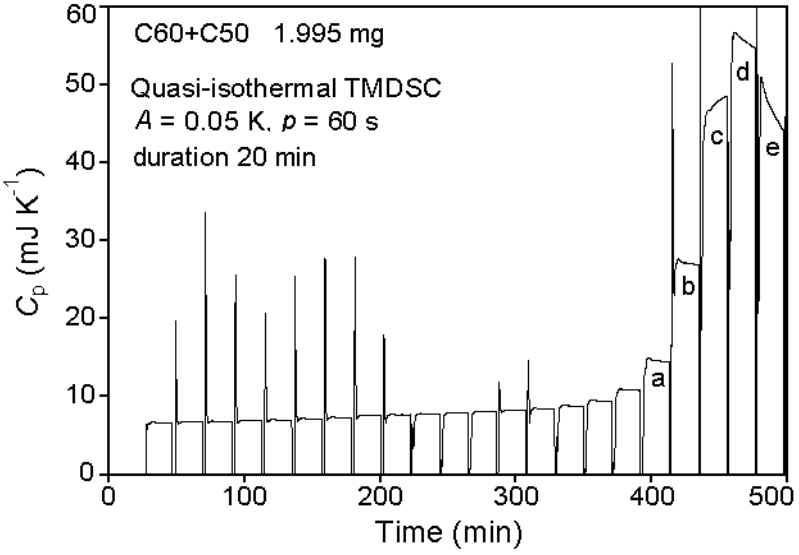

Figure 2.5. An example of the preliminary, reversing heat capacity from quasi-isothermal TMDSC measurements for each temperature, T_o in the time domain.

Each quasi-isothermal run lasted 20 min. The last 10 min data of the preliminary, reversing heat capacity in time domain are taken as the data point for the given T_o, and plotted as a function of sample temperature for each measurement. When data over the last 10 min are practically constant, as shown in most data in Figure 2.5, there is no problem to evaluate a reversing heat capacity. If the reversing heat capacity, however, keeps changing (increasing at 'c' in Figure 2.5 or decreasing at 'a', 'b', 'd', and 'e' in Figure 2.5) even after the 20 min run, not reaching a steady state which is necessary to evaluate a reversing heat capacity, the data must be discussed in the time domain. In this case the last data point is taken and recorded it as a reversing heat capacity after 20 min. To get a truly reversible heat capacity the duration of modulation should be extended up to 600 min. The reversing heat capacity from a 600 min measurement is fit into an appropriate exponential function and then extrapolated to infinite time. Outside the transition regions, 20 min modulation is enough to get the steady state. The details of the extrapolation to infinite time will be discussed in Section 4.

To approximately correct for the asymmetry of the equipment, the heat capacity of the empty run is subtracted from those of the sample run and the reference run. Data are recorded as specific quantities for a sample mass of one gram, J $g^{-1}K^{-1}$ or with the molar mass of small molecule or repeating unit of polymer, J $mol^{-1}K^{-1}$. As a final step the preliminary, reversing heat capacity of the sample run is multiplied by the heat capacity calibration constant (K_C), calculated from the reference run with sapphire at the given temperature, frequency and pan weights, as given by:

$$K_C = \frac{C_p^{lit}(sapphire)}{C_p^{pre}(sapphire)} \tag{2.3}$$

where C_p^{lit} (sapphire) is the literature heat capacity data of sapphire, available in ref. [81]. With this K_C, the constant $K(\omega)$ in eq (1.13) is also corrected.

For the data from the Mettler-Toledo DSC 820, the Fourier transformation of the experimental data of the heat-flow rate and the sample temperature had to be carried out separately using software provided by the manufacturer. The obtained amplitudes for the first harmonic of the heat-flow rate (A_Φ) and the sample temperature (A_{T_s}) were then transferred as ASCII data to a PC and the preliminary, reversing heat capacity, C_p^{pre}, was evaluated using eq (1.13) with $K(\omega) = 1$ through the commercial Sigma Plot™ program version 4.00. Once getting the preliminary, reversing heat capacity for all three runs, calculation process is same as done for data from TA Instruments.

2.4 Samples

The paraffin discussed in this thesis is *n*-hexacontane ($C_{60}H_{122}$, C60) with 98% purity. It was obtained from Aldrich Chemical Co., Inc., Milwaukee, WI. Data bank values (estimate based on ref. [82]) of thermal properties for this paraffin are listed in table 2.1 with other paraffins with shorter chain length analyzed in my master thesis.

Polyethylene (PE) standard materials were purchased from Scientific Polymer Products Inc., Ontario, NY. Their weight average molar masses (determined by scattered light photometry) are 560, 1150, 2150 and 15520 and the samples are labeled as PE560,

PE1150, PE2150, and PE15520. The number average molar masses are determined to be 515, 960, 1870 and 14400, respectively by membrane osmometry. The polydispersity indices are, thus, 1.09, 1.20, 1.15 and 1.08. The polymers PE560, PE1150 and PE15520 were synthesized by hydrogenation of polybutadiene.

Poly(oxyethylene) (POE) molar mass standard for 1500 Da with a M_w of 1500, a M_n of 1428, and a M_w/M_n = 1.05 was purchased from Polyscience, Inc., Warrington, PA (POE1500). Two additional poly(oxyethylene)s from Fluka Chemie AG have weight average molar masses of 1960 and 3060 (POE1960 and POE3060, respectively). They are polymer standards for Liquid chromatography (LC) and Gel permeable chromatography (GPC). Their polydispersity indices are 1.03. The thermal properties of PE and POE are summarized in Table 2.2. Also, the crystalline properties of PE and POE are listed in Table 2.3.

Table 2.1. Thermal properties of paraffins from *ATHAS* data bank

sample	equilibrium T (K)	heat of transition (kJ mol^{-1})
n-$C_{26}H_{54}$ [a]	T_d = 326.5	ΔH_d = 32.22
	T_i = 329.5	ΔH_i = 59.5
n-$C_{44}H_{90}$ [a]	T_f = 359.6	ΔH_f = 140.1
n-$C_{50}H_{102}$ [a]	T_f = 365.3	ΔH_f = 158.17
n-$C_{60}H_{122}$	T_f = 372.9	ΔH_f = 178.51

[a] Samples analyzed in [2].

Table 2.2. Thermal properties of equilibrium polyethylene and poly(oxyethylene) from *ATHAS* data bank

sample	equilibrium temperature (K)	heat of transition (kJ mol^{-1}) [a]	glass transition temperature (K)
polyethylene	T_f = 414.3	ΔH_f = 4.11	T_g = 237
poly(oxyethylene)	T_f = 342.0	ΔH_f = 8.66	T_g = 206

[a] The mole in the dimension refers to one CH_2-group in PE and one OCH_2CH_2-group in POE, i.e., it is 14.03 and 44.06 Da., respectively.

Table 2.3. Crystal properties of polyethylene and poly(oxyethylene) [a]

		PE	POE
crystal structure		orthorhombic	monoclinic
chain conformation ($A * u/t$) [b]		2 * 2/1	3 * 7/2
unit cell parameters (Å)	a	7.407	8.05
	b	4.949	13.04
	c	2.551	19.48
angle (°)		-	β = 125.4
density (g cm^{-3})		0.9961	1.229

[a] All data from fiber samples. PE data from ref. [83] and POE data from ref. [84].

[b] The symbol represents a helix with motifs of *A* chain atoms, *u* motifs and *t* turns of the helix per translatory identity period along the helix axis [85].

The reference sample (calibration material for heat capacity) is an aluminum oxide (Al_2O_3) single crystal disc (sapphire) of 22.56 mg purchased from TA Instruments Inc. It is a clear crystal and its melting temperature is 2323 K. The outer diameter is 0.135 inches and the thickness is 0.020 inches. The indium, calibration material for temperature and heat capacity is purchased from Mettler-Toledo. It is manufactured as a disc with 0.015 inches thickness and flattened for better heat conduct when it is encapsulated in a pan.

The sample masses used for analyses were 0.2) 1.0, 0.7) 2.1 and 2.1) 2.5 mg for C60, PE samples and POE samples, respectively. The samples were weighed on a Cahn C-33 electro-balance to an accuracy of ±0.001% of the total load (50 mg). For the Mettler-Toledo DSC 820 the samples were encapsulated in the 40 μL standard aluminum pans without center pins and with a cold-welded cover. The reference pan was an aluminum pan with a center pin and a cover. Thermal Analyst 2920 MDSC® from TA Instruments Inc. was used with 20 μL standard Al pans with cover for the samples and the empty reference. In all cases the reference pan was the same, and its mass was smaller than the sample pans.

The equation (2.4) is heat of fusion of low molar mass PE as a function of temperature derived from experimental data of paraffin and PE at the melting temperature [7]. Initially, the heat capacity-temperature relation was measured and the temperature dependence of the heat of fusion was derived from the relation. The heat of fusion is given in J g^{-1}. At 414.8 K this equation leads to a heat of fusion of 295 J g^{-1}, which corresponds to 4.14 kJ mol^{-1} in good agreement with the equilibrium heat of fusion at equilibrium melting temperature of PE.

$$\Delta H_f = 93.22 + (4.249 \times 10^{-3})T^2 - (7.413 \times 10^{-6})T^3 \qquad (2.4)$$

The PE samples analyzed in this thesis are low molar mass fractions much shorter than equilibrium PE. When one calculates the crystallinity, the equilibrium heat of fusion leads to

wrong result. The heat of fusion depending on the temperature should be used as reference for the crystallinity.

Also the POE samples in this thesis are low molar mass fractions, so the temperature dependence of the heat of fusion should be considered. For POE there is no derived equation. One can derive the heat of fusion as a function of temperature based on the definition of the heat of fusion expressed by:

$$\Delta H_f = H_a - H_c \tag{2.5}$$

where H_a is the enthalpy of amorphous and H_c, the enthalpy of crystalline.

Then, the expression of eq (2.6) is derived from eq (2.5).

$$\frac{d\Delta H_f}{dT} = C_p(a) - C_p(c) \tag{2.6}$$

That is, the heat of fusion depending on the temperature can be obtained from the difference between the heat capacities of 100% crystalline and 100% amorphous listed in ATHAS data bank. The data of PE and POE are summarized with the melting temperatures in Table 2.4.

Table 2.4. Melting temperature and heat of fusion of polyethylene and poly(oxyethylene) fractions calculated depending on their molar mass.

sample	melting temperature (K) [a]	heat of fusion (kJ mol^{-1}) [b]
PE560	T_m = 354.5	ΔH_f = 4.17
PE1150	T_m = 383.3	ΔH_f = 4.21
PE2150	T_m = 397.2	ΔH_f = 4.19
PE15520	T_m = 411.9	ΔH_f = 4.15
POE1500	T_m = 322.3	ΔH_f = 9.31
POE1960	T_m = 326.5	ΔH_f = 9.31
POE3060	T_m = 331.7	ΔH_f = 9.30

[a] The melting temperatures depending on the molar masses of PE fractions calculated by eq (3.1) and that of POE fractions by eq (3.2).

[b] The heats of fusion depending on the melting temperature of PE calculated by eq (2.4) and those of POE was taken from the differences between the crystalline and amorphous heat capacity at the corresponding temperatures listed in *ATHAS* data bank.

CHAPTER 3

RESULTS

3.1 n-Hexacontane, n-$C_{60}H_{122}$

The analysis of the n-paraffins $C_{50}H_{102}$, $C_{44}H_{90}$ and $C_{26}H_{54}$ which were chosen as simple model compounds for polyethylene was described in the master thesis of J. Pak, Department of Chemistry, The University of Tennessee, Knoxville, TN, 2000 [2]. All these paraffins solidify as extended chain crystals. Unexpectedly these paraffins did not show supercooling on crystallization from the melt as shown in Figure 3.1 [86, 87]. Also, in a

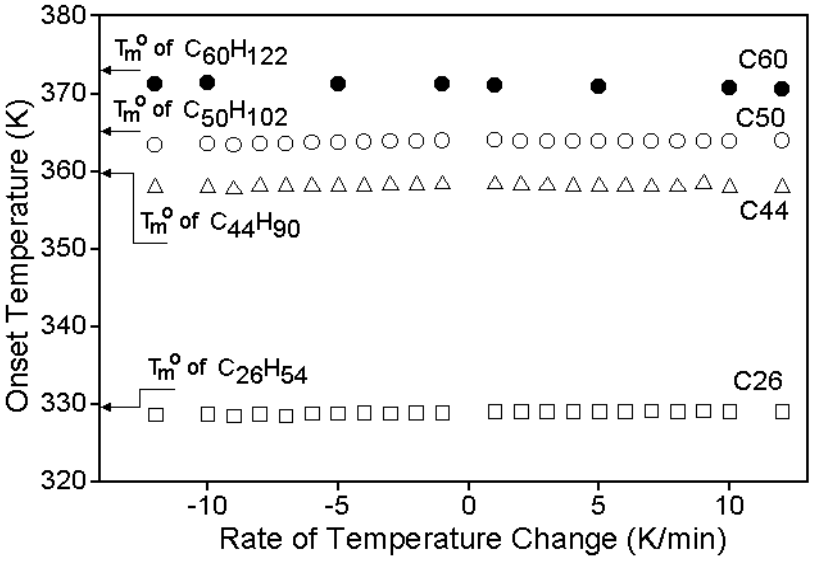

Figure 3.1. Onset temperatures of the phase transitions of *n*-paraffins as a function of the scanning rate, as measured by standard DSC. Melting and crystallization is marked by ●: C60, **F**: C50, Δ: C44, □: C26 (for C26 isotropization). Data from ref. [2] except for C60.

recent study of the heterogeneous and homogeneous nucleation of n-alkanes by Sirota *et al.* [3–5] such results were reported for n-paraffins with $21 \leq n \leq 37$ carbon atoms. The same authors reported an about 15 K supercooling before homogeneous nucleation of paraffins is possible. This is much smaller than the degree of supercooling of 50 K needed for homogeneous nucleation of polyethylene, which in turn is less than the supercooling of most other polymers analyzed [1].

Quite recently a longer n-paraffin sample became available, n-hexacontane, n-$C_{60}H_{122}$. This paraffin was used to extend the earlier analysis and to check on the phase diagram of a solution of n-$C_{60}H_{122}$ and n-$C_{50}H_{102}$.

3.1.1 Standard DSC of n-$C_{60}H_{122}$

The onset temperatures of crystallization and melting of n-hexacontane as a function of scanning rate when measured by standard differential scanning calorimetry (DSC) is added to Figure 3.1 (filled circles). The open symbols are the onset temperatures of the transition of the n-paraffins hexacosane, tetratetracontane, and pentacontane [2]. The onset temperatures of melting and crystallization of n-$C_{60}H_{122}$ are somewhat less than 372.9 K, the equilibrium melting temperature, T_m°, as calculated from the empirical equation of Broadhurst [88] which fits the experimental data from n-$C_{11}H_{24}$ to n-$C_{100}H_{202}$ with a root-mean-square deviation of ±0.41 K [7]:

$$T_m^\circ = \frac{414.6\ (x - 1.5)}{(x + 5.0)} \tag{3.1}$$

with x representing the number of carbon atoms in the n-paraffin.

There seems no supercooling for n-$C_{60}H_{122}$ melt crystallization and n-$C_{60}H_{122}$ behaves like all the other n-paraffins analyzed. More accurate data of the apparent reversing heat capacity were generated by quasi-isothermal TMDSC with a very small amplitude of 0.05 K and 60 s of period on heating and cooling sequences. The data are presented in Section 3.1.2.

3.1.2 TMDSC of n-$C_{60}H_{122}$

Figure 3.2 displays the results of the measurement of the apparent heat capacities by standard DSC on heating at 10 K min^{-1}, followed by quasi-isothermal TMDSC of melt-crystallized n-$C_{60}H_{122}$ after a cooling at a rate of 10 K min^{-1}, and a final sequence of quasi-isothermal TMDSC with successively lower temperatures starting from the melt. The

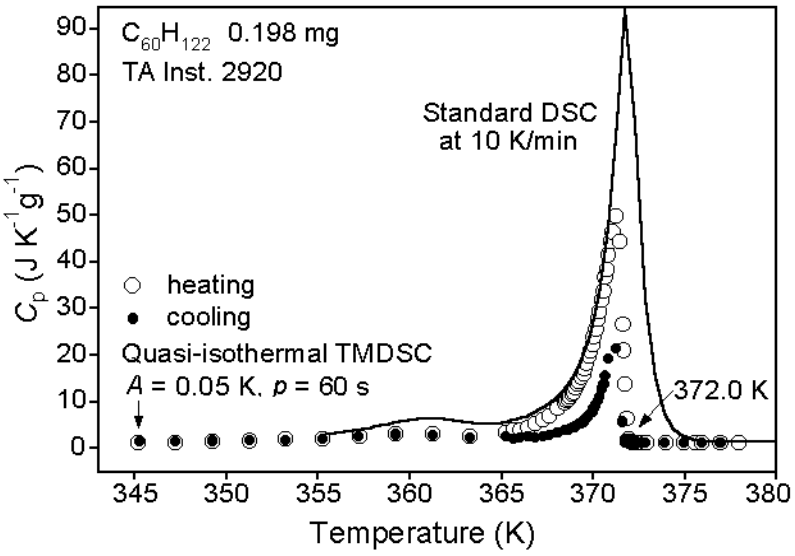

Figure 3.2. Heat capacity of n-$C_{60}H_{122}$ on heating by standard DSC and apparent reversing heat capacities on heating and cooling by quasi-isothermal TMDSC. Open circles and filled circles represent the first heating and subsequent cooling, respectively.

apparent total C_p by standard DSC, run prior to the quasi-isothermal measurements is indicated by the solid line. The open circles are the apparent, reversing heat capacities, obtained from the subsequent quasi-isothermal TMDSC at increasing temperatures. The quasi-isothermal measurements with decreasing temperatures depicted by the filled circles. The quasi-isothermal runs are started at the constant temperature, T_o and heated and cooled sinusoidally for 20 min within ±0.05 K temperature with a period of 60 s. Inside the transition region, the duration of the modulation was extended to 40 min to achieve steady state which is necessary to evaluate steady state heat capacity values.

The quasi-isothermal heating runs show that the end of melting is 372.0 K. The quasi-isothermal cooling run after the first heating proves that the beginning of crystallization occurs also at 372.0 K. There is, thus, also no supercooling of n-$C_{60}H_{122}$ in the quasi-isothermal TMDSC experiments with 0.05 K of amplitude as was also found for the other paraffins analyzed in ref. [2].

The apparent reversing heat capacity plot from the run at increasing temperature shows a sizeable contribution to the melting, but less for the run with decreasing temperature. The width of the region of melting of n-$C_{60}H_{122}$ is more than 5 K, and the maximum in the reversing C_p of heating run reaches about 60% of the C_p of the melting peak by standard DSC.

3.1.3 Eutectic study, 50:50 mixture of n-$C_{50}H_{102}$ and n-$C_{60}H_{122}$

An equalmolar mixture of the paraffins n-$C_{50}H_{102}$ and n-$C_{60}H_{122}$ was made by heating at 10 K min^{-1} followed by crystallization from the melt. In Figure 3.3, the apparent reversing

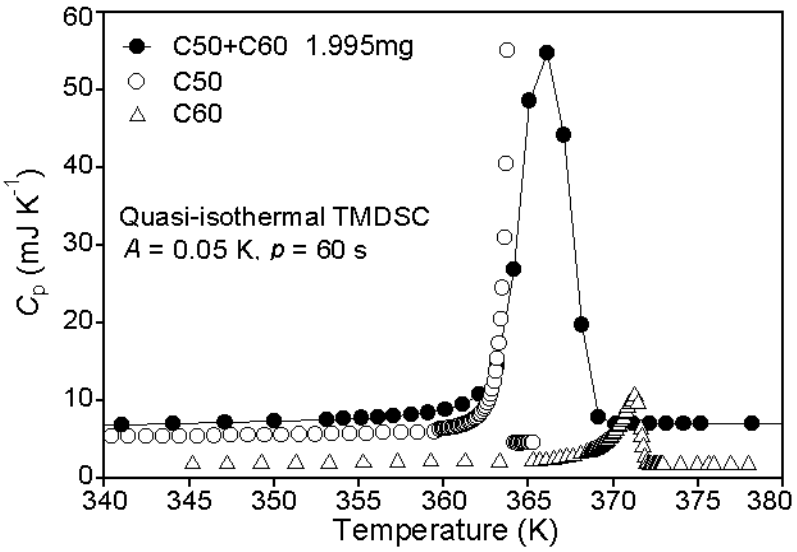

Figure 3.3. Apparent, reversing heat capacities of mixture of n-$C_{60}H_{122}$ and n-$C_{50}H_{102}$ compared with those of n-$C_{60}H_{122}$ and n-$C_{50}H_{102}$ on heating by quasi-isothermal TMDSC. Data for n-$C_{50}H_{102}$ was modified from [86].

heat capacities are plotted as a function of temperature. The open circles are n-$C_{50}H_{102}$ data from ref. [2] and the triangles are the n-$C_{60}H_{122}$ data recalculated from the identical experiments as for the open circles in Figure 3.2. As seen in Figure 3.3, the melting peak of the mixture shifts to higher temperature in comparison of the melting peak of pure n-$C_{50}H_{102}$ paraffin and it results in a peak temperature of 365 K. The detailed calculation of a phase diagram is given in the discussion section. The melting peak of the mixture is at a lower temperature than the melting peak of pure n-$C_{60}H_{122}$. Also, the width of melting of the mixture is about 12 K, wider than either melting peaks of n-$C_{50}H_{102}$ or n-$C_{60}H_{122}$.

3.2 Polyethylene-Extended Chain Crystals

As seen in section 3.1, n-paraffins up to n-$C_{60}H_{122}$ did not show any supercooling. Therefore, I decided to extend this research with n-paraffins with lengths that ultimately would exceed the length for chain folding. With such materials, the effects seen in multi-component systems could be avoided, simplifying the interpretation of the data. It is well known, that paraffins of different chain length, as well as polymer fractions below molar masses of about 20,000 Da can undergo eutectic phase separation on crystallization [7]. Sufficiently long paraffins to undergo chain folding were produced in the past in Great Britain with support of their Engineering and Physical Research Council (EPSRC). Our request for samples, known to be available, was denied because "universally and without exception" EPSRC imposed the condition that "no material must leave the country." Naturally, we are of the opinion that fundamental research will be impeded when national interests limit exchange of information. Fortunately, the commercially available sample PE560 is sufficiently similar in its crystal nucleation behavior to n-paraffins up to $C_{50}H_{102}$ studied earlier in my thesis [2], that major parts of the research did not have to be abandoned. The surprising finding that n-paraffins practically do not need primary, secondary, or molecular nucleation up to considerable lengths in typical experimental environments carries over into oligomer fractions generated out of polymers (PE560, PE1150, and PE2150) as main samples described in this thesis.

3.2.1 Melting temperatures as a function of scanning rates

To observe the difference between linear macromolecules and paraffins, the low-molecular mass polyethylene (PE560) with a molar mass close to the paraffin C40 was investigated first in the same manner prior to the further study with longer polyethylene oligomers.

Figure 3.4 contains a plot of the peak temperatures of crystallization and melting of the oligomers of this research as a function of the scanning rate when measured by standard differential scanning calorimetry (DSC). The squares in Figure 3.4 are the peak temperatures of the transition of PE560. The peak temperatures of melting of PE560 are somewhat less than 354.5 K, the equilibrium melting temperature, T_m°, of n-$C_{40}H_{82}$, as calculated from the empirical equation (3.1). The number-average molar mass of PE560 corresponds to n-$C_{37}H_{76}$

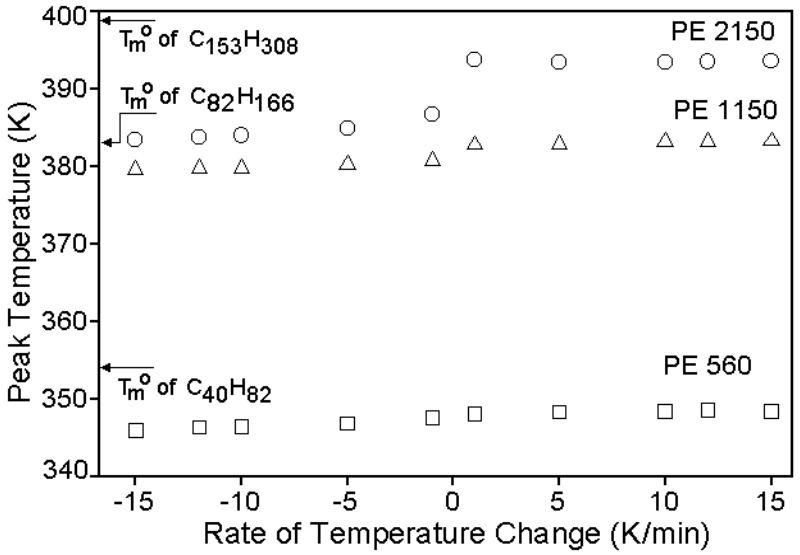

Figure 3.4. Temperatures of crystallization and melting peaks of polyethylene oligomers as a function of scanning rates when measured by standard DSC at 10 K min^{-1}. **F**: PE 2150, Δ: PE 1150, □: PE 560.

which has according to eq (3.1) a T_m° of 350.2 K. Between the data taken on heating and cooling there is at best a small indication of supercooling which is further investigated below by using quasi-isothermal TMDSC. Because of the molar mass distribution in PE560, one might assume that the smallest crystals melt first, but the largest molecules crystallize first, complicating the quantitative interpretation of the melting peaks that lead to Figure 3.4. The very small indication of supercooling is in need of further research and analyzed with TMDSC in Section 3.2.2.

The melting and crystallization temperatures of the longer polyethylene oligomers, PE1150 (≈C82) and PE2150 (≈C153) are also shown in Figure 3.4 with triangles and circles, respectively. In contrast to the paraffins and PE560, there is a significant amount of supercooling in the PE1150 and PE2150. The PE1150 and PE2150 are expected to have equilibrium melting temperatures of 383.0 K and 397.2 K, close to the observed values. From this observation, it is obvious that these two oligomers have the extended chain crystal morphologies. Of importance for the further discussion is that both, PE1150 and PE2150 show similar supercoolings of about 10 K on crystallization, compared to almost none seen for the n-paraffins and PE560.

3.2.2 TMDSC of PE560

Figure 3.5 displays the results of measurements by standard DSC and quasi-isothermal TMDSC of melt-crystallized PE560. The apparent total C_p by standard DSC, run prior to the quasi-isothermal measurements, is measured with a heating rate of 10 K min^{-1} and is indicated by the solid line. In this figure, and all subsequent ones, the mole in the

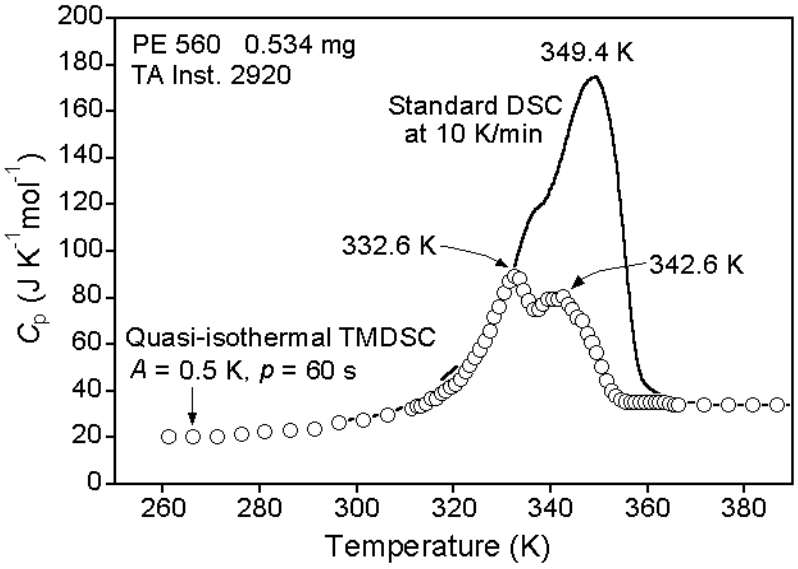

Figure 3.5. Apparent heat capacities measured by standard DSC and quasi-isothermal TMDSC for PE560 crystallized first from the melt on cooling at 10 K min^{-1}. The solid line is obtained by standard DSC at 10 K min^{-1} and the open circles represent the apparent, reversing heat capacity by quasi-isothermal measurements.

dimension of the heat capacity refers to one CH_2-group, i.e., it is 14.03 Da. The open circles are the apparent, reversing heat capacities, obtained from the subsequent quasi-isothermal TMDSC at increasing temperatures. A quasi-isothermal modulation TMDSC run is carried out at one temperature (mid-temperature of sinusoidal temperature cycle). Samples are raised to the chosen constant temperature, T_o and are heated and cooled for 20 min within ±0.5 K temperature range by the sinusoidal modulation program of a 60 s period. Outside the melting transition region, 20 min was enough to reach steady state, but inside the transition region, it was not enough so the duration of the modulation was sometimes extended up to 600 min to achieve steady state which is necessary to evaluate the accurate reversible, apparent heat capacities. Only when necessary, was the duration of the

modulation extended. The apparent, reversing heat capacities are obtained from 20 min modulation series. The measurement series, for example, are accomplished from 261 K to 388 K for PE560 in steps of 1.0 K (inside the transition region) to 5.0 K (outside the transition region). The crystallinity was determined by standard DSC using the heat of fusion at the average temperature of measurement [7]. It was 70% after cooling at 10 K min^{-1}, and improved to 82% after the long-time, quasi-isothermal runs on cooling in steps to different values of T_o which permit the increased annealing. The two peaks in the melting curve of Figure 3.5 are not clearly separated in the standard DSC run, but are revealed more clearly in the TMDSC runs. The melting temperature of 354.5 K for n-$C_{40}H_{82}$ with a similar molar mass to PE560, approximates the higher temperature peak. The first peak is most likely due to the eutectic separation of the different mass crystals and may also contain some of the enthalpies of transition to a high-temperature mesophase, observed in paraffins with a lower mass than n-$C_{40}H_{82}$. The apparent reversing heat capacity plot shows a sizeable contribution to the melting, but not as much as is seen for the pure n-$C_{50}H_{102}$ which crystallizes reversibly to almost 100%. When measured by quasi-isothermal TMDSC with an amplitude of as little as 0.05 K, 66% of the total crystals of n-$C_{50}H_{102}$ melt within 0.1 K or less, and all fusion is complete within 1.0 K [86], *i.e.*, with the present, larger modulation amplitude of 0.5 K, the melting would have been practically fully reversing. The width of the region of melting of PE560 is more than 30 K, and the maximum in the reversing C_p reaches only half the C_p of the melting peak by standard DSC. The broadening of the melting of PE560 in the quasi-isothermal measurements is, thus, most likely due to the chain-length distribution. The additional shift to higher temperature in the standard DSC experiment for the high-

temperature potion of the melting peak and the end of melting is due to the thermal lag of the calorimeter when heated at 10 K min^{-1} through the melting region [89].

Figure 3.6 contains three eutectic diagrams of PE560 with several paraffins, n-$C_{26}H_{54}$,n-$C_{37}H_{76}$ and n-$C_{50}H_{102}$. As depicted in the figure, the eutectic points are calculated to be 329.4 K, 347.6 K and 353.6 K, respectively. The arrows in the left Y-axis point to the equilibrium melting temperatures for each paraffin and the arrow in the right Y-axis for PE560. The detail of the eutectic diagram is given in discussion section.

In Figure 3.7, the experiment of Figure 3.5 is continued by quasi-isothermal measurements with decreasing temperatures starting from the melt. The apparent reversing heat capacities are plotted as a function of temperature, as before. The quasi-isothermal heating runs show that the end of melting is at 355 K. The quasi-isothermal cooling run after

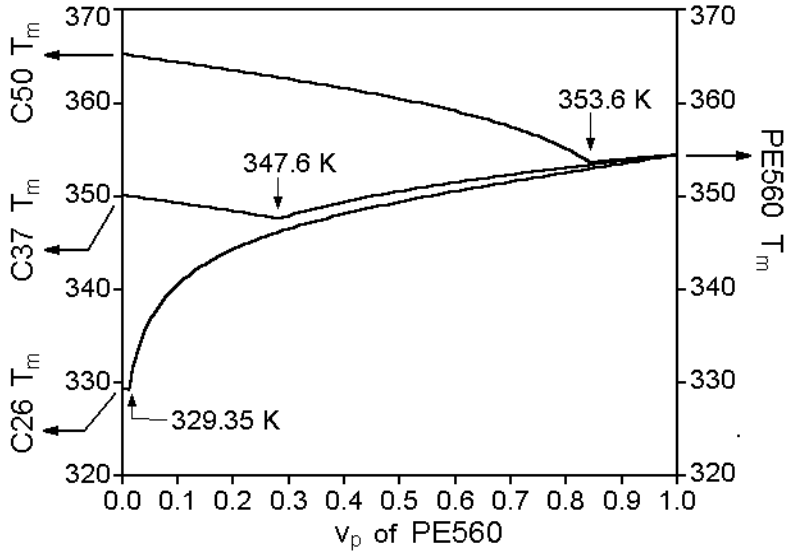

Figure 3.6. Eutectic phase diagrams computed for mixtures of PE560/C50, PE560/C37 and PE560/C26. (Note that PE560 has an average chain length of 40 chain atoms.)

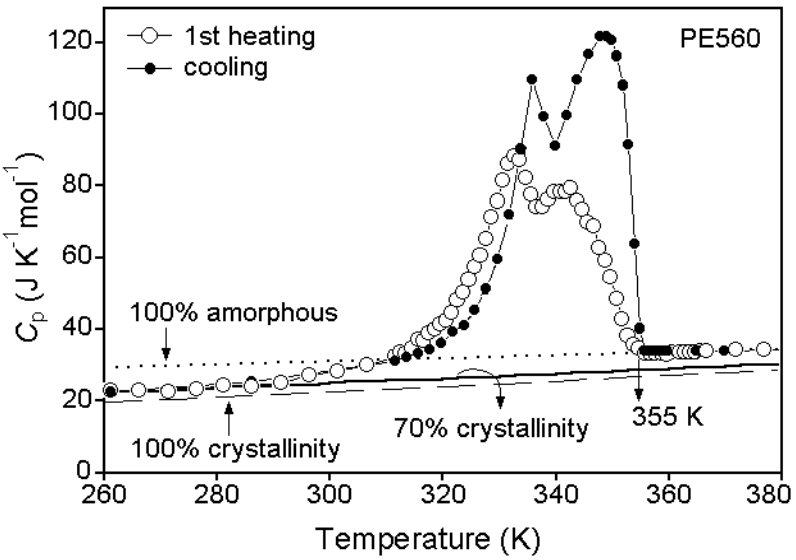

Figure 3.7. Apparent, reversing heat capacities of PE560 on heating and cooling by quasi-isothermal TMDSC. Open circles and filled circles represent the first heating and subsequent cooling, respectively.

the first heating proves that the beginning of crystallization occurs also at 355 K. There is no supercooling of PE560 in the quasi-isothermal TMDSC experiments with 0.5 K of amplitude.

In Figure 3.8, the experiment of Figure 3.7 is continued by quasi-isothermal measurements with increasing temperatures starting from 260 K, followed by a subsequent second cooling run. The apparent reversing heat capacities from the second heating runs are added to Figure 3.7. A second cooling run is not depicted in Figure 3.8, but it was identical to the first and proves that the beginning of crystallization occurs also at 355 K. The quasi-isothermal second heating runs show that the end of melting is at 355 K, therefore, it is obvious that there is no supercooling of PE560 in the quasi-isothermal TMDSC experiments with 0.5 K of amplitude. The shifts of the peak positions between first and second heating

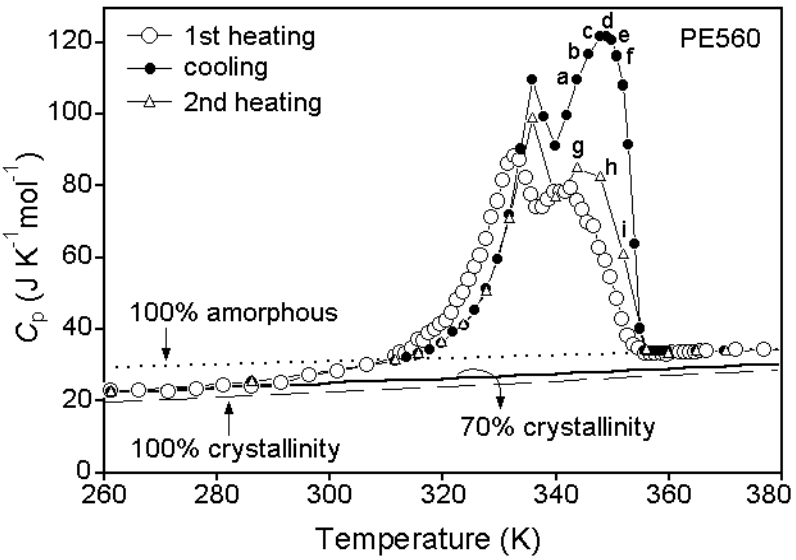

Figure 3.8. Apparent, reversing heat capacities of PE560 on heating and cooling by quasi-isothermal TMDSC. Open circles, filled circles, and triangles represent the first heating, subsequent cooling, and the second heating, respectively.

runs can be explained by changes in the co-crystallization of different chain lengths and perfection in the crystal morphology, as is also indicated by the increase in the overall crystallinity mentioned above.

The higher apparent reversing heat capacities in the regions of the points marked a–f in the cooling sequence relative to g–i in the heating sequence are analyzed in the more detailed graphs in discussion section.

3.2.3 TMDSC of PE1150

Figure 3.9 represents the results for PE1150. The thick, continuous solid line is the apparent total C_p from the standard DSC at 10 K min^{-1}, carried out prior to the quasi-isothermal TMDSC measurements. The open circles are the apparent reversing C_p obtained

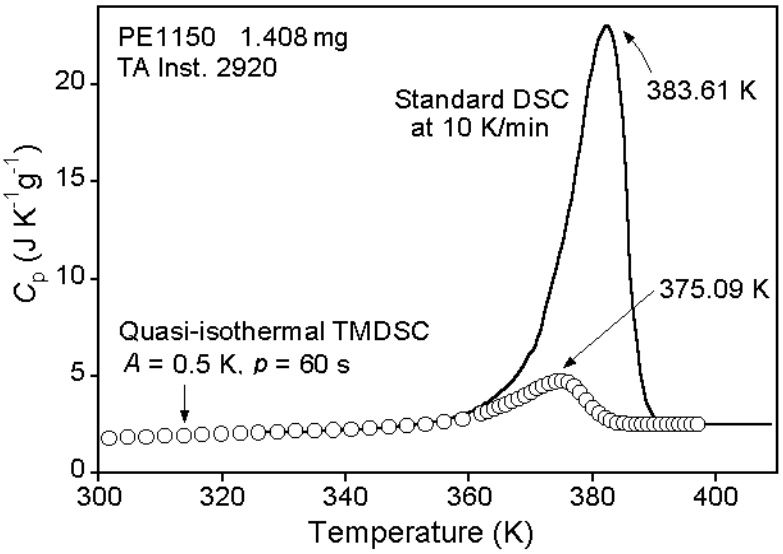

Figure 3.9. Apparent heat capacities of PE1150 crystallized first from the melt on cooling at 10 K min^{-1}. The solid line is obtained by standard DSC at 10 K min^{-1} and the open circles represent the apparent, reversing heat capacity by quasi-isothermal TMDSC.

from the first quasi-isothermal heating TMDSC runs. The peak temperature of 383.61 K of the standard DSC run is close to the equilibrium melting temperature of n-$C_{82}H_{166}$ (383.0 K). The crystallinity is 82.9%, calculated from the heat of fusion obtained from the standard DSC run, and the melting range is, again, about 30 K wide.

Figure 3.10 displays only the reversing heat capacity plots of PE1150 as a function of temperature, enlarging the ordinate. The dotted line indicates the heat capacity of a 100% amorphous, liquid sample, as given in the ATHAS data bank.[26] The solid line is computed for an 83% crystalline sample. The end of melting on first heating is at 386.2 K, and the onset of crystallization on first cooling is 382.1 K. The difference of about 4.1 K represents the supercooling of PE1150.

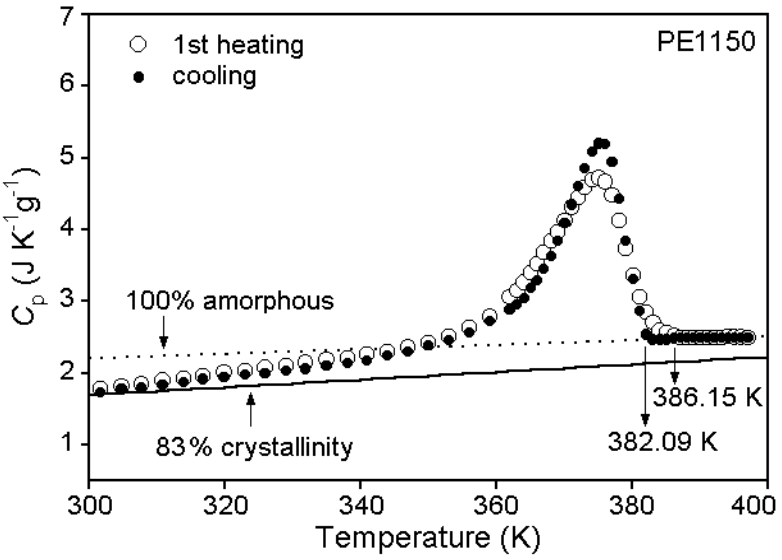

Figure 3.10. Apparent, reversing heat capacities of PE1150 on heating and cooling by quasi-isothermal TMDSC. Open circles and filled circles represent the first heating and subsequent cooling, respectively.

In Figure 3.11, the experiment of Figure 3.10 is continued by quasi-isothermal measurements with increasing temperatures starting from 301 K, followed by a subsequent second cooling run. The apparent reversing heat capacities from the second heating runs are added to Figure 3.10. A second cooling run is not depicted in Figure 3.11, but it was identical to the first. The second heating runs exhibit that the end of melting is also at 386.2 K. The apparent reversing plots of C_p on cooling and on second heating are matched from low temperature to around 354 K. After 354 K, the C_p on second heating starts to deviate and the maximum becomes higher than on first heating and on cooling. The apparent reversing C_p on first heating is somewhat higher in the low temperature region, but the maximum is lower than for the other runs. The magnitude of the apparent reversing C_p in

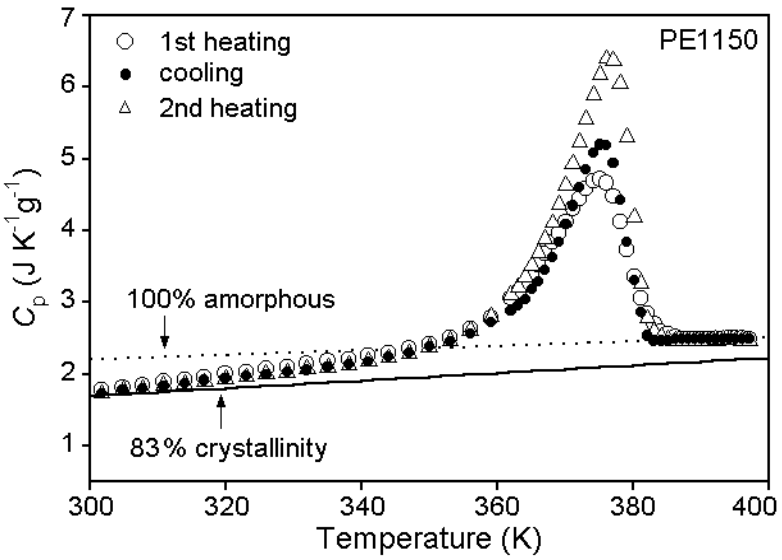

Figure 3.11. Apparent, reversing heat capacities of PE1150 on heating and cooling by quasi-isothermal TMDSC. Open circles, filled circles, and triangles represent the first heating, subsequent cooling, and the second heating, respectively.

the melting is smaller than for PE560, but is similar to that found for other polymers [32–35], but still larger than that for most polymers. At low temperature, the expected heat capacity without latent heat contributions is reached only below 301 K.

3.2.4 TMDSC of PE2150

Figure 3.12 represents the results for PE2150. Again, the thick, continuous solid line is the apparent total C_p from the standard DSC at 10 K min^{-1}, carried out prior to the quasi-isothermal TMDSC measurements. The open circles are the apparent reversing C_p obtained from the first quasi-isothermal heating TMDSC runs. The peak temperature of the standard DSC run is close to the equilibrium melting temperature of n-$C_{153}H_{308}$ (397.2 K). The crystallinity is 89%, calculated from the heat of fusion obtained from the standard DSC run,

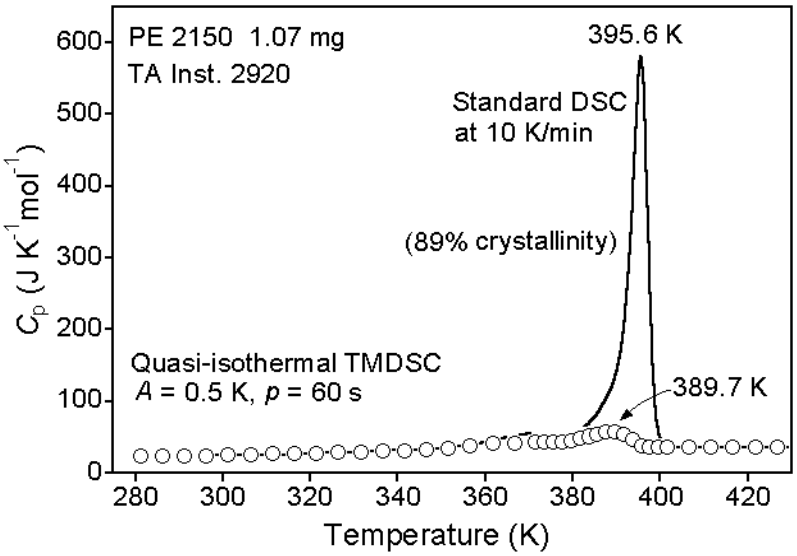

Figure 3.12. Apparent heat capacities measured by standard DSC and quasi-isothermal TMDSC for PE2150 crystallized first from the melt on cooling at 10 K min^{-1}. The solid line is obtained by standard DSC at 10 K min^{-1} and the open circles represent the apparent, reversing heat capacity by quasi-isothermal measurements.

and the melting range is, again, about 30–40 K wide, although the main melting peak is much narrower and steeper than seen in PE560. The apparent reversing heat capacity plot shows only a very small contribution to melting. The shallow peak at about 370 K in the standard DSC trace is also largely irreversible, *i.e.*, it is very much reduced in the quasi-isothermal TMDSC runs. Enlarging the ordinate, as shown in Figure 3.13, reveals that the remaining 370 K-peak on first heating disappears fully on cooling, and does not reappear on second heating, due to the better crystallization on cooling under TMDSC conditions.

Figure 3.13 displays the apparent, reversing heat capacity plots of PE2150 as a function of temperature as described in Figure 3.7 for PE560. The dashed line is the C_p for 100% crystalline PE without latent heat contributions, and the dotted line is for a 100%

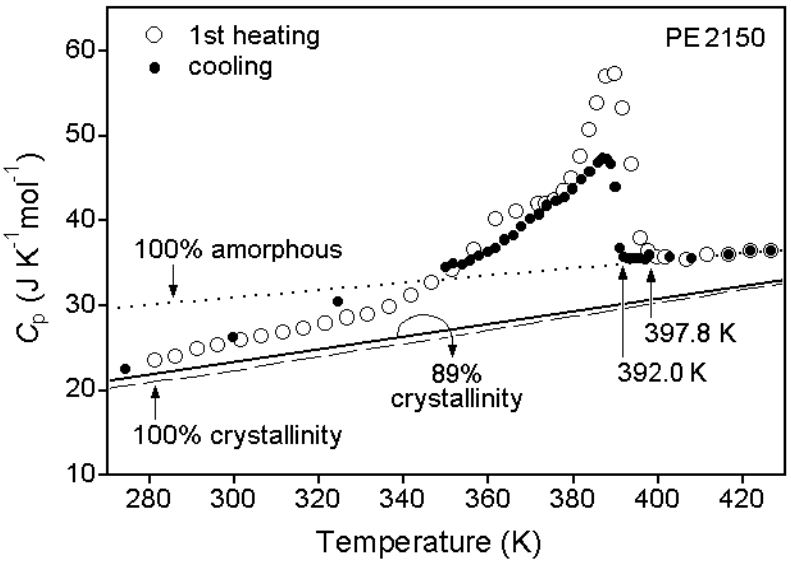

Figure 3.13. Apparent, reversing heat capacities of PE2150 on heating and cooling by quasi-isothermal TMDSC. Open circles and filled circles represent the first heating and subsequent cooling, respectively.

amorphous sample, as given in the *ATHAS* data bank [90]. The solid line is computed for an 89% crystalline sample, as measured by standard DSC. The end of melting on heating is at 397.8 K, and the onset of crystallization on cooling is 392.0 K. The difference of about 5.8 K represents the supercooling of PE2150.

In Figure 3.14, the experiment of Figure 3.13 is continued by quasi-isothermal measurements with increasing temperatures starting from 281 K, followed by a subsequent second cooling run. The apparent reversing heat capacities from the second heating runs are added to Figure 3.13. A second cooling run is not depicted in Figure 3.14, but it was identical to the first and ascertains that the beginning of crystallization occurs also at 392.0 K. The second heating runs exhibit that the end of melting is at 397.9 K, little bit higher than the first heating runs. However, it is not significant. The difference of about 5.8 K

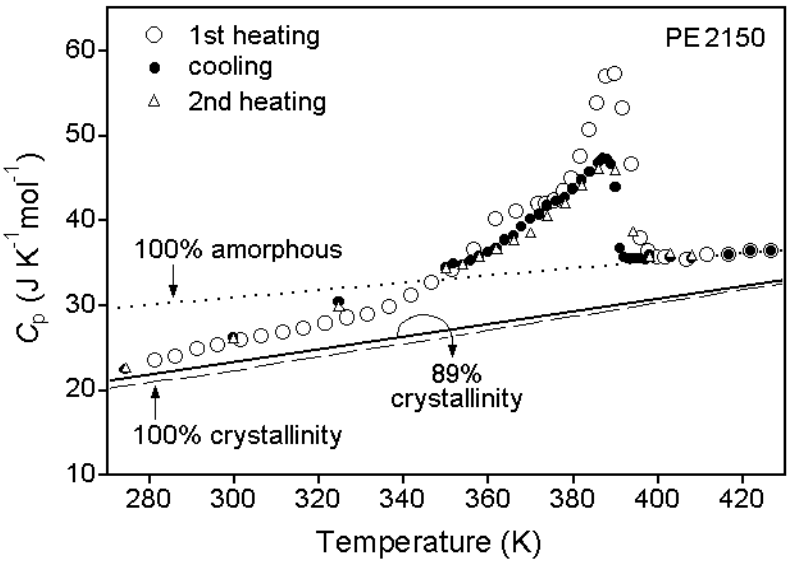

Figure 3.14. Apparent, reversing heat capacities of PE2150 on heating and cooling by quasi-isothermal TMDSC. Open circles, filled circles, and triangles represent the first heating, subsequent cooling, and the second heating, respectively.

represents the supercooling of PE2150. The apparent reversing plots of C_p on cooling and on second heating are matched from low temperature to the temperature of the maximum. The maximum on first heating is higher than on second heating and on cooling. The initial crystals melt during the first heating sequence and then crystallize into better crystals on subsequent cooling, due to the slower quasi-isothermal heating and cooling experiments. The better crystals melt on subsequent second heating with a retracing of the reversing C_p of the prior cooling experiment. The magnitude of the small amount of apparent reversing C_p in the melting range is similar to that found for other polymers [32–35]. At low temperature, the expected heat capacity without latent heat contributions is reached only at about 280 K, *i.e.*, a small amount of reversing melting and crystallization exists even below room temperature. This increase in heat capacity below room temperature is known from standard

calorimetry for almost 40 years [91]. It increases substantially with decreasing crystal perfection, as was studied recently by an extensive analysis of poly(ethylene-co-octene-1) [27, 28]. More details about the crystallization and melting are displayed in the time domain in the discussion section.

PE1150 and PE2150 behave similarly and are examples of extended-chain crystals which crystallize with supercooling.

3.3 Polyethylene-Folded Chain Crystal

3.3.1 Melting temperatures as a function of scanning rates

The true polyethylene PE15520 (≈C1106) is analyzed next. Figure 3.4 is plotted again now with the additional data for PE15520 as filled circles in Figure 3.15. In contrast to PE560 and similar to PE1150 and PE2150 there is a significant supercooling in PE15520, as indicated by the mark]. The PE1150 and PE2150 melt not far from the expected equilibrium melting temperatures extrapolated from eq (3.1) in Section 3.2.1 as marked in Figures 3.4 and 3.15. However, the melting temperature of PE15520 is about 30 K lower than that expected for an equilibrium crystal of polyethylene of this molar mass with an extended chain macroconformation (411.9 K), and even approximately13 K lower than that for PE2150, in spite of the fact that PE15520 is 7 times longer than PE2150. It is obvious that chain folding, which has been observed for chain lengths above 37 nm [46, 47], is the main reason for the large difference between the expected and measured melting temperature of PE15520 [7]. Furthermore, one might expect a difference between extended chains and folded chains for the molecular nucleation process, but there seems to be no difference. Of

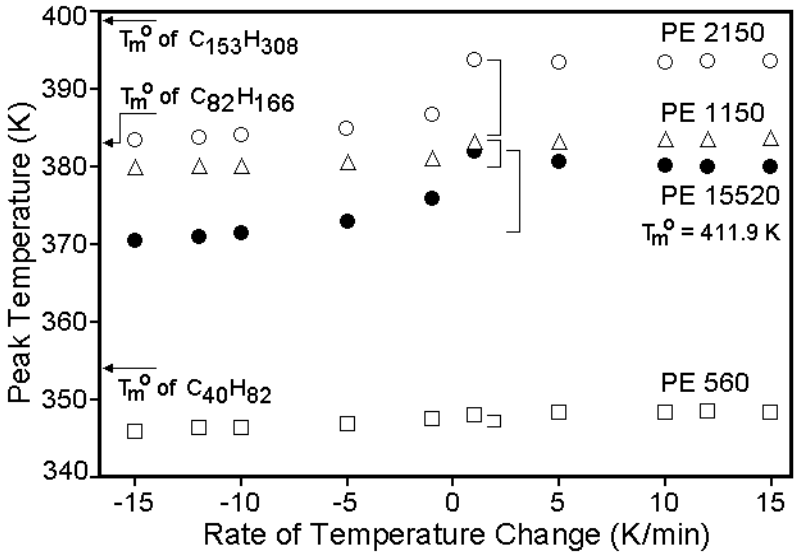

Figure 3.15. Temperatures of crystallization and melting peaks of polyethylene and its oligomers as a function of scanning rates when measured by standard DSC at 10 K min^{-1}. **M**: PE 15520, **F**: PE 2150, Δ: PE 1150, □: PE 560. (Compare to Figure 3.4)

importance for the further discussion is, thus, that both, the chain-folded PE15520 and the extended-chain PE2150 show similar supercoolings of almost 10 K as depicted in Figure 3.15.

3.3.2 TMDSC of PE15520

Figure 3.16 represents the results for PE15520. Again, the thick, continuous solid line is the apparent total C_p by standard DSC at 10 K min^{-1}, carried out prior to the quasi-isothermal TMDSC measurements. The open circles are the apparent reversing C_p, obtained from the quasi-isothermal heating TMDSC. The crystallinity determined from the heat of fusion measured by standard DSC is 55%. On the standard DSC trace, there are two peaks which are close to each other. Probably, the second peak results from better crystals

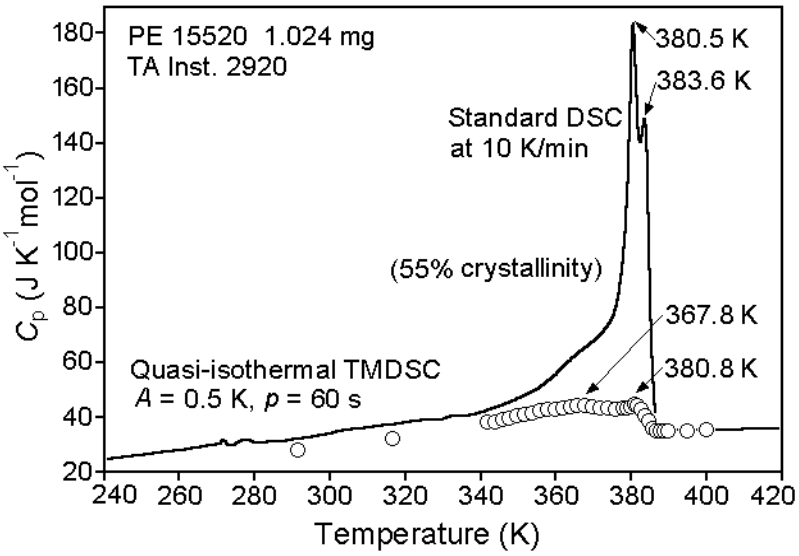

Figure 3.16. Apparent heat capacities measured by standard DSC and quasi-isothermal TMDSC for PE15520 crystallized first from the melt on cooling at 10 K min^{-1}. The solid line is obtained by standard DSC at 10 K min^{-1} and the open circles represent the apparent, reversing heat capacity by quasi-isothermal measurements.

produced by annealing during heating [7]. In the apparent, reversing C_p trace, the two peaks merge to one very small peak at 380.8 K. There is also a very broad, shallow maximum at 367.8 K which seems to correspond to the shoulder at 370 K in the standard DSC trace. Overall, the quasi-isothermal, apparent reversing heat capacity covers only a small part of the total melting peak, but extends to low temperature. Melting and crystallization is thus largely irreversible with an extended low-temperature, reversing contribution.

Figure 3.17 shows again an enlarged representation of the reversing melting with additional cooling TMDSC traces. The double-peak by standard DSC in Figure 3.16 at about 380 K reduces to a single peak on first heating by TMDSC, and is barely visible on cooling.

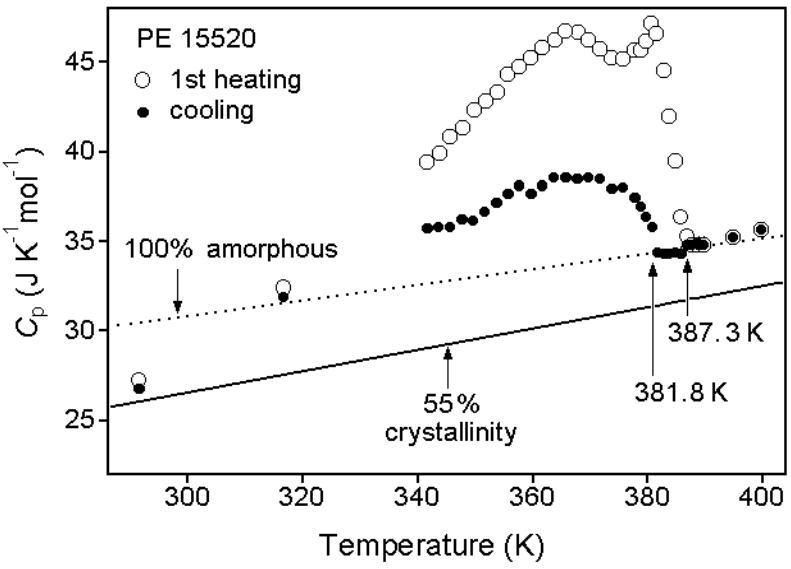

Figure 3.17. Apparent, reversing heat capacities of PE15520 on heating and cooling by quasi-isothermal TMDSC. Open circles and filled circles represent the first heating and subsequent cooling, respectively.

The end of melting on first is at 387.3 K, and the onset of crystallization on first cooling is at 381.8 K. The difference of about 5.5 K is the supercooling of PE15520.

In Figure 3.18, the experiment of Figure 3.17 is continued by quasi-isothermal measurements with increasing temperatures starting from 291 K (second heating run), followed by a subsequent second cooling run. The apparent reversing heat capacities from the second heating runs are added to Figure 3.17. The double-peak by standard DSC at about 380 K in Figure 3.16 is also barely visible on second heating after disappearance on first cooling. A second cooling run is identical to the first, and not plotted in Figure 3.18. The first peak in Figure 3.18 on TMDSC is at the position of the weak shoulder at 367.8 K. The end of melting on second heating is at 386.8 K, 0.5 K lower than the first heating and the onset of crystallization on second cooling is at 381.8 K, too. The difference is still about 5 K

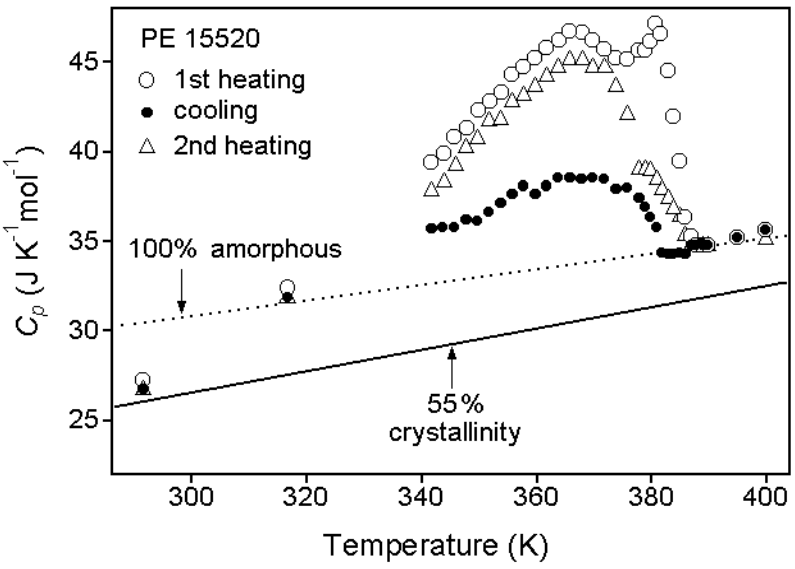

Figure 3.18. Apparent, reversing heat capacities of PE15520 on heating and cooling by quasi-isothermal TMDSC. Open circles, filled circles, and triangles represent the first heating, subsequent cooling, and the second heating, respectively.

and it is the supercooling of PE15520. The dotted line represents the heat capacity of a 100% liquid amorphous sample, as given in the *ATHAS* data bank [90], and the solid line is for the expected heat capacity for a sample of 55% crystallinity, as it was determined by standard DSC, measured after all quasi-isothermal TMDSC runs were completed.

The reversing C_p measured on first heating has higher values than on second heating over the entire temperature range. On cooling the reversing heat capacity is much lower. For the first effect, it is assumed that the initially poorer crystals melt during the first heating sequence and then recrystallize to higher perfection on subsequent cooling, due to the slower cooling in the TMDSC experiments. These better crystals anneal less on subsequent heating, eliminating the peak at 380 K, but show, otherwise, a similar apparent reversing heat capacity as the first heating. Of further interest is the much higher C_p on heating than on

cooling, in contrast to PE2150, which retraced the reversing C_p of the prior cooling experiment on second heating (see Figure 3.14) and to PE560 where the TMDSC on cooling showed the larger reversing C_p (see Figure 3.8). Integrating the reversing heat capacity over the whole melting range leads to less than 10% reversing crystallinity for the cooling runs.

PE15520 as an example of the folded-chain crystal with supercooling is described in more detail about the crystallization and melting in the time domain in the discussion section.

3.4 Poly(oxyethylene)-Extended Chain Crystal

To increase the examples of linear macromolecules with extended-chain crystals, low molecular mass poly(oxyethylene)s with lengths close to those of polyethylene fractions investigated in the previous section 3.2 were studied.

3.4.1 Melting temperatures as a function of scanning rates

Figure 3.19 contains a plot of the peak temperatures of crystallization and melting of the poly(oxyethylene)s as a function of the scanning rate when measured by standard differential scanning calorimetry (DSC). The squares in Figure 3.19 are the peak temperatures of the transition of PE1500. The peak temperatures of melting of POE1500 are somewhat less than 322.3 K, the equilibrium melting temperature, T_m° as calculated from the experimental equilibrium melting temperature equation which fits the experimental data from 42 fractions of different molecular weights of extended chain crystals or close to

extended chain crystals as collected by Buckley and Kovacs with a root-mean-square deviation of ±1.43 K [92]:

$$T_m^\circ = 340.8 - \frac{1890}{x} \tag{3.2}$$

with x representing the number of backbone atoms (3 times the number of repeating units).

The melting and crystallization temperatures of the longer poly(oxyethylene) oligomers, POE1960 ($x \approx 133$) and POE3060 ($x \approx 208$) are also shown in Figure 3.19 with triangles and circles, respectively. The POE1960 and POE3060 are expected to have equilibrium melting temperatures of 326.6 K and 331.7 K, close to the observed values. From this observation, it is obvious that these three poly(oxyethylene) oligomers have the extended chain crystal morphologies.

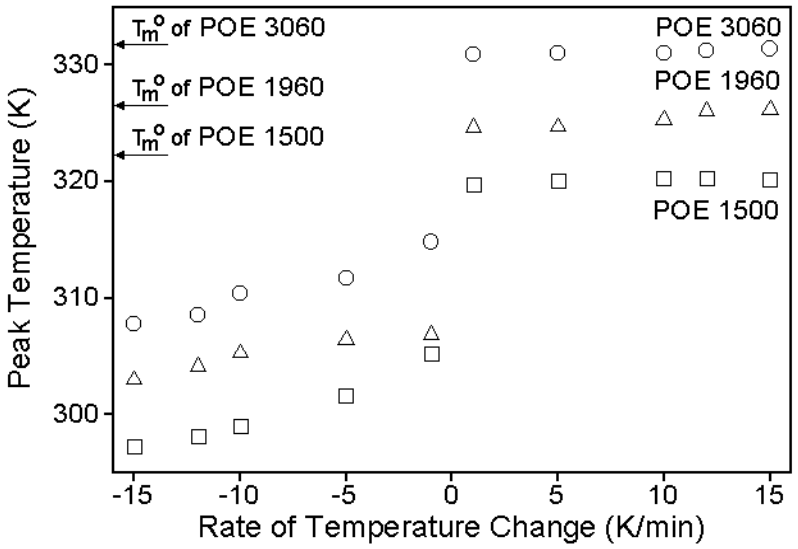

Figure 3.19. Temperatures of crystallization and melting peaks of poly(oxyethylene) oligomers as a function of scanning rates when measured by standard DSC at 10 K min^{-1}. **F**: POE 3060, Δ: POE 1960, and □: POE 1500.

3.4.2 Standard DSC of POE1500

Selected from several standard DSC runs, the raw data of heat-flow rate on heating and cooling of 10 K min^{-1} are depicted in Figure 3.20 as a function of sample temperature. In each heat-flow rate curves the upward direction is the exothermic direction, in contrast to heat capacity plots. There exist two peaks on cooling and only one peak on heating. A more careful look at the peak on heating shows that it seems to consist of two peaks that merged into one. All measurements at the different scanning rates from 1 K min^{-1} to 15 K min^{-1} show the same results with two separated peaks on cooling and a merged single peak on heating. Based on the fact that the equilibrium temperature of POE1500 is 322.3 K and POE1500 is too short to form folded-chain crystals, it is clear the high-temperature peak is

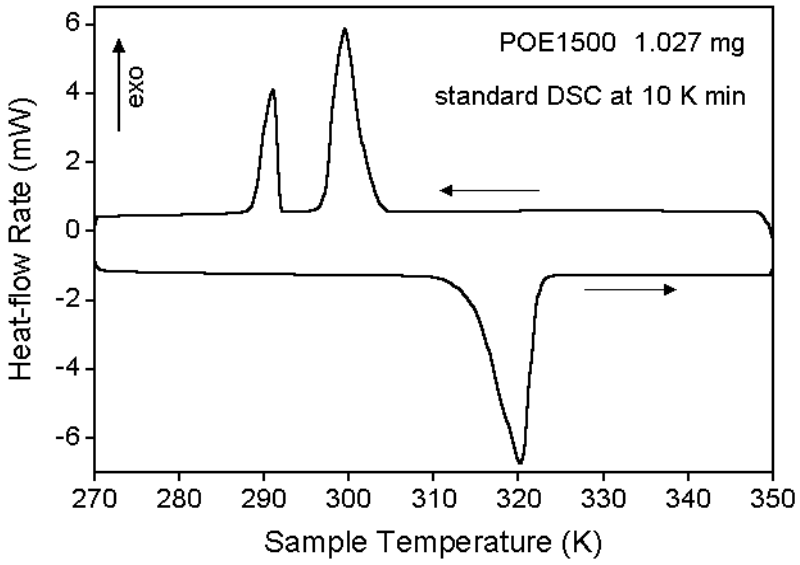

Figure 3.20. *HF*(*t*) of POE1500 *versus* sample temperature. The upward direction *HF*(*t*) is exothermic. Heating and cooling rates are 10 K min^{-1}.

the main melting peak which is main interest in this thesis. Therefore, the peak temperature of high-temperature peak was chosen to generate the Figure 3.19.

3.4.3 TMDSC of POE1500

Figure 3.21 displays the apparent, reversing heat capacity plots of POE1500 as a function of temperature, originally measured by Dr. Kazuhiko Ishikiriyama in our laboratory several years ago. The open circles are the apparent reversing C_p obtained from the first quasi-isothermal heating TMDSC runs, the triangles from the cooling runs and the squares from the second heating runs. The dotted line is for a 100% amorphous sample, as given in the *ATHAS* data bank [90]. The solid line is computed for an 93.8% crystalline sample, as

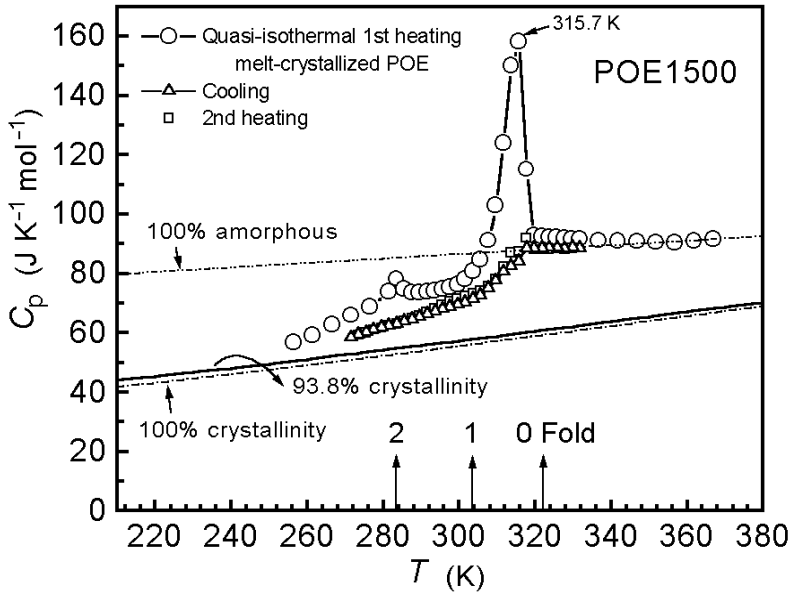

Figure 3.21. Apparent, reversing heat capacities of POE1500 on heating and cooling by quasi-isothermal TMDSC. Open circles, triangles and squares represent the first heating, subsequent cooling, and the second heating, respectively. Copied from [32].

measured by standard DSC prior to quasi-isothermal TMDSC. In this figure the mole in the dimension of the heat capacity refers to one OCH_2CH_2-group, i.e., with a mass of 44.06 Da. The end of melting on heating is at 318.7 K, and the beginning of crystallization on cooling is at 316.7 K. The difference of about 2 K represents the supercooling of POE1500. In contrast to previous paraffin and PE samples, the apparent reversing heat capacity plot on cooling shows that there is no contribution to crystallization, the amount of contribution to the melting on first heating is much smaller than paraffin and PE samples, and there is a barely visible peak on second heating.

As shown in Figure 3.20 in section 3.4.2, there were two peaks which were not fully separated on heating but clearly separated on cooling. In Figure 3.21, only on quasi-isothermal first heating runs, the low-temperature peak is visible at about 282 K separately. However, there is no peak on quasi-isothermal cooling runs and second heating, in contrast to the results from standard DSC measurement.

3.4.4 TMDSC of POE1960

Figure 3.22 represents the results for POE1960. The thick, continuous solid line is the apparent total C_p from the standard DSC at 10 K min^{-1}, carried out prior to the quasi-isothermal TMDSC measurements. The open circles are the apparent reversing C_p obtained from the first quasi-isothermal heating TMDSC runs. The peak temperature of the standard DSC run is identical to the equilibrium melting temperature (326.6 K). The crystallinity is 61.7%, calculated from the heat of fusion obtained from the standard DSC run, and the melting range is, again, about 13 K wide, much narrower and steeper than seen in PE

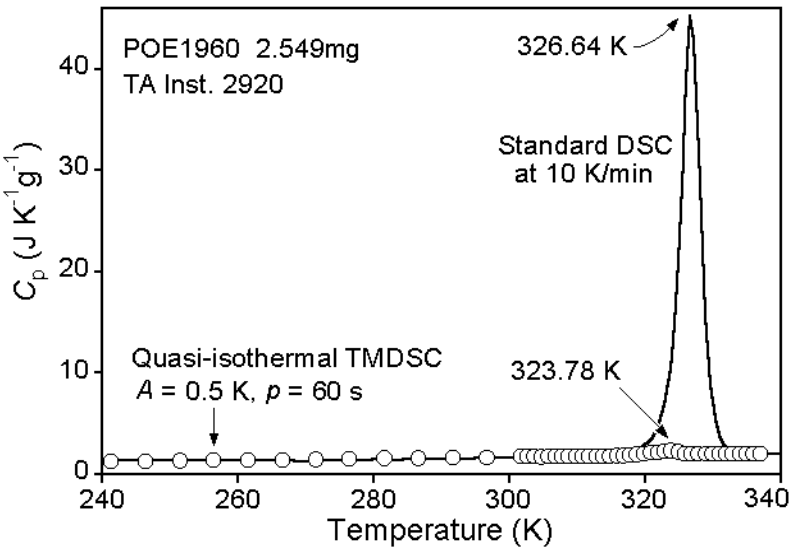

Figure 3.22. Apparent heat capacities measured by standard DSC and quasi-isothermal TMDSC for POE1960 crystallized first from the melt on cooling at 10 K min^{-1}. The solid line is obtained by standard DSC at 10 K min^{-1} and the open circles represent the apparent, reversing heat capacity by quasi-isothermal measurements.

samples in sections 3.2 and 3.3. The apparent reversing heat capacity plot shows only a very small (almost negligible) contribution to melting.

Figure 3.23 displays the enlarged apparent, reversing heat capacity plots of POE1960 as a function of temperature. The dotted line is for the heat capacity of a 100% liquid amorphous sample, as given in the *ATHAS* data bank [90]. The solid line is computed for an 62% crystalline sample, as measured by standard DSC. The end of melting on heating is at 324.9 K, and the beginning of crystallization on cooling is at 319.6 K. The difference of about 5.3 K represents the supercooling of POE1960. In contrast to previous paraffin and

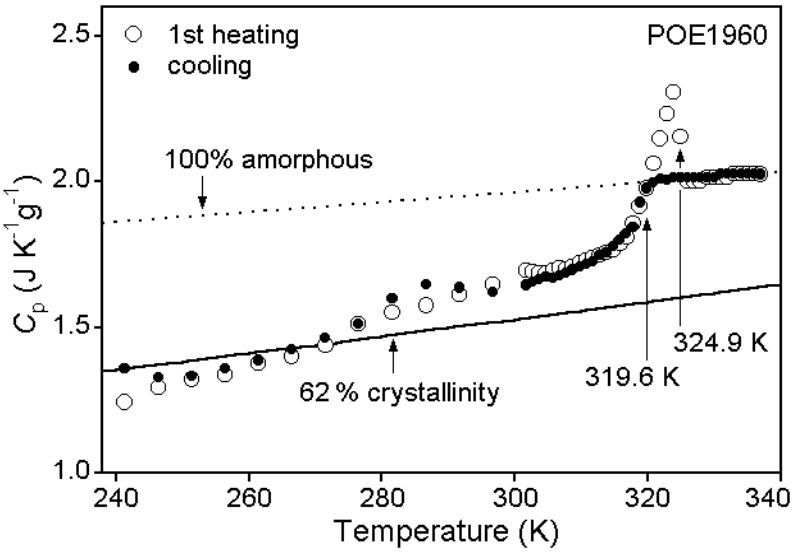

Figure 3.23. Apparent, reversing heat capacities of POE1960 on heating and cooling by quasi-isothermal TMDSC. Open circles and filled circles represent the first heating and subsequent cooling, respectively.

PE samples, the apparent reversing heat capacity plot on cooling shows that there is no contribution to crystallization and the amount of contribution to melting is much smaller than paraffin and PE samples.

In Figure 3.24, the experiment of Figure 3.23 is continued by quasi-isothermal measurements with increasing temperatures starting from 241 K, followed by a subsequent second cooling run. The apparent reversing heat capacities from the second heating runs are added to Figure 3.23. A second cooling run is not depicted in Figure 3.14, but it was identical to the first. The second heating runs exhibit that the end of melting is at same temperature of the first heating runs. The apparent reversing plots of C_p on cooling and on first heating are matched at low temperature regions except 241 K measurement but that on second heating is somewhat higher than others in the same regions. The maximum on

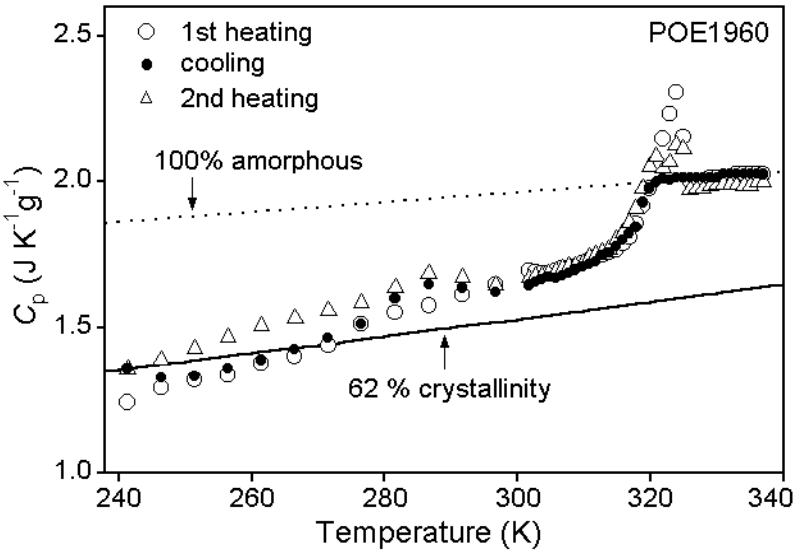

Figure 3.24. Apparent, reversing heat capacities of POE1960 on heating and cooling by quasi-isothermal TMDSC. Open circles, filled circles, and triangles represent the first heating, subsequent cooling, and the second heating, respectively.

second heating is lower than on first heating but there is still a small contribution to melting in contrast to the cooling runs. The magnitude of the small amount of apparent reversing C_p in the melting range and no contribution to crystallization is similar to that found for the other POE samples as shown in section 3.4.2.

3.4.5 TMDSC of POE3060

Figure 3.25 represents the results for POE3060. The thick, continuous solid line is the apparent total C_p by standard DSC at 10 K min^{-1}, carried out prior to the quasi-isothermal TMDSC measurements. The open circles are the apparent reversing C_p, obtained from the quasi-isothermal heating TMDSC. The crystallinity determined from the heat of fusion measured by standard DSC is 62.2%. In the standard DSC trace, there are two peaks at

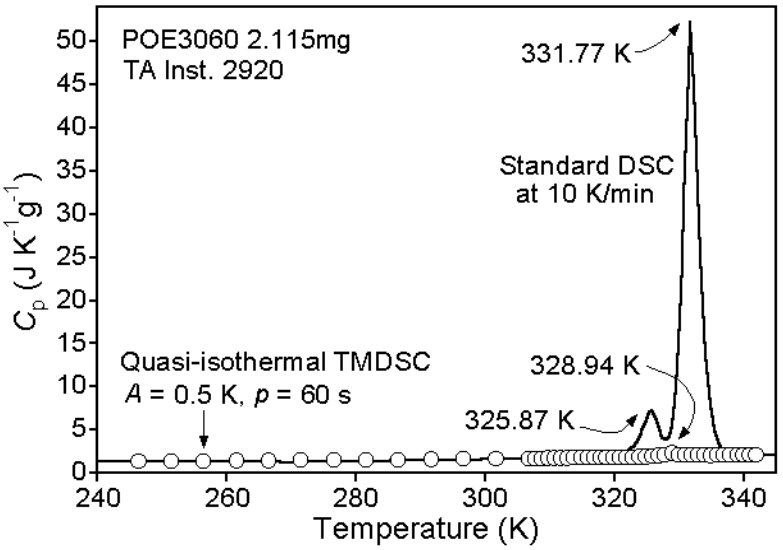

Figure 3.25. Apparent heat capacities measured by standard DSC and quasi-isothermal TMDSC for POE3060 crystallized first from the melt on cooling at 10 K min^{-1}. The solid line is obtained by standard DSC at 10 K min^{-1} and the open circles represent the apparent, reversing heat capacity by quasi-isothermal measurements.

325.87 K and 331.77 K. Probably, the first peak results from poor crystals produced when the samples are manufactured because this run was done with fresh sample from the bottle without any pre-heating or cooling. In the apparent, reversing C_p trace, there is only one small peak at 328.94 K. To make sure, a second heating by standard DSC was carried out after the TMDSC followed by cooling at 10 K min^{-1}. The results are shown in Figure 3.26. The peak was practically disappeared.

The dotted line in Figure 3.26 which is an enlarged figure of Figure 3.25 shows the second heating trace. The double-peak by standard DSC (solid line) is seen as a single peak with a small shoulder on second heating by standard DSC. The peak on heating by TMDSC is at the onset of melting on second heating. Therefore, the second peak on first heating

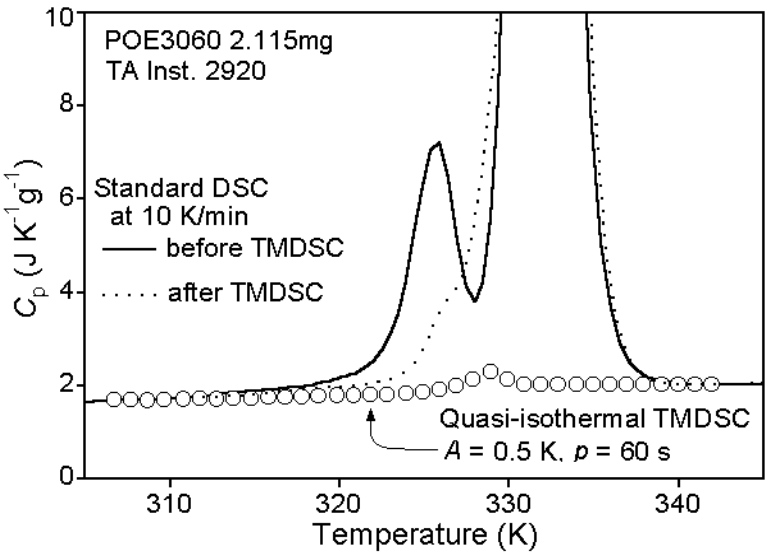

Figure 3.26. Heat capacities of POE3060 measured by standard DSC at 10 K min^{-1} before and after the quasi-isothermal TMDSC.

(solid line in Figure 3.25) is the main melting peak most interested.

Figure 3.27 shows only the enlarged TMDSC traces including the cooling experiment. The dotted line represents the heat capacity of the 100% liquid amorphous sample, as given in the *ATHAS* data bank [90], and the solid line is for the expected heat capacity for a sample of 64% crystallinity, as it was determined by standard DSC, measured after all quasi-isothermal TMDSC runs were completed. As shown in TMDSC results of POE1960 there is no apparent reversing heat capacity contribution to crystallization on cooling. When the crystallization starts, the value of reversing heat capacity drastically drop below the liquid heat capacity and then gradually decreases to the value of semicrystalline heat capacity. The end of melting on first heating occurs at 329.9 K, lower than the equilibrium melting temperature. And the onset of crystallization on first cooling is at 318.7 K. The difference of about 11.2 K is the degree of supercooling of POE3060. The heat

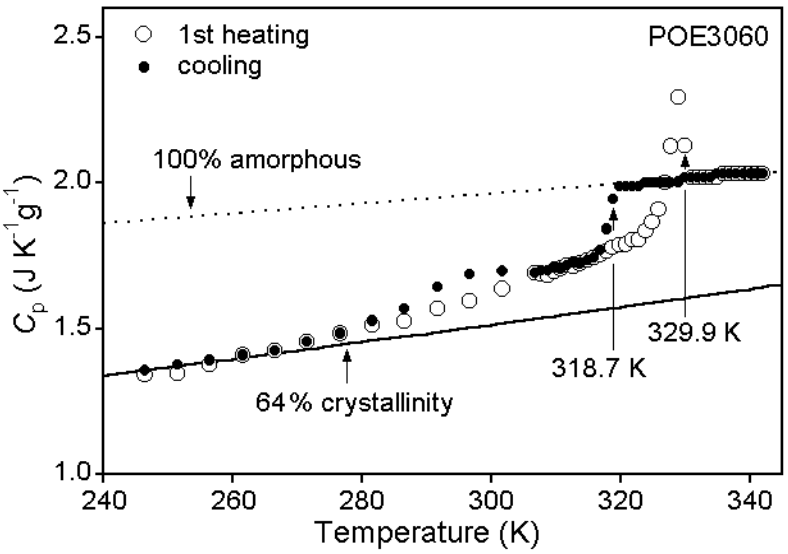

Figure 3.27. Apparent, reversing heat capacities of POE3060 on heating and cooling by quasi-isothermal TMDSC. Open circles and filled circles represent the first heating and subsequent cooling, respectively.

capacities measured on heating and cooling are matched a low temperature starting from 317 K, except in the 282–302 K region.

In Figure 3.28, the TMDSC experiment of Figure 3.27 is continued by quasi-isothermal measurements with increasing temperatures starting from 244 K (second heating run), followed by a subsequent second cooling run. The apparent reversing heat capacities from the second heating runs are added to the Figure 3.27. The second cooling run is identical to the first, and not plotted in Figure 3.28. The reversing C_p measured on first heating has almost same values than on second heating over the entire temperature range, but the maximum on second heating runs is somewhat lower than on first heating. And this reduced heat capacity values on second heating at the maximum is the same as observed in POE1960.

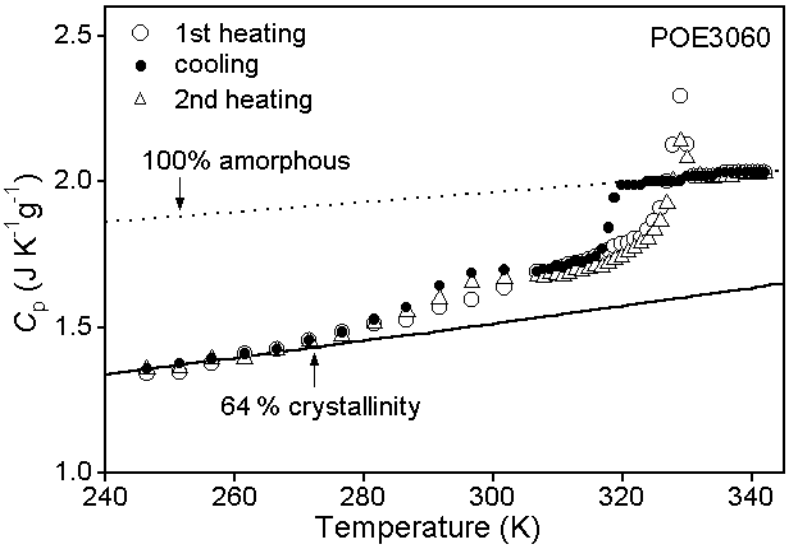

Figure 3.28. Apparent, reversing heat capacities of POE3060 on heating and cooling by quasi-isothermal TMDSC. Open circles, filled circles, and triangles represent the first heating, subsequent cooling, and the second heating, respectively.

3.5 Effect of seeding on degree of supercooling

The polyethylene fractions analyzed in this thesis except for PE560 showed some degree of supercooling. It can be due to any kind of nucleation. Melts of small molecules, such as metals or water, supercool before crystallization because of the need to nucleate crystals before growth can commence. Crystal nucleation is, thus, the first step of any crystallization, but it can be circumvented by either incomplete melting before crystallization (self nucleation) or by adding of foreign nuclei (crystallization by heterogeneous nucleation) [1]. For example, indium shows reversible melting and crystallization on analysis by temperature-modulated differential scanning calorimetry (TMDSC). In this technique the temperature is cycled about a mean value. As long as the melting during the previous heating

cycle is incomplete and nuclei are left for re-crystallization during the cooling cycle there is no supercooling [13, 14]. Once, melting is completed; *i.e.*, no nuclei are left, the sample needs to be supercooled by an amount ΔT (= $T_m - T_c$) of 1–1.5 K [13, 14]. In this case the 1–1.5 K of supercooling is needed for the crystal nucleation of indium.

To make sure that the degree of supercooling observed in this thesis is not for crystal nucleation as in indium crystallization, the seeding of PE with a high-melting temperature into the PE oligomers and polymer was done. PE fiber which has approximately 1 M Da. of molar mass and a melting temperature of about 406 K was used as a seed. The PE2150 and PE15520 fractions, whose melting temperatures are about 15 K below that of the fiber were heated from 350 K to 396 K, to melt the PE samples completely, but the seeds do not start their melting. Next the samples were cooled to 350 K to recrystallize the PE fraction samples to see if the degree of supercooling decrease or not. The samples were then reheated to 416 K, above the melting temperature of the seed and then cooled down again to 350 K to make sure that the PE fiber was still present and not miscible with the PE fractions. The result for PE15520 is depicted in Figure 3.29 as a function of time. There is only one peak on each first heating and cooling cycle as shown in beginning of Figure 3.29 and second peak appears on each second heating and cooling cycle. For clarifying the crystallization temperature of PE15520 with the seed the Figure 3.29 is transposed to a plot *versus* sample temperature in Figure 3.30. On first cooling, a crystallization peak appears at about 375 K and the crystallization temperature is same as in other experiments of PE15520 without any seed, i. e., there is no effect of the seed to supercooling of PE15520. On second run an

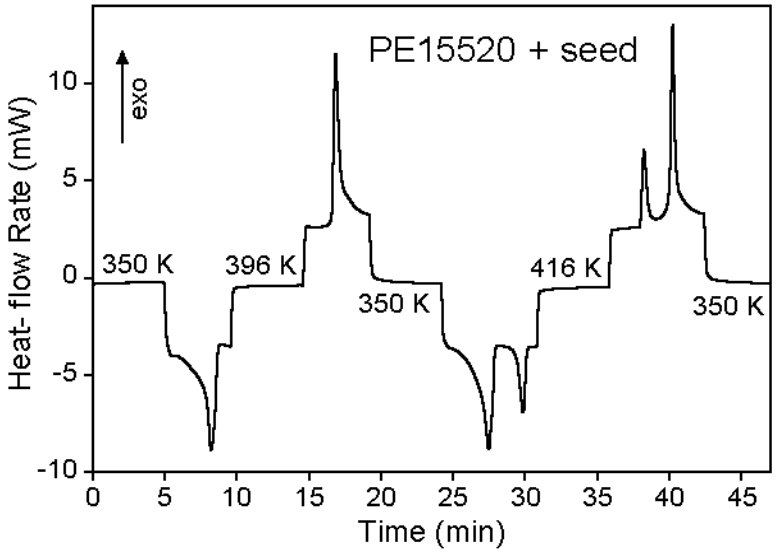

Figure 3.29. *HF*(*t*) of PE15520 with seeds *versus* time. The upward direction *HF*(*t*) is exothermic. Heating and cooling rates are 10 K min^{-1}. The temperatures indicated in each isothermal region are corresponding minimum and maximum.

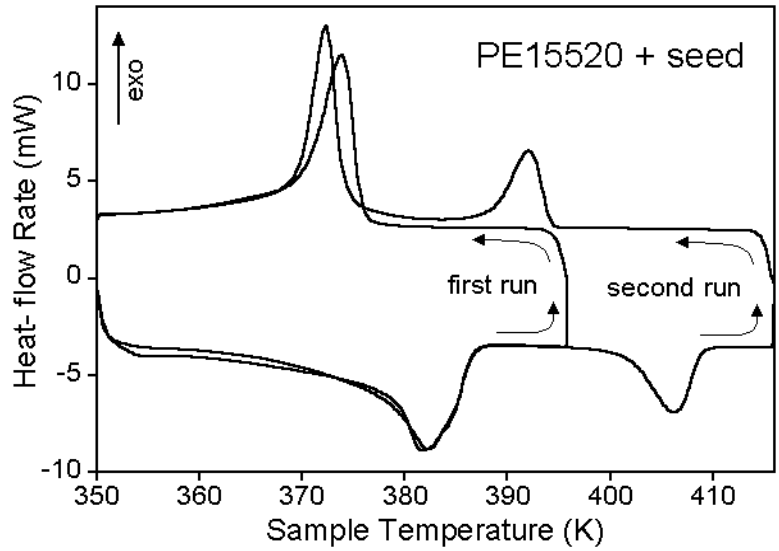

Figure 3.30. *HF*(*t*) of PE15520 with seeds *versus* sample temperature. The upward direction *HF*(*t*) is exothermic. Heating and cooling rates are 10 K min^{-1}.

endothermic peak and an exothermic peak at 406 K and 393 K, respectively are evidences of seed existence during the first measurement. With PE2150 I got same results.

Similar experiments of seeding of polyethylene with higher melting samples were done long time ago in our laboratory [93] and the results agree well with the present ones.

CHAPTER 4

DISCUSSION

4.1 Melting and Crystallization of PE Observed by Quasi-isothermal TMDSC

4.1.1 Comparison of PE560 with n-Paraffins

The $C_{50}H_{102}$, $C_{44}H_{90}$, and $C_{26}H_{54}$ n-paraffins were analyzed previously with standard and temperature-modulated DSC [86, 87]. As depicted in Figure 4.1 for n-$C_{50}H_{102}$ the paraffins n-$C_{44}H_{90}$ and n-$C_{50}H_{102}$ show only a single, largely reversible melting transition, as expected from the well-known fact that n-paraffins above n-$C_{36}H_{74}$ exhibit only one crystal

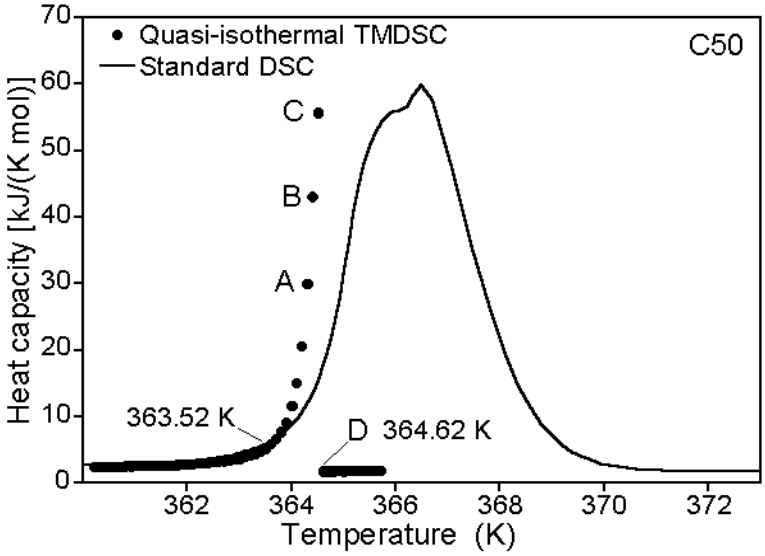

Figure 4.1. Heat capacity of n-$C_{50}H_{102}$. The filled circles represent the reversing heat capacities by quasi-isothermal TMDSC, the solid line, the heat capacity by standard DSC. Copied from ref. [86].

phase, while paraffins between n-$C_{21}H_{44}$ and n-$C_{36}H_{74}$, as analyzed by us by TMDSC for the example of n-$C_{26}H_{54}$, display a disordering transition to a mesophase below T_m in addition to the melting transition (see Figure 4.2). In this case, the melting transition should be called more precisely an isotropization transition since the mesophase can be considered as being already "partially melted [94]." The PE560 oligomer whose mass and number-average lengths correspond to n-$C_{40}H_{82}$ and n-$C_{37}H_{76}$, respectively, shows two transition peaks. In a recent reference [3], the mesophase transition was detected up to n-$C_{37}H_{76}$. The peak on TMDSC and the shoulder on DSC at about 333 K in Figure 3.5 might, thus, contain contributions from the mesophases of n-$C_{37}H_{76}$ and shorter chains, as observed in n-$C_{26}H_{54}$ [87]. The main part of the melting peak at 333 K, as well as the broadening of the melting range, however, should be caused by the eutectic phase behavior, known to occur on careful

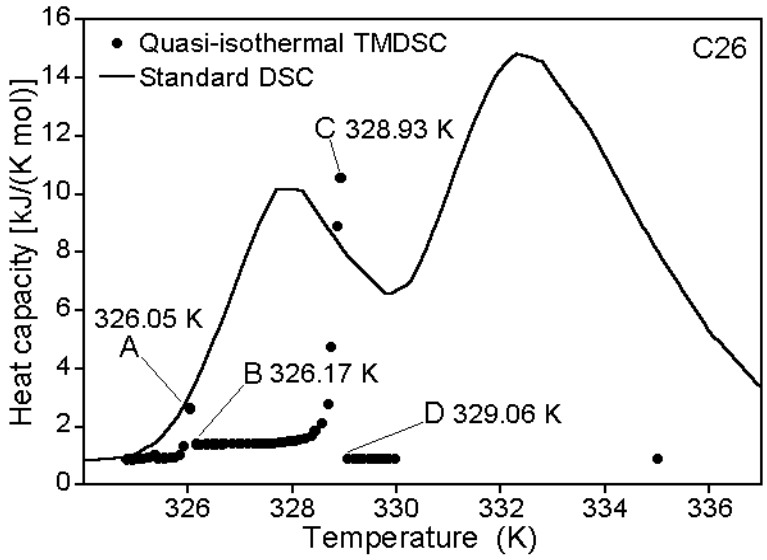

Figure 4.2. Heat capacity of n-$C_{26}H_{54}$. The filled circles represent the reversing heat capacities by quasi-isothermal TMDSC, the solid line, the heat capacity by standard DSC. Copied from ref. [87].

crystallization of paraffin solutions [7].

To understand typical eutectic phase diagrams in paraffins, the eutectic temperature of the PE560 system can be analyzed using the Flory-Huggins equation or its extension to multi-component systems [95]:

$$\frac{1}{T_m} - \frac{1}{T_m^\circ} = \frac{R}{\Delta H_p}[-\ln v_p + (\bar{x} - 1)(1 - v_p) - \bar{x}\chi(1 - v_p)^2] \qquad (4.1)$$

where T_m is the temperature of the chosen equilibrium, and T_m^o, the equilibrium melting temperature of the pure species of the molar mass considered and given by eq (3.1). The partial molar volume fraction of the considered species in the melt is v_p and χ, the interaction parameter. The appropriate average size-ratio of the considered species relative to all other species of length *i* is:

$$\bar{x} = \frac{\sum v_i x_i}{\sum v_i} \qquad (4.2)$$

For two components only, $\bar{x} = x$, and the Flory- Huggins equation is recovered. A eutectic point about 1.3 K below T_m^o of PE560 can, thus, be calculated for a PE560/n-$C_{50}H_{102}$ solution assuming $\chi = 0$. The calculated eutectic phase diagram is displayed in Figure 3.6 together with the two additional mixtures, PE560/n-$C_{26}H_{54}$ and PE560/n-$C_{37}H_{76}$. For PE560/n-$C_{37}H_{76}$ this difference between eutectic and equilibrium melting temperatures increased to 7 K, and for PE560/n-$C_{26}H_{54}$, to 25 K. Therefore, a broadened eutectic can easily contribute to the secondary peak in Figure 3.5, seen 10 K below the melting peak. Experimental data of extended-chain crystals of polyethylene of a weight-average molar mass of 2550 Da and a polydispersity of 1.6, much larger than in PE560, showed an even broader melting range with

several lower-temperature eutectic peaks [96], while a phase diagram of a mixture of pure n-$C_{30}H_{62}$ and n-$C_{22}H_{46}$ has a melting range between the eutectic and the melting temperature of n-$C_{30}H_{62}$ of up to 24 K [1], making the eutectic crystallization a likely cause for the broadening of the melting in PE560 of Figure 3.5.

The apparent reversing heat capacity plot shows a sizeable contribution to the melting (see Figure 3.5), but not as much as seen for the pure n-$C_{50}H_{102}$, which crystallizes reversibly to almost 100%. When measured by quasi-isothermal TMDSC with an amplitude of 0.05 K, 66% of the total crystals of n-$C_{50}H_{102}$ melt within 0.1 K or less, and all fusion is complete within 1.0 K as seen in Figure 4.1 [86], *i.e.*, with the present, larger modulation amplitude of 0.5 K, the melting would have been practically fully reversing. The width of the region of melting of PE560 is more than 30 K, and the maximum in the reversing C_p reaches only half the C_p of the melting peak by standard DSC. The broadening of the melting of PE560 in the quasi-isothermal measurements is, thus, most likely due to the chain-length distribution. The additional shift to higher temperature in the standard DSC experiment for the high-temperature potion of the melting peak and the end of melting is due to the thermal lag of the calorimeter when heated at 10 K min^{-1} through the melting region [89].

As shown in Figures 3.5 and 3.16, the reversibly melting fraction of PE560 is much larger than for the high molar mass PE15520, and the biggest crystals in PE560 which melts last on heating also crystallize first on cooling without supercooling. Again, such behavior is expected from a eutectic phase diagram at equilibrium. On heating, the last crystals melting and on cooling, the first crystals growing, both consist of the pure component of

highest molar mass, as observed in Figure 3.8. Quite similar results were found on TMDSC of a sample of not quite pure n-$C_{44}H_{90}$ in Figure 4.3 [87].

The quasi-isothermal measurements on paraffins with smaller modulation amplitudes when compared to the present data in Figure 3.8, showed incomplete melting and crystallization in the temperature-range of modulation due to limitations of the heat flow for the given small changes in temperature (±0.05 K) coupled with the low thermal conductivity of the paraffins [87]. In the modulation cycle of the next higher value of T_o, the crystals that should have melted at the lower temperature melted irreversibly during the first few cycles at a rate until the new steady state was reached. In this case, the reversing heat-flow rate is strongly asymmetric (see Figure 4.4) due to the larger melting contribution during heating,

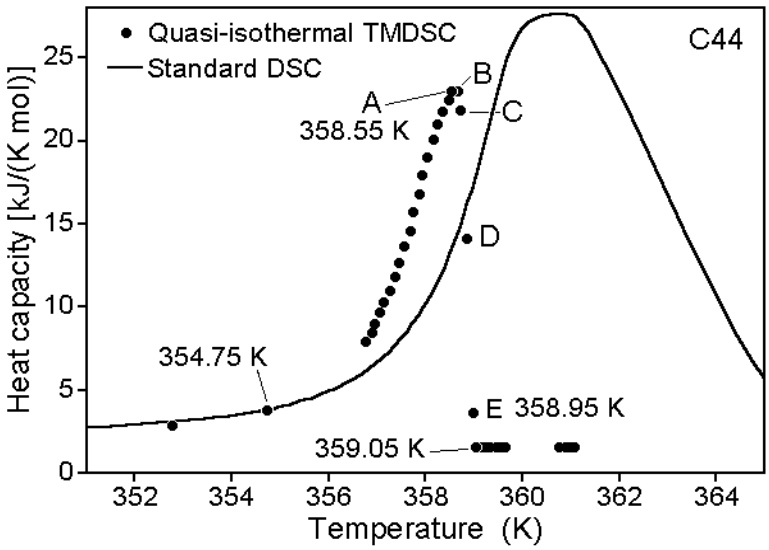

Figure 4.3. Heat capacity of n-$C_{44}H_{90}$. The filled circles represent the reversing heat capacities by quasi-isothermal TMDSC, the solid line, the heat capacity by standard DSC. Copied from ref. [87].

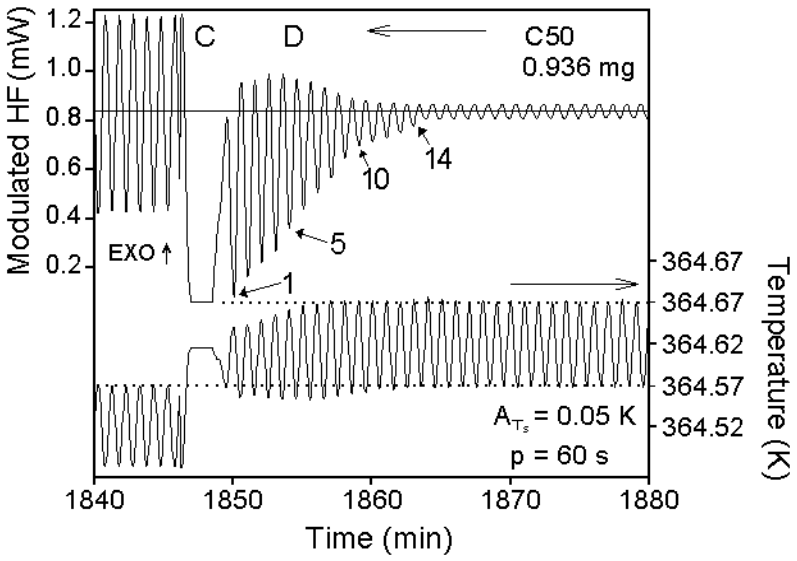

Figure 4.4. Modulated heat-flow rate and sample temperature of modulation set D in Figure 4.1. Copied from ref. [2].

and naturally, the first harmonic of this asymmetric response of the sample alone is not usable for a quantitative analysis. In the present analysis of PE560, these problems were largely avoided by choosing larger modulation amplitudes, and helped by the inherently smaller amount of change in crystallinity over the much broader melting range in the corresponding runs.

The higher apparent reversing heat capacities in the regions of the points marked a–f in the cooling sequence relative to g–i in the heating sequence in Figure 3.8 are analyzed in the more detailed graphs in Figure 4.5. Corresponding data for the marked points are given in the graphs for the apparent, reversing, specific heat capacity in the time domain. After attainment of steady-state, the specific heat capacity continues to decrease at the temperatures from f–a and converges towards the measurements on heating at points g–i which show a constant reversing heat capacity in each run after about 10 min.

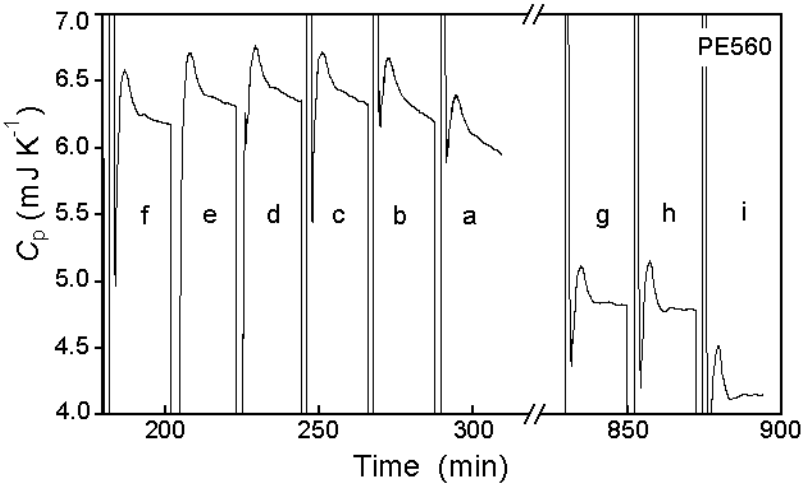

Figure 4.5. Detailed analysis in the region of the reversing melting peak of PE560. Apparent reversing heat capacity during cooling and subsequent heating. Corresponding points to Figure 3.8 are marked.

Figure 4.5 shows the practically constant apparent reversing heat capacity at points g–i after reaching steady state. Every modulation-cycle is symmetric in crystallization and melting, so that the overall progress of melting occurs when the temperature is increased from one quasi-isothermal T_o to the next, and the amplitude of the apparent reversing heat capacity can be separated into a contribution due to the reversible thermodynamic heat capacity and the reversible latent heat exchanged on crystallization and melting as graphed in Figure 3.8. If measurements would have been carried out with an underlying heating rate $\langle q \rangle$ and not quasi-isothermally, the modulation amplitudes in successive cycles would overlap, and the integral reversible heat of fusion would erroneously exceed the total heat of fusion, as was demonstrated for the reversible melting of indium [89].

4.1.2 Comparison of PE2150 to PE560 and PE15520

Although PE2150 is an oligomer and much shorter than PE15520, it has a similar amount of supercooling and higher melting temperature as seen in Figure 3.15. The melting temperature is close to the equilibrium melting temperature of n-$C_{153}H_{308}$ with a 19.2 nm chain length. Therefore, PE2150 should be an extended-chain crystal as in the paraffins, PE560 discussed above, and expected from the well-established upper limit of 37 nm for extended-chain crystallization of paraffins at atmospheric pressure [46, 47]. The extended chain crystal, PE2150 grows at about six kelvins below the melting temperature, as seen in Figure 3.13.

In contrast, PE15520 shows in Figure 3.17 an end of melting about 25 kelvins below the equilibrium melting temperature of 411.9 K (see Figure 3.15). This agrees with a reasonable lamellar crystal thickness of about 10.5 nm, as can be calculated from an equation derived from a large number of data on the melting temperatures of polyethylenes of known lamellar thickness [7]:

$$L = 0.627 \frac{T_m^o}{T_m^o - T_m} \tag{4.3}$$

where T_m is melting temperature of the folded-chain crystal, T_m^o the melting temperature of the extended chain crystal represented by eq (3.1), and L is the lamellar thickness in nm. The three analyzed samples, thus, show much different crystallization and melting behaviors. While PE560 shows no supercooling and crystallizes largely reversibly, PE2150 shows a supercooling of 5.8 K and PE15520 one of about 30 K based on T_m^o, i.e., both crystallize irreversibly. While PE2150 melts close to the equilibrium temperature, PE15520 melts 25

kelvins below, at a temperature close to the zero-entropy-production temperature where the free enthalpy of the metastable crystal (with lamellar thickness L = 10.5 nm, in this case) is equal to the free enthalpy of the supercooled melt as illustrated in Figure 4.6. From this zero-entropy-production melting temperature the crystallization of PE15520 shows a supercooling of 5.5 K, as shown in Figure 3.17.

Comparing the shape of the melting curves by standard DSC in Figures 3.5, 3.12, and 3.16, one finds the broadest melting peak for PE560 (≈40 K), the narrowest for PE2150 (≈15 K), and a broad peak of about 40 K with a superimposed sharper peak of about 20 K for PE15520. The more detailed analysis shown in Figures 3.8, 3.14, and 3.18 reveals a beginning deviation from the heat capacity due to vibrations-only at 260 to 280 K, only little above the glass transition. For PE560 this early deviation is fully reversible, as found earlier for the paraffins [82]. The first separation between reversing and total C_p is seen at 330 K,

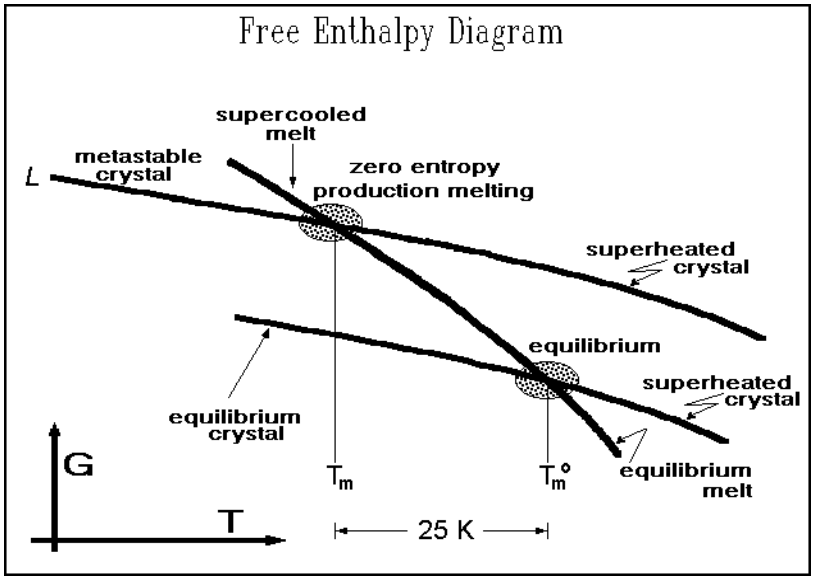

Figure 4.6. Free enthalpy diagram illustrating the zero entropy production melting. Modified from ref. [97].

well into the melting peak, at an apparent heat capacity of 95 J $K^{-1}mol^{-1}$ (see Figure 3.5). For PE2150, the first separation between total and reversing heat capacity occurs at about 360 K, before major melting, at an apparent C_p of about 30 J $K^{-1}mol^{-1}$, while for P15520 this separation is seen at about 260 K, at an apparent C_p of about 25 J $K^{-1}mol^{-1}$ (see Figures 3.12 and 3.16). For all three samples the apparent reversing heat capacity reaches the level of the melt before major melting has begun. These observations point to the difficulties that arise when attempting to define a baseline for the determination of the heat of fusion.

The next question concerns the reversing portion of the melting, as revealed in Figures 3.8, 3.14, and 3.18. The discussion of PE560 was done in connection with the similarity of paraffins. A large portion of the melt is reversible within the range of modulation. The remaining irreversible part is expected to be connected with incomplete separation of the various species, as is seen on cooling at temperatures a–f in Figure 4.5 and discussed in the section on the kinetics. The PE2150 is characterized by a minimum of reversible melting, as also seen for poly(oxyethylene)s in the same molar mass range (POE1500 to POE5000) [32, 33]. The remaining reversible increase in heat capacity seems to be largely reversible since the quasi-isothermal reversing heat capacities are independent of time (see Figure 4.7). The polymer PE15520, behaves quite differently. It shows an irreversible melting component at all temperatures between the glass and melting transitions and the reversing contribution to the melting peak is larger than for PE2150 when one considers that the crystallinity is little more than half that of PE2150 (compare Figures 3.14 and 3.18). To discuss more of the details of the small amount of reversing melting and assess the truly reversible fraction the possible annealing of the sample must be analyzed as

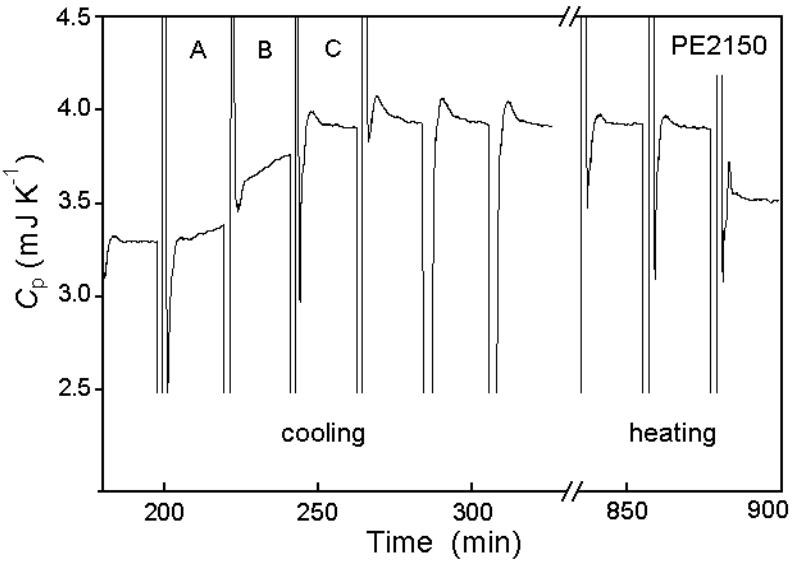

Figure 4.7. Detailed analysis in the region of the reversing melting peak of PE2150. Apparent reversing heat capacity during cooling and subsequent heating in the first crystallization steps and at the melting peak. A to C indicate runs that can be used for the study of crystallization.

done in the section 4.2. The large difference between reversing heat capacity on cooling and on heating indicates that as much as half of the species contributing to the reversing melting crystallize irreversibly at temperatures below the melting temperature, different from PE2150, which grows all reversibly melting species close to the melting temperature after the initial supercooling, while PE560 has a larger reversing C_p on cooling, as discussed above.

4.2 Kinetics of the Processes Seen by TMDSC

The kinetics of the changes in the quasi-isothermal analysis of PE560 in terms of the apparent, reversing heat capacity and the total heat-flow rate is shown in Figure 4.8. The higher apparent reversing heat capacities in the regions of the points marked a–f in the

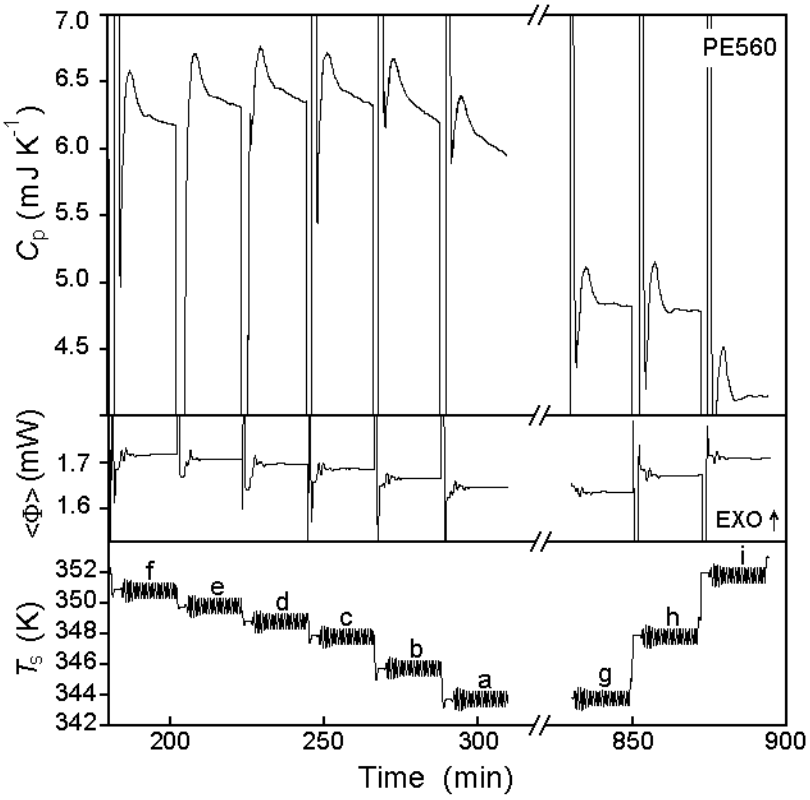

Figure 4.8. Detailed analysis in the region of the reversing melting peak of PE560. Apparent reversing heat capacity, total heat-flow rate <Φ>, and sample temperature $T_s(t)$ during cooling and subsequent heating. Corresponding points to Figure 3.8 are marked.

cooling sequence relative to g–i in the heating sequence in Figure 3.8 are analyzed in the more detailed graphs in Figure 4.8. Corresponding data for the marked points are given in the graphs for the modulation of the temperature (bottom), the total heat-flow rate (center), and the apparent, reversing, specific heat capacity (top).

For PE560 much of the response is reversible within the parameters of modulation. The larger apparent total heat capacity of the final melting peak in Figure 3.5 is linked to the kinetics of the processes which may arise not so much from lags of the calorimeter, but from

slow kinetics to reach equilibrium within the sample by diffusion and selection of the various species attaining equilibrium only at the proper crystal thickness. The instrument-caused effects have been seen in earlier work on pure paraffins, analyzed with a different calorimeter using sawtooth modulation [87]. The missing reversing heat of fusion was in the latter cases evolved during the heating from one base temperature to the next and at the melting peak also in the first few modulation cycles at the higher temperature. With the present instrumentation, no recording of the heat-flow rate is possible between runs, but we assume that it may occur, although to a smaller degree. The melting range of PE560 is sufficiently broad, so that no additional melting at the higher temperature can be distinguished during the approach to steady state as seen, for example, in Figure 4.9 in runs during the time up to the 277 min point. Reversible low-latent-heat transitions of liquid crystals where similarly analyzed [98]. Temperature lags in the sample pan could also be documented directly by

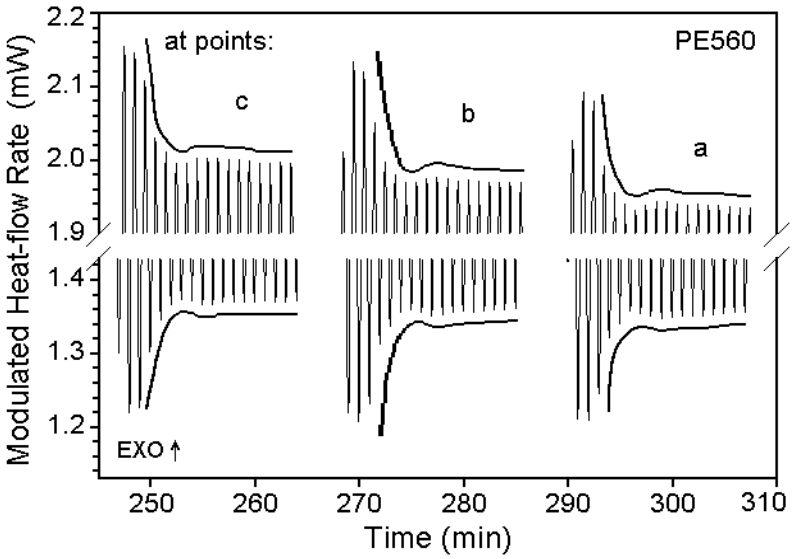

Figure 4.9. Raw heat-flow rate data $\Phi(t)$ as a function of time. Data for PE560 as a function of time for points a, b and c in Figures 3.8.

contact-less measurements within the DSC cell by infrared thermography [99].

Slow, irreversible processes within the sample of PE560 can be seen from the decrease of the reversing heat capacity with time in the cooling sequence f–a of Figure 4.8. It was suggested in the discussion, above, that this decrease in reversing heat capacity may, in time, reach agreement with the quasi-isothermal experiments on heating (sequence g–i). Approximately 100 min should be sufficient to reach such true equilibrium.

Figure 4.9 adds the actual, raw data in the time domain of the heat-flow rate of PE560 for selected temperatures in order to judge the symmetry of the response to the modulation and find causes for the nonreversing contributions. Figure 4.9 indicates a largely symmetrical heat-flow rate, but from 277–287 minutes into the experiment, after attainment of steady state, the amplitude of the endothermic cycle decreases faster than the exothermic one. This observation indicates that in every cycle a small amount of the recrystallized material achieves a sufficiently higher melting point due to better crystal perfection to fall outside the temperature range covered on the subsequent heating. We speculate that with time a better segregation of the molar mass distribution into crystals of equal length is possible. Similar decreases in apparent reversing heat capacity are seen also in polymers on annealing. Examples are seen in linear low density polyethylenes on annealing in the melting range of sequences of paraffinic lengths [27, 28], and on annealing of poly(ethylene terephthalate) in the melting region [34, 35].

The analysis of the PE2150 in Figure 3.12 shows that its melting is largely irreversible. Only a small reversing contribution to the apparent heat capacity begins at about 260 K and develops to a 10 J K^{-1} mol^{-1} peak, as seen in Figure 3.13. Figure 4.10 displays

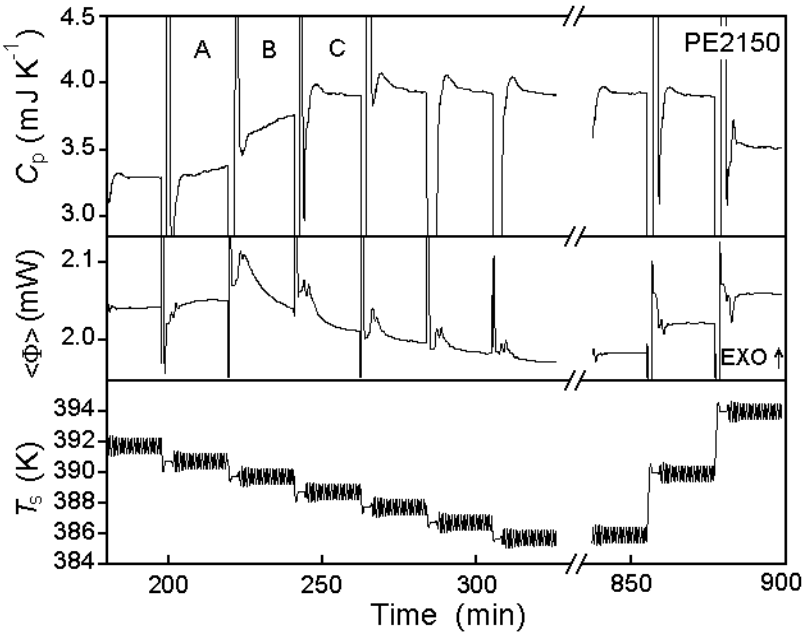

Figure 4.10. Apparent reversing heat capacity, total heat-flow rate <Φ>, and sample temperature $T_s(t)$ during cooling and subsequent heating in the first crystallization steps and at the melting peak. A to C indicate runs that can be used for the study of crystallization. Corresponding points to Figure 3.14 are marked.

more details about the crystallization and melting in the time domain, using graphs for the modulation of the temperature (bottom), the total heat-flow rate (middle), and the apparent, reversing, specific heat capacity (top). At the initial crystallization (marked A) <Φ> reaches an almost constant, but slightly elevated exothermic level, while the apparent reversing heat capacity increases continuously. Next, at temperature B the total heat-flow rate <Φ> decreases from a strongly exothermic level, while the reversing C_p continues to increase. At point C and lower temperatures, both <Φ> and the reversing C_p decrease. These changes will be discussed below on hand of the raw data of the heat-flow rate and compared to the lower and higher molar mass materials.

Figure 4.10 reveals that except for temperatures A, B, and C, little changes occur in the apparent reversing heat capacities with time, i.e., the effect has reversible causes. The small irreversible peaks, like the one at 370 K and the increased reversing peak at 390 K disappear from the reversing heat capacity on more careful crystallization, an indication that poorer crystallization increases the apparent reversing heat capacity. Quite similar increases in apparent reversing heat capacity were observed for POE with molar masses of 1500 and 5000 Da and most other polymers analyzed to date [29, 89]. Their existence has been linked to surface melting either on fold surfaces [39, 40], or on side surfaces [30, 34].

The kinetic effect at points A, B, and C, in Figure 4.10, which represent the initial temperatures of crystallization, may shed some light on the development of the reversing melting on crystallization. At the point A in Figure 4.10, one observes the first linear increase in the apparent reversing heat capacity. It starts only after steady state is reached and the total heat-flow rate is slightly more exothermic than the response of the melt, indicating a constant rate of crystallization starts slightly earlier and causes a continuing linear increase in reversibly melting material. Figure 4.11 shows at the temperature A that the amplitude of the response to modulation is largely symmetric with slight increases in the exotherm. The endotherm increases also, but only half as much, i.e., about half of the added crystallization in each cooling cycle is melted again in the subsequent heating. Full reversibility is not reached in the time of analysis. At temperature B, the increase in apparent reversing heat capacity continues and reaches a constant level at C (see Figure 4.10). The total heat-flow rate, in turn, is much different. A large, irreversible crystallization exotherm that decreases with time and is less in each subsequent analysis step is superimposed on the

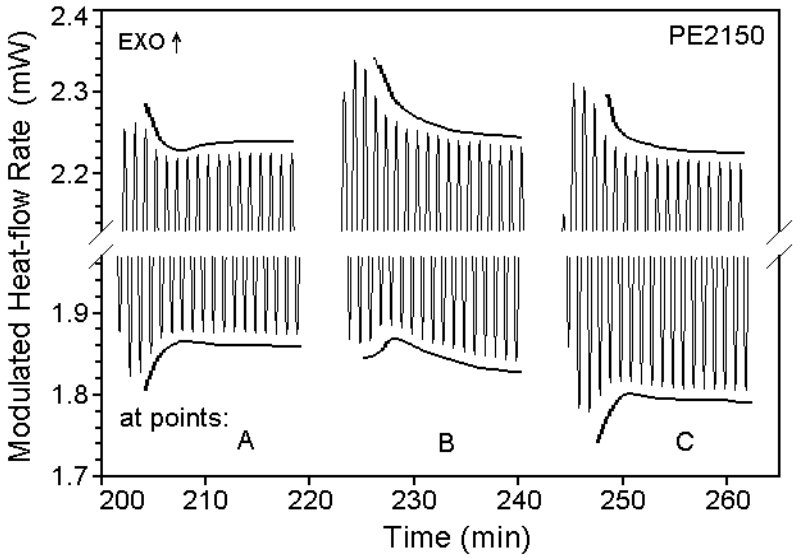

Figure 4.11. Raw heat-flow rate data $\Phi(t)$ as a function of time. Data for PE2150 as a function of time for points A, B, and C in Figure 3.14.

modulation effect, as seen in Figures 4.10 and 4.11. At temperature B, the reversing heat-flow rate, again, is largely symmetric and increases somewhat by increasing the exotherm slightly more than the endotherm in successive steps. In C there is hardly any asymmetry detectible and, judging from the total heat flow, by this time the bulk of the irreversible crystallization has taken place. The reversible crystallization stays constant for several more steps of cooling before decreasing, but reaches zero only close to the glass transition. Below about 370 K, the total and reversing apparent heat capacities are equal which means that all of the early melting is reversible.

The PE15520, true polymer behaves different from PE oligomers. The low-temperature melting is, in this case, only partially reversible, and the fraction of reversing apparent heat capacity is more than in PE2150 and is larger in the more poorly crystallized sample (see Figures 3.16 and 3.18). Figure 4.12 displays, as before, more details about the

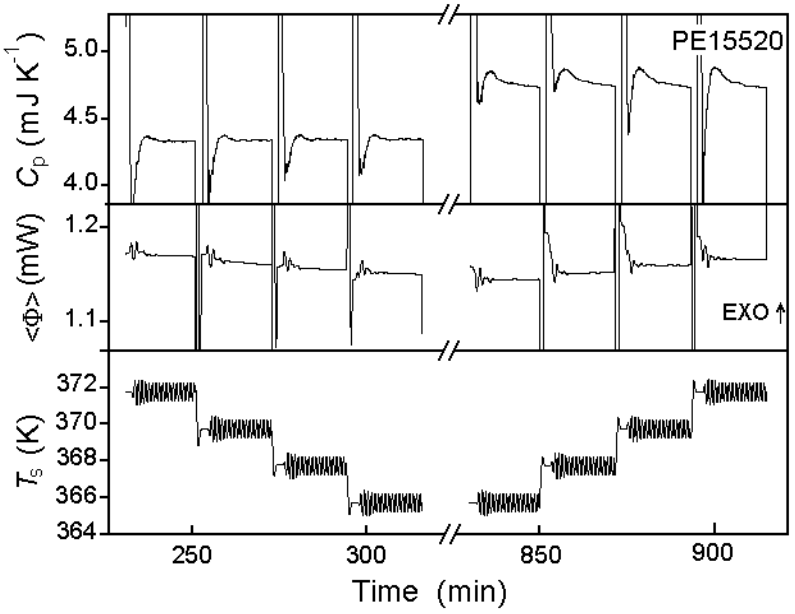

Figure 4.12. Detailed analysis in the region of the reversing melting peak of PE15520. Apparent reversing heat capacity, total heat-flow rate <Φ>, and sample temperature $T_s(t)$ during cooling and subsequent heating in the region of the melting peaks.

crystallization and melting, using graphs for the modulation of the temperature (bottom), the total heat-flow rate (middle), and the apparent, reversing heat capacity (top). The points chosen for analysis are in the temperature region of the broad peak of the cooling data of Figure 3.18. In the given scale all values of <Φ> are constant with time after attainment of instrumental steady state. The reversing C_p on cooling also changes only little, but in the heating sequence, it starts at higher values and decreases with time. Therefore, the gap of reversing C_p between heating and cooling run decreases, but on extrapolation to longer times does not reach equal levels.

Figure 4.13 shows that on cooling the reversing apparent heat capacity is constant with time, while on heating it is larger and decreases with time. Figures 4.14 and 4.15

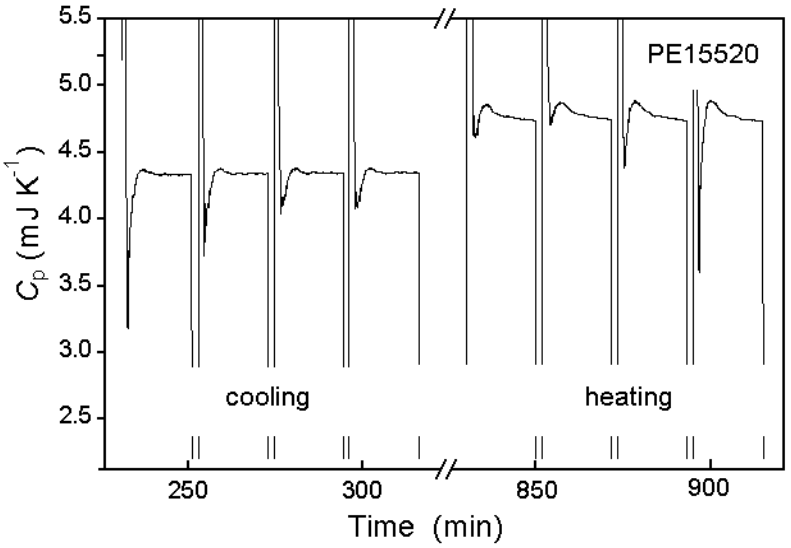

Figure 4.13. Detailed analysis in the region of the reversing melting peak of PE15520. Apparent reversing heat capacity during cooling and subsequent heating in the region of the melting peaks.

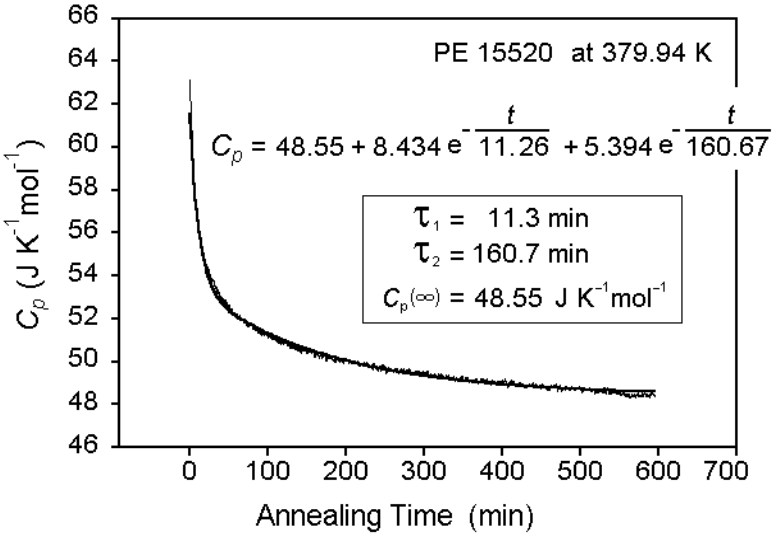

Figure 4.14. Plot of the change in apparent, reversing heat capacity as a function of annealing time for the data of Figure 4.15.

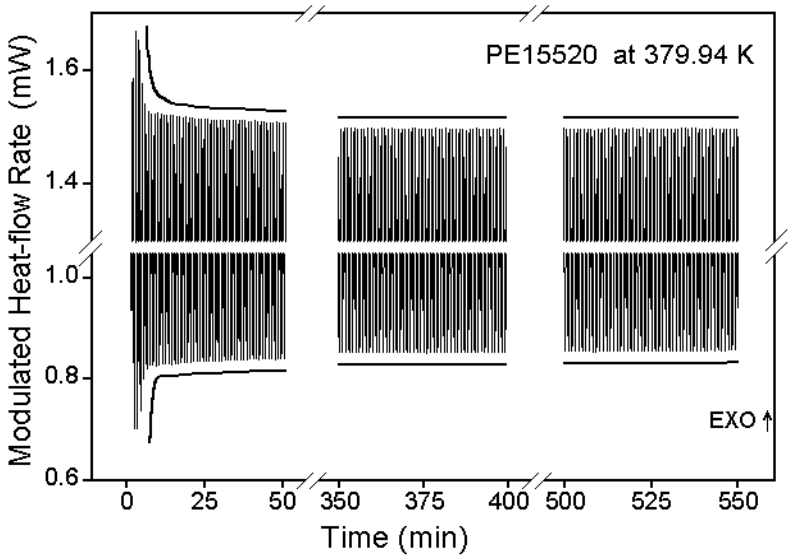

Figure 4.15. Raw heat-flow rate data $\Phi(t)$ for PE15520 as a function of time from a long-time quasi-isothermal experiment at 379.94 K at the high-temperature peak of a sample of specially poor crystallization history. Shown are excerpts at 0–50, 350–400 and 500–550 min. The center areas are omitted to be able to increase the ordinate. The solid line is drawn somewhat above the endothermic and exothermic maximum amplitudes for clarity.

illustrate the changes at 379.9 K in a long-time experiment for a sample with an even larger peak in the reversing, apparent heat capacity than shown in Figure 3.18. The ultimately reached level of reversing heat capacity of 48.55 J K^{-1} mol^{-1} in Figure 4.14 is still much above the constant level reached on cooling. As for all other polymers of high molar mass that have been analyzed in this fashion, two processes seem to be involved in the kinetics with the indicated relaxation times. Both are longer than the response of the calorimeter, and Figure 4.15 indicated that a slightly larger exotherm leads the change, which is otherwise largely symmetric. One expects thus that an annealing process is involved in the decrease of the reversing heat capacity, starting with a small exotherm of crystal perfection which then

is removed as a perfected crystal from the subsequent melting cycle. It takes several hundred minutes until this process is completed.

4.3 Melting and Crystallization of POE Observed by Quasi-isothermal TMDSC

The study of the reversing melting and crystallization of POE1500 was carried out several years ago in our laboratory [32]. When it is analyzed with standard DSC recently, there exist two peaks on cooling and only one peak on heating as seen in Figure 3.20. The two peaks on cooling may be caused by primary and secondary crystallization with different rates of crystal perfection on prior heating run. The quasi-isothermal TMDSC results show different melting and crystallization behavior compared to that of PE. The reversing heat capacity peak of POE1500 on heating is relatively smaller than for PE1150, even thought they are similar in molar mass and chain length. (See Figure 4.16 and compare to Figure 3.9). In addition to the smaller melting peak in reversing heat capacity, POE1500 also shows no peak in reversing heat capacity on cooling as shown by the triangles in Figure 3.9. The reversing heat capacities, however, after the beginning of crystallization on cooling are above the heat capacity of semicrystalline expected from the crystallinity, so still one can say there is a reversing apparent heat capacity contribution on the reversing heat capacity from cooling runs that may arise from a latent heat.

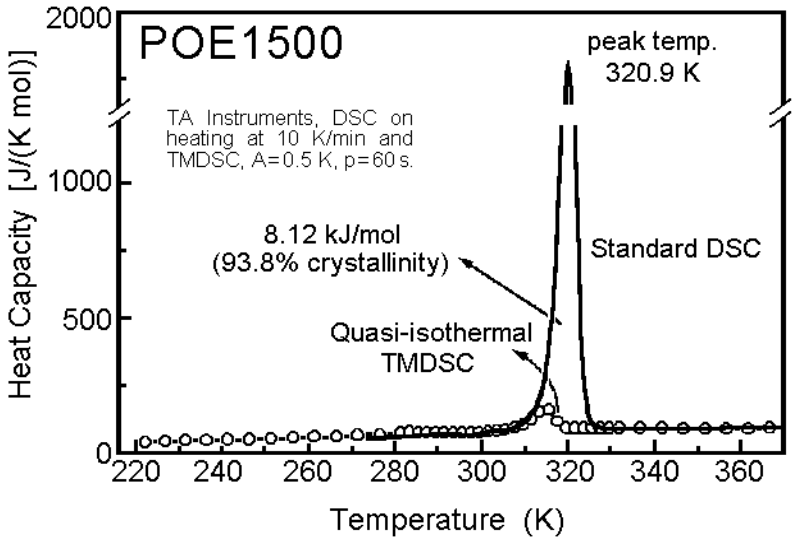

Figure 4.16. Heat capacity measured by standard DSC and quasi-isothermal TMDSC for POE1500 crystallized at 300 K. The solid curve was obtained by standard DSC at 10 K min^{-1}, and the open circles represent the reversing heat capacity, obtained by quasi-isothermal experiments. Copied from [32].

When the molar mass of POE increases, these small melting peak on heating and no peak on cooling remain. The newly analyzed samples, POE1960, as seen in Figure 3.22, and POE3060, in Figure 3.25 have very small peak in reversing heat capacity on heating. Also, there is no peak for these POE1960 and POE3060 on cooling. (See Figure 3.23 and 3.27).

The longer POE sample, POE5000 (its actual molar mass is 4540) has extremely small peak on heating, almost no peak (see Figure 4.17) and no peak on cooling. The degree of supercooling based on this Figure is about 20 K, much higher than the other POE samples in this thesis. On first and second heating, the last melting took place at 333.7 K which is close to the equilibrium temperature of 333.8 K calculated by eq (3.2) in the section 3.4.1. On cooling POE5000 is still liquid amorphous at 313.7 K, i.e., the first crystallization occurs at lower temperature. The beginning of crystallization is about 6 K below the melting

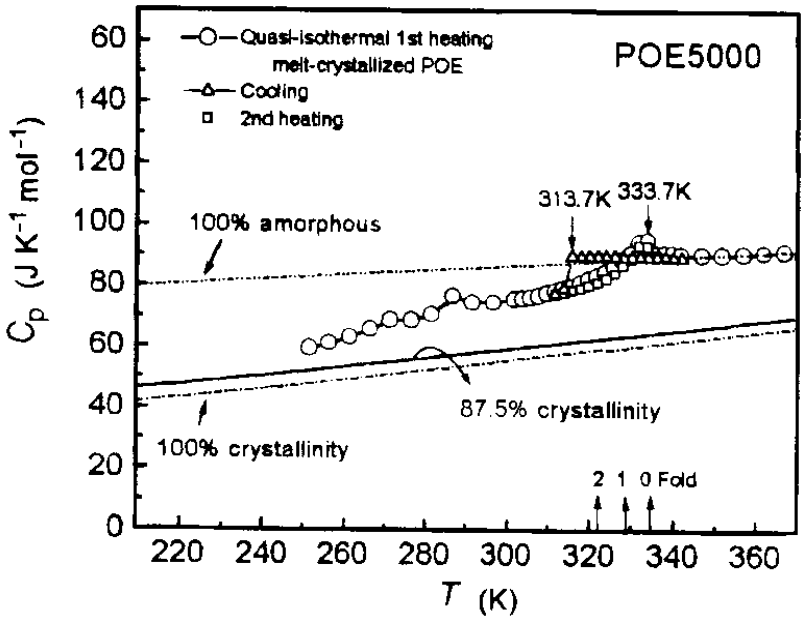

Figure 4.17. Quasi-isothermal TMDSC of POE5000 on heating and cooling. Circles, triangles, and squares represent the first heating sequence, a subsequent cooling sequence, and a second heating sequence, respectively. Indicated also are data bank heat capacities. Copied from [32].

temperature of twice-folded chain crystal of POE5000. It seems that the POE5000 is an extended-chain crystal when it melts on heating, but it is not re-formed by following crystallization on subsequent cooling, and then on second heating it anneals to the extended-chain crystal again during long time quasi-isothermal TMDSC measurements, resulting in the melting temperature close to the equilibrium temperature. This annealing behavior is quite similar to the chain-folded crystal of polyethylene, but the annealing in this case is just faster.

When POE1500 was modulated at 315.7 K for 600 min quasi-isothermally, the reversing heat capacity curve was increasing and settled to constant, as depicted in Figure 4.18 [32]. This long-time modulation shows that at the peak temperature on heating of Figure 3.21, it takes a long time to approach the steady state. The reversing heat capacity slowly reaches a higher level than initially observed. This observation is in contrast to changes to lower levels that were observed in the analysis of poly(ethylene terephthalate) (PET) [34], and PE15520 as seen in Figure 4.14. A polymer shows the decreasing reversing heat capacity on long time modulation and it is usually explained as a loss of restraint of the molecules with time due to crystal perfection.

The explanation for the increasing reversing heat capacity of POE1500 has several possibilities. As time goes on, the crystallinity decreases from 92.3% to 69.5%. The

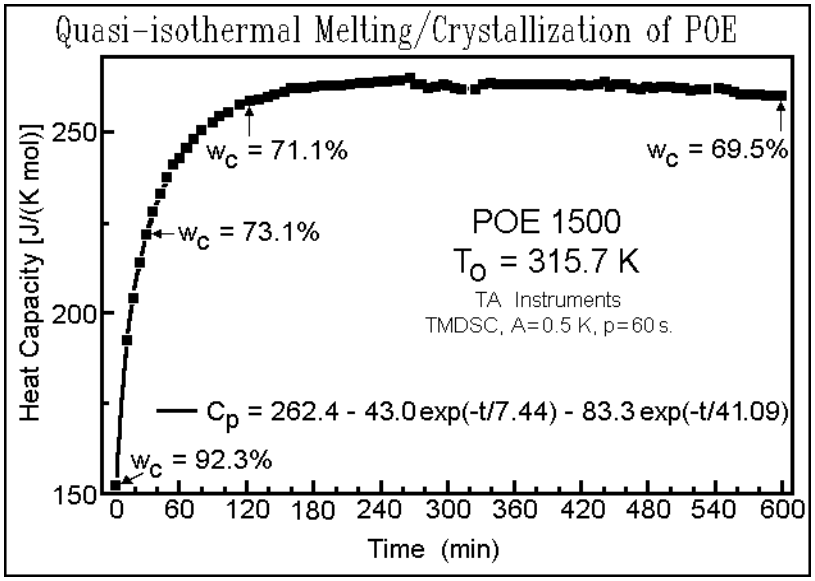

Figure 4.18. Change of the apparent heat capacity at 315.7 K of POE1500 as a function of time (temperature close to the maximum in apparent reversing heat capacity, sample of Figure 4.16; see also Figure 3.21, open circles). Copied from [32].

reducing crystallinity can be one reason for the increasing reversing heat capacity with time. The crystal with 92.3% in the beginning might be a mixture of different length crystals. During the long-time heating and cooling cycles, shorter chain crystals could be extracted from the longer chain crystals and the resulting crystals have uniformed chain length but lower crystallinity. A chain which was originally partially attached to higher melting crystals can be detached on a heating cycle, but on next cooling cycle the detached chain (now it is a random coil) may not be re-attached.

4.4 Critical length for nucleation

4.4.1 Degree of Supercooling vs. Number of Carbons

In Figure 4.19 data are given to answer the question of 'how long must a molecule be before a noticeable nucleation barrier exists for crystallization?' The data of Figure 4.19 include information from the literature on n-paraffins [2, 3, 86, 87], on polyethylene fractions [100] and on POE1500 [33], and the new polyethylene and poly(oxyethylene) fractions measured in this thesis. All physical property data for these samples analyzed in our laboratory are listed in Table 4.1.

The degree of supercooling listed in Figure 4.19 is the temperature difference between the zero-entropy-production melting temperature and the crystallization temperature, as determined by quasi-isothermal TMDSC data to eliminate any instrumental effect. The zero-entropy-production melting temperature is the equilibrium melting temperature or the lower nonequilibrium melting temperature at which a metastable crystal melts into a similarly metastable melt so that no entropy production occurs. The supercooling depends

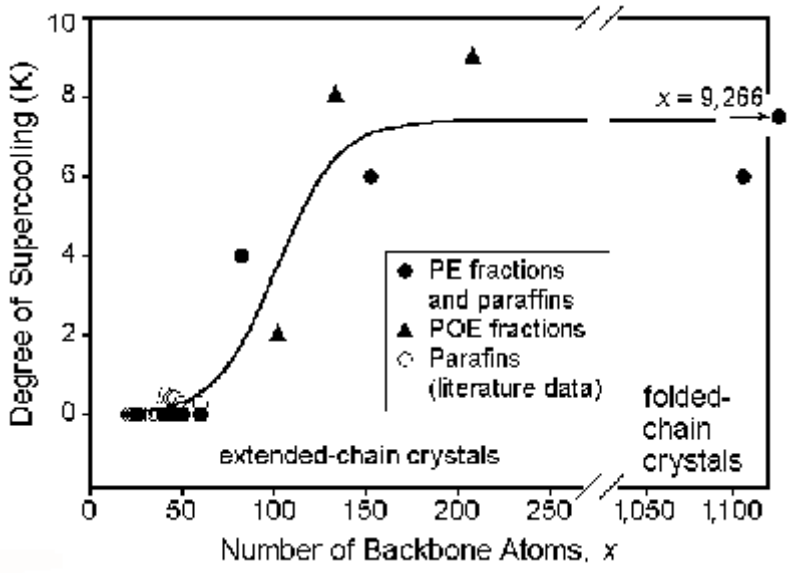

Figure 4.19. Degree of supercooling as a function of the number of chain atoms in the backbone. Open circles are paraffin data from ref. [2], the filled circles are paraffins analyzed in ref. [87] and the polyethylene polymer fractions, triangles refer to poly(oxyethylenes).

on primary, secondary, and molecular nucleation rate. At faster cooling rates, the degree of supercooling gets larger. Primary, homogeneous nucleation does not need to be considered because its degree of supercooling is known to be much larger than observed in the present experiments. For example, it reaches 56 K for linear PE and 66 K for POE (M_w 12400) [15, 101]. In this research we need to measure the intrinsic degree of supercooling due to the molecules themselves, i.e., the molecular nucleation may be involved. Crystal growth after molecular nucleation is, again, expected to be much faster than the capacity of measurement by calorimetry. Quasi-isothermal TMDSC with a zero underlying heating and cooling rates during melting and crystallization is the analysis method of choice since it is the only method permitting long-time measurements of calorimetry.

Table 4.1 Molar masses, chain-lengths, and melting temperatures of paraffins, polyethylenes and poly(oxyethylene)

Samples	Number of backbone atoms	Molar mass (Da)	Chain length [a] (nm)	Equilibrium temperatures [b] (K)
n-$C_{26}H_{54}$ [c]	26	366.70	3.16	T_i = 329.5
n-$C_{44}H_{90}$ [c]	44	619.20	5.44	T_m = 359.6
n-$C_{50}H_{102}$ [c]	50	703.37	6.20	T_m = 365.3
n-$C_{60}H_{122}$	60	843.64	7.46	T_m = 372.9
PE560	40	560	4.93	T_m = 354.5
PE1150	82	1150	10.25	T_m = 383.3
PE2150	153	2150	19.23	T_m = 397.2
PE15520	1106	15520	139.78	T_m = 411.9
PE130000 [d]	9266	130000	1172.02	T_m = 414.3
POE1500	102	1500	9.39	T_m = 322.3
POE1960	133	1960	12.27	T_m = 326.5
POE3060	208	3060	19.15	T_m = 331.7
POE5000	309	4540	28.41	T_m = 333.8

[a] For POE samples, it is replaced with the c-axis lengths.

[b] All melting temperatures, T_m, and the isotropization temperature, T_i, for the paraffins and polyethylenes refer to the approximate values for the extended chain crystals as calculated from eq (3.1). The disordering temperature, T_d, of n-$C_{26}H_{54}$ from the orthorhombic to the conformationally disordered crystal (the "rotor phase") occurs at 326.5 K. On cooling, this transition typically supercools by 4.0 K, while T_i is close to reversible. The TMDSC of the POE1500 and POE5000 has been studied earlier [32, 33].

[c] The detailed analyses of these samples are in the master thesis of J. Pak, Department of Chemistry, The University of Tennessee, Knoxville, TN, 2000.

[d] Polydispersity index is 13.26. Studied earlier [93].

One expects for the paraffins that the most perfect crystals melt last and the analysis has shown that they also crystallize first. On quasi-isothermal TMDSC heating runs, the poorer crystals melt at lower T_o and a crystal which is close to equilibrium (in the case of extended-chain crystals) melts last, so at the next higher T_o, the reversing heat capacity reaches the heat capacity of an 100% amorphous liquid. The temperature where the last crystal melts is taken as the melting temperature of the sample. On subsequent cooling runs of quasi-isothermal TMDSC, the next lower temperature after finding a heat capacity of an 100% amorphous liquid is taken as the crystallization temperature. It was proven earlier [93] that no primary nucleation via heterogeneous nuclei is involved in these supercooling since seeding with higher melting polyethylene crystals does not change the supercooling. Similar experiments were performed with the materials analyzed in this thesis.

The crystals to the left of the break in the temperature scale in Figure 4.19 are all of the extended-chain type as can be deduced from these melting temperatures. This study was originally planned to be limited to these extended-chain types, but the PE15520, which has a folded-chain macroconformation shows also similar degree of supercooling. Even though the PE15520 is 7 times longer than PE2150, the degree of supercooling is 6 K, i.e., it does not increase with molecular weight. It seems that the degree of supercooling is related to the initial lamellar thickness rather than the molecular weight. In this respect, the PE15520 seems to melt and crystallize with same lamellar thickness. For the POE5000, however, the evaluation was not easy as was mentioned in section 4.3. It seems that the extended-chain crystals which melt on heating is not reformed by the following crystallization from melt on subsequent cooling, i.e., thinner lamellar

crystals are initially formed. But, they are annealed very quickly during the subsequent heating runs and the much higher melting temperatures of the extended-chain crystals are measured on heating. So PE15520 is added to the right of the break in Figure 4.19 and POE5000 is excluded. That is, the Figure 4.19 includes only crystals whose lamellar thicknesses is not changed significantly during the TMDSC measurements. Using a sigmoidal equation with three parameters, the fit of the solid line in Figure 4.19 was attained. It is clearly seen that there is a critical number for the backbone atoms at which secondary or molecular nucleation starts to be important for the description of the crystal growth. From Figure 4.19, one can define this critical number as the mid point between n-$C_{60}H_{122}$ and n-$C_{82}H_{164}$ as fixed by PE1150 which are the last datum of zero supercooling and the first datum of substantial supercooling, respectively. It is reached at about 75 backbone atoms or about 10 nm of chain-length, much less than the 37 nm which is the critical chain length for n-paraffin to chain-fold [46, 47] under similar crystallization conditions.

An extensive DSC analysis of crystallization and melting of polyethylene of a much higher mass average of 130,000 Da and a polydispersity of 13 was made earlier in the presence and absence of equilibrium crystal seeds. The average degree of supercooling for the initial growth of chain-folded crystals was 7.5 K from their subsequent melting temperature, in good agreement with Figure 4.19 [86]. Recently, poly(oxytetramethylene) with molar mass of 2000 (POTM2000) was measured using the quasi-isothermal TMDSC [102]. The number of backbone atoms of POTM2000 is 139. Its degree of supercooling was revealed to be four kelvins, which again fits well into the sigmoidal curve in Figure 4.19.

4.4.2 Entropic work of extension

Although 37 nm is the critical length to chain-fold [46, 47], the lamellar thickness for polymer crystals is usually known to be 10-20 nm. Of course, for flexible macromolecules the lamellar thickness can be increased by an annealing process. It seems, however, there are reasons for the thickness that commonly appears in polymer crystals and the critical chain length discussed in the section 4.4.1. To reveal these reasons, the force was calculated which is needed to stretch a random coil to an extended zig-zag chain as shown schematically in Figure 4.20. Using the entropy elasticity concept, the force for extension can be expressed by [103]:

$$f = 3RT\frac{\Delta r}{\langle r^2 \rangle} \tag{4.4}$$

where f is the force in J m^{-1}mol^{-1}, R is the gas constant, 8.31 J K^{-1} mol^{-1}, Δr is the extension of the random coil in nm, and $\langle r^2 \rangle$ is the mean square end-to-end distance assuming a Kuhn length of 0.398 nm for the chain length with an expansion ratio, c = 6.7 for PE [104].

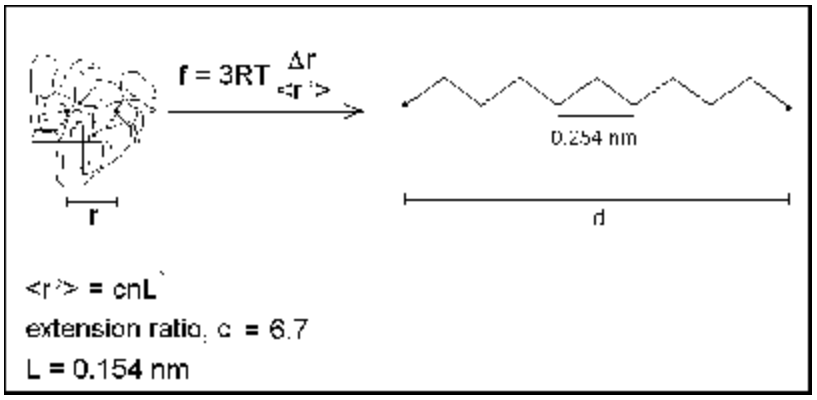

Figure 4.20. Illustration of the extension from a random coil to a fully extended chain of n-paraffin.

The force is computed for n-paraffins with the number of carbon atoms from 20 to 300. The parameters used in this computation and the resulting force are listed as the calculated force and work done to the chain in Table 4.2.

The n-paraffin, $C_{75}H_{152}$ was established as a critical chain length for the crystal growth without supercooling in this thesis (see Figure 4.19) and corresponds to the chain length of 10 nm. It matches the common lamellar thickness of 10 ! 20 nm, typically observed in polymer crystals. It can be also considered a critical limit for the spontaneous extension from random coils to fully extended chains. In Figure 4.21 the values of the work are plotted *versus* the number of carbon atoms. The entropic work of extension, i.e., the overall free energy barrier ΔG^* is 14 kJ mol^{-1} for n-$C_{75}H_{152}$. At 381 K which is the melting temperature of n-$C_{75}H_{152}$, the thermal energy of a degree of freedom without potential energy is 1.6 kJ mol^{-1} ($RT/2$). This is one-ninth of the 14 kJ mol^{-1} calculated and enough to find a sufficient fraction of energetic molecules that can activate the crystallization (0.008%).

One may interpret the Figure 4.21 that the overall free energy barrier, ΔG^* leads to the speculation that on crystallization of long chain molecules only a segment of about 10 nm might be stretched sufficiently by random fluctuations to permit crystallization. Perhaps the segment length of a longer molecule that may initially crystallize is also related to the size of a molecular nucleus. Once the molecular nucleation occurs for a portion of the molecule, the rest of the chain can crystallize easily, similarly, on temperature-modulated DSC a molecule that melts only partially and retains a molecular nucleus can recrystallize reversibly during the cooling cycle.

Table 4.2 The parameters and resulting work for random coils to be stretched with comparison to the thermodynamic entropic term on crystallization.

number of carbon atoms	T (K)	*d* (nm)	*r* (nm)	Δ*r* (nm)	calculated [a] *f* ($\times 10^{12}$ J $m^{-1}mol^{-1}$)	calculated [b] work (J mol^{-1})
20	306.80	2.40	1.74	0.66	1.68	560.69
30	337.60	3.67	2.15	1.52	2.78	2117.10
40	354.71	4.93	2.49	2.44	3.48	4245.81
50	365.30	6.20	2.79	3.41	3.99	6792.72
60	372.87	7.46	3.06	4.40	4.37	9605.58
70	378.67	8.73	3.31	5.42	4.67	12648.73
80	382.89	10.00	3.54	6.46	4.91	15857.63
90	386.23	11.26	3.76	7.50	5.11	19150.25
100	388.93	12.52	3.97	8.55	5.27	22550.84
120	393.00	15.00	4.35	10.65	5.52	29382.76
150	397.21	18.85	4.86	13.99	5.85	40940.17
300	405.76	37.82	6.89	30.93	6.59	101844.21

[a] $3RT\Delta r/\langle r^2\rangle$, see Figure 4.20.

[b] $3RT\Delta r^2/2\langle r^2\rangle$

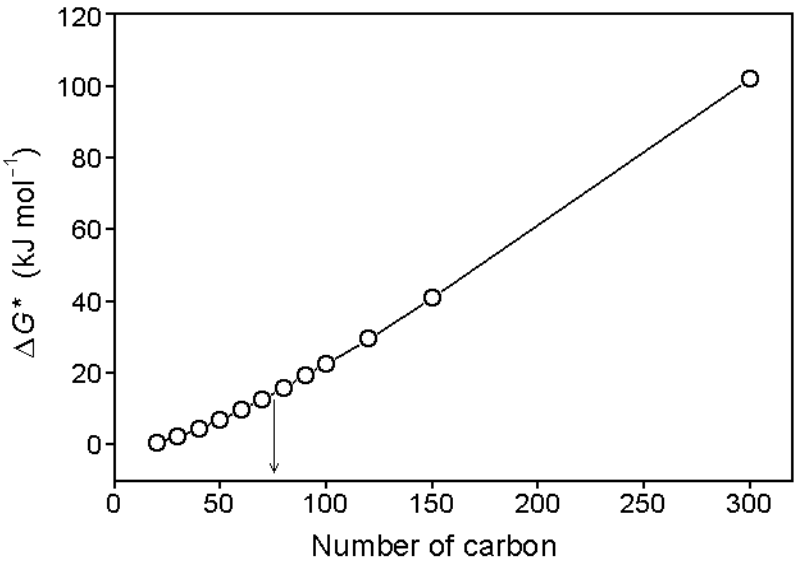

Figure 4.21. The work *versus* the number of carbon atoms. The circles represent the amount of work that should be done for the random coils to be fully stretched.

We propose this to be the reason for the experimental fact of no supercooling in melt-crystallization of n-paraffins up to $C_{60}H_{122}$ documented in this thesis. One can easily estimate that the longer chains than $C_{75}H_{152}$ will need certain degree of supercooling for their crystallization. From this fact, the critical chain length, 10 nm established in this thesis can get an explanation. It also can be a reason why polymers have usually 10–20 nm lamellar thickness.

4.5 Contributions to apparent heat capacities

As mentioned in the section 1.1.4, there are six different thermodynamic contributions to an apparent heat capacity in the melting and crystallization region of the analyzed polymer. In our laboratory, TMDSC studies on several polymers show that this reversible and irreversible contribution were analyzed separately. The PET is one of the

polymers. A quasi-isothermal TMDSC analysis of the poorer crystallized PET showed a surprising, apparent reversing heat capacity although it is smaller than the apparent heat capacity from standard DSC run. By extending the time of quasi-isothermal TMDSC measurement in the melting region, it could be observed that the apparent reversing heat capacity decreases with time and the kinetics could be followed similarly to PE15520 as described in the section 4.2. Figure 4.22 is a plot of the apparent reversing heat capacity of PET from the quasi-isothermal TMDSC runs. The open circles are evaluated from normal 20 min modulation and the two filled circles are extracted along the long-time modulation at T_o = 522 K after given time. The triangles with marked with '∞' is extrapolate one to infinite time. It reveals that after six hours, the reversing melting and crystallization had practically disappeared, i.e., the reversing heat capacity reached the heat capacity for 100%

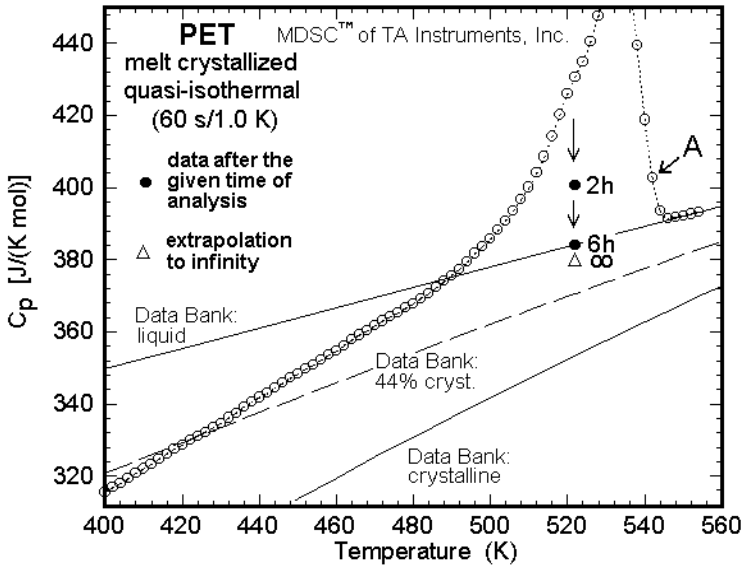

Figure 4.22. Apparent reversing heat capacity of PET. The open circles are evaluated from normal 20 min modulation and the two filled circles are extracted along the long-time modulation at T_o = 522 K after given time. Copied from ref. [105].

amorphous liquid. These experiments were interpreted as showing that the melting of polymers is basically irreversible, but specific details of the crystals can be uncovered that were never before seen by calorimetry.

The same analysis was attempted for PE15520. Figure 4.23 is a plot of the apparent reversing heat capacity of PE15520. The thin line with the large melting peaks is the apparent heat capacity from standard DSC and the thick solid line is the reversing heat capacity from 20 min modulation experiments. The open circles are the reversing heat capacity at various stages of the 600 min modulation at T_o = 380 K. For clear view the outlined region is enlarged at the top of the left corner. The reversing heat capacity at initial time decreases continuously like observed in PET (see Figure 4.22), but even after the infinite time it reaches neither to the heat capacity of 100% amorphous liquid nor the value

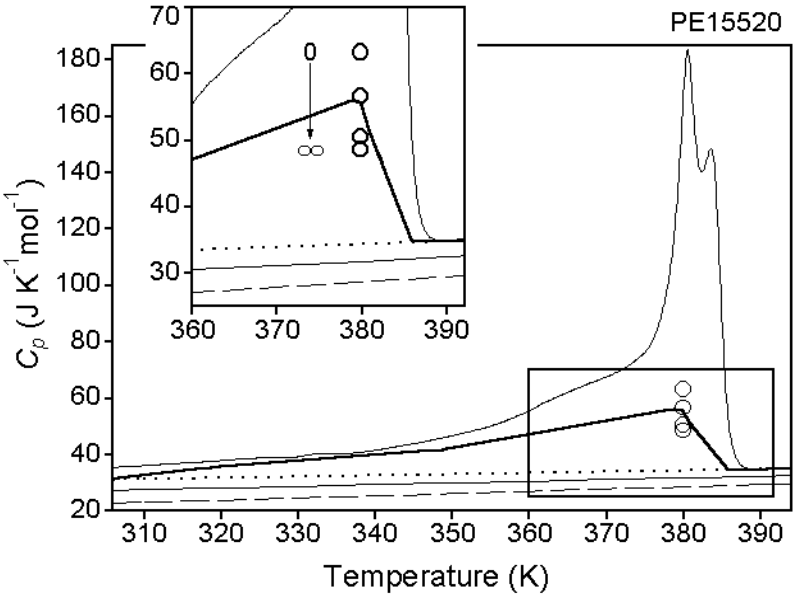

Figure 4.23. Heat capacities of PE15520 on heating by standard DSC (thin line) and quasi-isothermal TMDSC (thick line). Open circles represent the change in apparent, reversing heat capacity for the data of Figure 4.15.

for a semicrystalline polymer (in this case, 55%). It seems the PE15520 involves the relatively large amount of irreversible contributions at 380 K, which is 7 and 2 kelvins below its melting and crystallization temperatures, respectively. This reversing heat capacity is measured from one quasi-isothermal run at T_o = 380 K among heating sequences from 300 K to 400 K. The similar analysis was done at same temperature, T_o = 380 K, but among cooling sequences starting from 400 K to 300 K. In this opposite direction sequence, the measured reversing heat capacity from 600 min at T_o = 380 K was much smaller than that depicted in Figure 4.23 and it was almost constant.

The reversing heat capacity extrapolated to infinity is now a truly reversible heat capacity. It may consist of the vibration, conformational, and reversible melting and crystallization contributions. The vibration contribution can be obtained from the crystallinity of the polymer analyzed, for example, in Figure 4.22 the PET has 44% crystallinity. So the true heat capacity, vibration contribution should be the long dashed line in Figure 4.22 and the small difference between the dashed line and the triangle results from the conformation and reversible melting/crystallization contributions. The subtraction of the truly reversible heat capacity (heat capacity at infinity) from the reversing heat capacity at the given time gives us the three irreversible contributions, which are yet hard to be separated one another, at the corresponding given time. In this respect, the amount of irreversible contributions to the reversing heat capacity of PET is decreasing with time in Figure 4.22.

Same interpretation can go to Figure 4.23. PE15520 has 55% crystallinity and the thin line at the bottom is the computed heat capacity, vibration contribution only. The reversing heat capacity at infinity which is identified to be a truly reversible heat capacity in

the prior paragraph, is now further from the thin line. It can be said that the PE15520 has more local reversible melting/crystallization than the PET at that temperature(380 K).

The truly reversible heat capacity with temperature is most important to interpret the melting/crystallization behavior of semicrystalline polymers. For example, in Figure 4.22, if the long-time quasi-isothermal TMDSC run had been done at higher temperature (marked by A in Figure 4.22) and the reversing heat capacity decreases, it could have reached the heat capacity of 100% amorphous liquid (the top solid line). In this case, one can conclude that the melting of the sample can be completed at that temperature although the measured reversing heat capacity (as shown with the circles in Figure 4.22) appears higher than C_p of liquid. But if the reversing heat capacity had reached below the C_p of liquid at the same temperature, the interpretation should be that the melting of the sample cannot be completed at that temperature, i.e., there exist some crystals which need higher temperature to melt. Whenever one interprets the six contributions to the truly reversible heat capacity (infinity C_p) should be determined first.

4.6 Degree of reversibility

4.6.1 Reversibility in n-paraffins

The reversibility in n-$C_{50}H_{102}$ is calculated by the equation (1.4), modified from ref. [39] with a process described in a section 1.1.5. The total crystallinity is 100% and Δw_c(rev) varies little from 1.3-2%. Figure 4.24 is a plot of the Δw_c(rev) as a function of time. It is the same experiment depicted in Figures 4.1 and 4.4. Therefore, 'C' and 'D' is corresponding the modulation sets which gave maximum in the reversing heat capacity and the first liquid

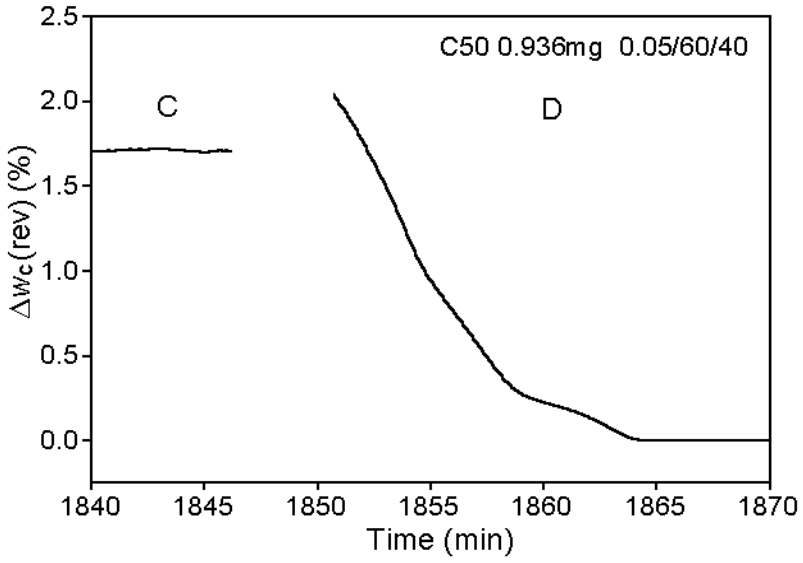

Figure 4.24. The Δw_c(rev) as a function of time for n-$C_{50}H_{102}$. 'C' and 'D' correspond to the modulation sets which gave maximum in the reversing heat capacity and the first liquid heat capacity in Figure 4.1, respectively.

heat capacity, respectively). The modulation sets up to 'C' which is completely symmetric in melting and crystallization peaks gave constant Δw_c(rev) as expected (only 'C' is depicted in Figure 4.24). The modulation set 'D' where the melting occurs more dominantly and finally reaches to liquid state, i.e., the T_o is already higher than the melting temperature, gave the decreasing Δw_c(rev) curve starting from 2% and reaching to zero. At the end of 'D' the reversible crystalline fraction also melt completely. This is just an trial evaluation and further studies are required.

There is no clear evidence for the location where the reversible melting/crystallization in polymer can take place as mentioned in the section 1.1.5. It can be the lateral surface, the fold surface or both. We thought it might be the lateral surface. To make sure the reversible melting in the lateral surfaces, a set of experiments was planned on n-$C_{50}H_{102}$ single crystals

in different sizes. Maybe we could see how many surface layers melt reversibly. Unfortunately, the size of the single crystal of the paraffin was too small to observe. We chose PE2150 and PE11520 for the same experiment. It will be future work.

CHAPTER 5

CONCLUSIONS

Quantitative calorimetry supported by temperature-modulated calorimetry opens the possibility to gain considerable new insight into the crystallization and melting of polymers. Of special importance is the observation that there exists a narrow range of chain lengths below which paraffinic and related flexible chain molecules act like small molecules and can melt reversibly in the presence of primary crystal nuclei (see Figure 4.19). For n-paraffins, oligomeric fractions of polyethylene and poly(oxyethylene), and polyethylene, this range centers around a critical chain length of about 75 chain atoms. This corresponds to a chain length of about 10 nm, a molar mass of about 1050 Da, and for paraffins, an equilibrium melting temperature of about 380 K. For poly(oxytetramethylene) the melting temperature for reversible crystallization should be about 300 K, and the measurements of the equivalent oligomers to the short-chain paraffins are in progress.

The observed increase of the apparent reversing heat capacity in the melting range of n-paraffins, oligomeric fractions of polyethylene and poly(oxyethylene), and polyethylene can be related to one or more of the following three causes:

(1) A gauche-trans equilibrium within the crystals. Using the known vibrational heat capacity as a quantitative baseline, it is seen, that a slow increase of the heat capacity of the crystals starts at about 250 K. The cause of this increase was documented for n-paraffins [82] and polyethylene [90, 91] and was linked to the introduction of gauche defects into the crystals which collect at higher concentrations at the chain ends or fold surfaces [106]. The

main increase in heat capacity is the potential-energy increase caused by the addition of the gauche defects. In this thesis the increase was shown in all analyzed samples.

(2) Equilibrium melting and crystallization of short-chain oligomers as illustrated in this thesis by the paraffins. These paraffins melt reversibly at a temperature that can be estimated from eq 3.1, and modified by the changes of multicomponent systems, as described by the Flory-Huggins formalism [95, 96]. It must be remembered in that chain-ends (cilia) or segments connected on both ends to polymer crystals can act as paraffins when given sufficient mobility, as was shown for polymers with sufficiently long side chains [7].

(3) Partially melted polymer segments that remain attached to polymer crystals. These were identified by their inability to be removed physically after melting [25], and may be able to crystallize and melt reversibly without the need to go through any nucleation process. This is the major contribution in the high-temperature reversible melting peaks of polymers since the melting temperatures, as judged by eq 3.1, exceed in this case the limit where the small-molecule behavior changes to the polymer behavior (see Figure 4.19). Since global equilibria do not exist in the melting region of polymers, the reversible processes must take place locally within a metastable structure, set up by the main body of the interconnected crystals of the macromolecules. Other components of this metastable structure are the mobile- and rigid-amorphous fractions [107] that can also be studied by TMDSC [108].

The study of the kinetics of changes of the reversing heat capacity allows the separation of annealing processes from truly reversible processes, even in the presence of fully irreversible crystallization. The best means to study the irreversible behavior is to compare separate standard DSC data which yield the total, apparent heat capacity data with the

reversing data from quasi-isothermal measurements, as shown in Figures 3.5, 3.9, 3.12, and 3.16. The quasi-isothermal analyses permit the identification of instantaneous processes relative to the time scale of calorimetry, as well as slower processes, as shown in Figures 4.8–4.12 and 4.14.

To summarize the results on polyethylene and the three fractions analyzed in this paper, only PE560 approaches equilibrium and much of it's reversible melting can be explained by effects (1) and (2), in addition to the possible existence of mesophase transitions for the lower molar mass fractions and some irreversible effects due to instrument lag and sample kinetics (diffusion and recrystallization). Practically all chain lengths of its components are below the critical chain length of Figure 4.19. The crystals of PE1150 and PE2150 are also of the extended chain macroconformation, as are the paraffins, but the molecular lengths are within the range of change form reversible to irreversible melting of Figure 4.19. These two samples have the most completely irreversible melting and crystallization behavior of the four samples. All increases in the apparent reversible heat capacity at low-temperatures beyond that of the vibrational contribution are probably of cause (1). The true reversibility of PE560 changes increasingly from cause (2) to cause (3) (peaks in Figures 3.11 and 3.14). In the polymer PE15520, finally, the apparent, reversing heat capacity increases and stretches over a wider temperature range. At low temperature it is less than the total heat capacity, i.e., the effect (1) is mixed with some irreversible melting or annealing and possibly contains some reversible melting of small paraffinic crystals (2), as seen to a much larger extent in the poly(ethylene-co-octene)s [27, 28]. The final, small amount of reversing melting above about 380 K, again, is expected to result from cause (3).

Obviously these assignments make up only a first attempt of separating the various reversible processes between the glass and melting transition. It is also obvious that the limit of the TMDSC method has not been reached. Further work, coupling quantitative kinetics of the various slow processes with specific, morphological studies can probably give specific insights into the interplay between flexible chains in the crystal on the crystal surface, and in the melt within their overall irreversible nanophase-separated superstructure. For example, reversible effects described at the fold surface of polyethylene [39] must still be separated quantitatively from possible additional side-surface effects as are expected from the molecular nucleation and proven, for example, for polypropylene [30] which shows no reversible effects on the fold surface. Finally, the possible complication from rigid amorphous fractions can be separated, removing a complication of particular importance for the stiffer polymer chains, as shown for polycarbonate [108].

LIST OF REFERENCES

LIST OF REFERENCES

[1] B. Wunderlich, Macromolecular Physics, Vol. 2, Crystal Nucleation, Growth, Annealing, Academic Press, New York, 1976.

[2] J. Pak, Master Thesis, Department of Chemistry, the University of Tennessee, Knoxville, Tennessee, 2000.

[3] H. Kraack, E. B. Sirota, and M. Deutsch, Measurements of Homogeneous Nucleation in Normal-alkanes, *J. Chem. Phys.* **112**, 6873-6885 (2000).

[4] H. Kraack, M. Deutsch, and E. B. Sirota, –Alkane Homogeneous Nucleation: Crossover to Polymer Behavior, *Macromolecules* **33**, 6174-6184 (2000).

[5] E. B. Sirota, Supercooling, Nucleation, Rotator Phases, and Surface Crystallization of *n*-Alkane Melts, *Langmuir* **13**, 3133-3136 (1998).

[6] U. Eisele, Introduction to Polymer Physics, Springer-Verlag Berlin Heidelberg, New York, 1990.

[7] B. Wunderlich, Macromolecular Physics, Vol. 3, Crystal Melting, Academic Press, New York, 1980.

[8] L. H. Sperling, Introduction to Physical Polymer Science, 2nd edition, John Wiley and Sons, Inc., New York, 1992.

[9] TAM16-24*

[10] R. J. Young, Introduction to Polymers, Chapman and Hall, New York, 1981.

[11] TAM16-25

[12] HG. Elias, Macromolecules, Vol.1, Structure and Properties, 2nd edition, Plenum press, New York, 1984.

[13] B. Wunderlich, I. Okazaki, K. Ishikiriyama, and A. Boller, Melting by Temperature-Modulated Calorimetry, *Thermochim. Acta.*, **324**, 77-85 (1998); see also: *Proc. 25th NATAS Conf.* in McLean, Va., Sept. 7-9, 1997, R. G. Morgan, ed., 49-56.

[14] K. Ishikiriyama, A. Boller, and B. Wunderlich, Melting of Indium by Temperature-Modulated Differential Scanning Calorimetry, *J. Thermal Analysis*, **50**, 547-558 (1997).

[15] R. L. Cormia, R. P. Price, and D. Turnbull, Kinetics of Crystal Nucleation in Polyethylene, *J. Chem. Phys*, **37**, 1333-1340 (1962).

[16] TAM 16-51

[17] B. Wunderlich, and A. Mehta, Macromolecular Nucleation, *J. Polymer Sci., Polymer Phys. Ed.* **12**, 255-263 (1974).

[18] A. Mehta, and B. Wunderlich, A Study of Molecular Fraction during the

---

* References TAMab-xy refer to screen xy of lecture ab (from 01 to 36) of the computer-assisted course "Thermal Analysis of Materials", by Bernhard Wunderlich, downloadable from the world-wide web: web.utk.edu/~athas/courses/tham99.html, or the LAN of the Department of Chemistry (user: Chem-690; password ATHAS).

Crystallization of Polymers, *Colloid and Polymer Sci.* **253**, 193-205 (1975).

[19] S. Z. D. Cheng, D. W. Noid and B. Wunderlich, Molecular Segregation and Nucleation of Poly(ethylene Oxide) Crystallized from the Melt. IV. Computer Modeling, *J. Polymer Sci., Part B: Polymer Phys.* **27**, 1149-1160 (1989).

[20] S. Z. D. Cheng, and B. Wunderlich, Molecular Segregation and Nucleation of Poly(ethylene Oxide) Crystallized from the Melt. I. Calorimetric Study. *J. Polymer Sci., Part B: Polymer Phys.* **24**, 577-594 (1986).

[21] S. Z. D. Cheng, H. S. Bu, and B. Wunderlich, Molecular Segregation and Nucleation of Poly(ethylene Oxide) Crystallized from the Melt. III. Morphological Study. *J. Polymer Sci.: Part B, Polymer Phys.* **26**, 1947-1964 (1988).

[22] B. Wunderlich, Molecular Nucleation and Segregation, *Disc. Farad. Soc.*, **68**, 239-243 (1979).

[23] TAM 16-39 to 16-41

[24] A. Mehta and B. Wunderlich, Molecular Fractionation during Crystallization and its Application to the Study of Lamellar Thickening during Isothermal Crystallization, *Makromol. Chem.*, **153**, 327-330 (1972).

[25] A. Mehta and B. Wunderlich, Detection of Tie-Molecules by Thermal Analysis, *Makromol. Chem.*, **175**, 977-982 (1974).

[26] R. Androsch, Melting and Crystallization of Poly(ethylene-*co*-octene) Measured by Modulated DSC and Temperature-resolved X-ray Diffraction, *polymer* **40**, 2805-2812 (1999).

[27] R. Androsch, and B. Wunderlich, A Study of the Annealing of Poly(ethylene-*co*-octene)s by Temperature-modulated and Standard Differential Scanning Calorimetry, *Macromolecules*, **32**, 7238-7247 (1999).

[28] R. Androsch and B. Wunderlich, Analysis of the Degree of Reversibility of Crystallization and Melting in Poly(ethylene-*co*-octene), *Macromolecules*, **33** (24), 9076-9089 (2000).

[29] B. Wunderlich, M. Pyda, J. Pak, and R. Androsch, The Measurement of Heat Capacity at Time Scales from Pico to Megaseconds. *Thermochim. Acta.*, accepted for publication (2001).

[30] R. Androsch and B. Wunderlich, Reversible Crystallization and Melting at the Lateral Surface of Isotactic Polypropylene Crystals, *Macromolecules*, to be published (2001).

[31] TAM9-28

[32] K. Ishikiriyama and B. Wunderlich, Melting of Poly(oxyethylene) Analyzed by Temperature-Modulated Calorimetry, *Macromolecules*, **30**, 4126-4131 (1997).

[33] K. Ishikiriyama and B. Wunderlich, Crystallization and Melting of Poly(oxyethylene) Analyzed by Temperature-Modulated Calorimetry, *J. Polymer Sci., Part B, Polymer Phys.*, **35**, 1877-1886 (1997).

[34] I. Okazaki and B. Wunderlich, Reversible Melting in Polymer Crystals Detected by Temperature Modulated Differential Scanning Calorimetry, *Macromolecules*, **30**, 1758-1764 (1997).

[35] I. Okazaki and B. Wunderlich, Reversible Local Melting in Polymer Crystals, *Macromol. Chem. Phys., Rapid Commun.*, **18**, 313-318 (1997).

[36] M. Pyda, A. Boller, J. Grebowicz, H. Chuah, B. V. Lebedev and B. Wunderlich, Heat Capacity of Poly(trimethylene terephthalate), *J. Polymer Sci., Part B: Polym. Phys.* **36**, 2499-2511 (1998).

[37] M. Pyda and B. Wunderlich, Reversible and Irreversible Heat Capacity of Poly(trimethylene terephthalate) Analyzed by Temperature-Modulated Differential Scanning Calorimetry, *J. Polym. Sci., Part B: Polymer Phys.* **38**, 622-631 (2000).

[38] K. Ishikiriyama, M. Pyda, G. Zhang, T. Forschmer, J. Grebowicz and B. Wunderlich, Heat Capacity of Poly-*p*-Dioxanone, *J. Macromol. Sci. -Phys.*, **B37**, 27-44 (1998).

[39] B. Goderis, H. Reynaers, V. B. F. Mathot, R. Scherrenberg and M. H. J. Koch, Temperature Reversible Transitions in Linear Polyethylene Studied by TMDSC and Time-resolved, Temperature-modulated WAXD/SAXS, *Macromolecules*, **34** (6), 1779-1787 (2001).

[40] W. Hu, T. Albrecht and G. Strobl, Reversible surface melting of PE and PEO crystallites indicated by TMDSC, *Macromolecules*, **32** (22), 7548-7554 (1999).

[41] T. Albrecht and G. Strobl, Temperature-Dependent Crystalline-Amorphous Structures in Linear Polyethylene: Surface Melting and the Thickness of the Amorphous Layers, *Macromolecules*, **28**, 5827-5833 (1995).

[42] C. L. Hill, ed., Activation and Functionalization of Alkanes, John Wiley and Sons.

Inc., New York, 1989.

[43] GY. Môzes, ed., Paraffin Products in the series of Developments in Petroleum Science 14, Elsevier Scientific Publishing Company, New York, 1982.

[44] TAM29-53

[45] B. Wunderlich, The Heat Capacity of Polymers, *Thermochim. Acta*, **300**, 43-65 (1997).

[46] D. C. Bassett, R. H. Olley, S. J. Sutton, and A. S. Vaughan, On Spherulitic Growth in a Monodisperse Paraffin, *Macromolecules*, **29**, 1852-1853 (1996).

[47] D. C. Bassett, R. H. Olley, S. J. Sutton, and A. S. Vaughan, On chain conformations and spherulitic growth in monodisperse n-C294H590, *Polymer*, **37**, 4993-4997 (1996).

[48] G. M. Stack, L. Mandelkern, and I. G. Voigt-Martin, Crystallization, Melting, and Morphology of Low Molecular Weight Polyethylene Fractions, *Macromolecules* **17**, 321-331 (1984).

[49] D. L. Dorset, Bridged Lamellae: Crystal Structure(s) of Low Molecular Weight Linear Polyethylene, *Macromolecules* **32**, 162-166 (1999).

[50] D. L. Dorset, The Bridged Lamellar Structure of Synthetic Waxes Determined by Electron Crystallographic Analysis, *J. Phys. Chem. B*, **104**, 4613-4617 (2000).

[51] A. Prasad, and L. Mandelkern, Equilibrium Dissolution Temperature of Low Molecular Weight Polyethylene Fractions in Dilute Solution, *Macromolecules* **22**, 914-920 (1989).

[52] B. Wunderlich, Thermal Analysis, Academic Press, San Diego, 1990.

[53] TAM19-39

[54] B. Wunderlich and M. Pyda, Application of the Advanced THermal Analysis System (ATHAS) to Differential Scanning Calorimetry (DSC) and Temperature-Modulated DSC of Polymers, *J. Reinforced Plastics and Composites*, **18**, 487-498 (1999).

[55] TAM20-53

[56] TAM20-56

[57] A. Boller, M. Ribeiro, and B. Wunderlich, A Detailed Comparison of First Order Transitions by DSC and TMC, *J. Thermal Analysis and Calorimetry*, **54**, 545-563 (1998).

[58] TAM20-54

[59] B. Wunderlich, Differential Thermal Analysis, in Physical Methods of Chemistry, A. Weissberger and B. W. Rossiter, eds. Vol. 1, Part 5, Chapter 8, John Wiley and Sons, Inc., New York, 1971.

[60] B. Wunderlich, Heat Capacity of Polymers in S. Z. D. Cheng Editor, "Handbook of Thermal Analysis and Calorimetry," Vol. III, Elsevier Publ., 1999.

[61] M. Reading, D. Elliot and V. L. Hill, A new approach to the calorimetric investigation of physical and chemical transitions. *J. Thermal Anal*., **40**, 949-955 (1993).

[62] P. S. Gill, S. R. Sauerbrunn and M. Reading, Modulated differential scanning

calorimetry. *J. Thermal Anal.*, **40**, 931-939 (1993).

[63] M. Reading, Modulated differential scanning calorimetry - a new way forward in materials characterization, *Trends in Polymer Sci.*, **8**, 248-253 (1993).

[64] B. Wunderlich, Y. Jin, and A. Boller, Mathematical Description of Differential Scanning Calorimetry Based on Periodic Temperature Modulation, *Thermochim. Acta*, **238**, 277-293 (1994).

[65] P. F. Sullivan and G. Seidel, Steady-State, ac-Temperature Calorimetry, *Phys. Rev.*, **173** (3), 679-685 (1968).

[66] B. Wunderlich, Y. Jin, and A. Boller, Mathematical Description of Differential Scanning Calorimetry Based on Periodic Temperature Modulation, *Thermochim. Acta*., **238**, 277-293 (1994).

[67] R. Androsch, I. Moon, S. Kreitmeier, and B. Wunderlich, Determination of Heat Capacity with a Sawtooth-type, Power-compensated Temperature-Modulated DSC, *Thermochim. Acta*, **357**/**358**, 267-278 (2000).

[68] R. Androsch, and B. Wunderlich, Temperature-Modulated DSC Using Higher Harmonics of the Fourier Transform, *Thermochim. Acta*, **333**, 27-32 (1999).

[69] B. Wunderlich, The Basis of Thermal Analysis. In: "Thermal Characterization of Polymeric Materials." E. Turi, ed., Academic Press, New York, 205-482 (1997).

[70] B. Wunderlich, R. Androsch, M. Pyda, and Y. K. Kwon, Heat Capacities by Multi-Frequency Saw-Tooth Modulation, *Thermochim. Acta*, **348**, 181-190 (2000).

[71] J. Pak, and B. Wunderlich, Heat Capacity by Sawtooth-Modulated, Standard Heat-Flux Differential Scanning Calorimeter with Close Control of the Heater Temperature, *Thermochim. Acta,* **367/368**, 367-368 (2001).

[72] M. Pyda, Y. K. Kwon, and B. Wunderlich, Heat Capacity Measurement by Sawtooth Modulated Standard Heat-Flux Differential Scanning Calorimeter with Sample-Temperature Control, *Thermochim. Acta,* **367/368**, 217-227 (2001).

[73] Y. K. Kwon, R. Androsch, M. Pyda, and B. Wunderlich, Multi-Frequency Saw-Tooth Modulation of a Power-Compensation Differential Scanning Calorimeter, *Thermochim. Acta,* **367/368**, 203-215 (2001).

[74] A. Boller, Y. Jin and B. Wunderlich, Heat Capacity Measurement by Modulated DSC at Constant Temperature, *J. Thermal Analysis*, **42**, 307-330 (1994).

[75] TAM20-55

[76] T. Hütter, New Ceramic Sensor (FRS5) for the DSC 82X Instruments, *UserCom 5*, Mettler-Toledo, Schwerzenbach, 1997.

[77] private communication from the software engineers of Mettler-Toledo.

[78] B. Wunderlich, I. Okazaki, K. Ishikiriyama, and A. Boller, Melting by Temperature-Modulated Calorimetry, *Thermochim. Acta.*, **324**, 77-85 (1998).

[79] S. M. Sarge, E. Gmelin, G. W. H. Höhne, H. K. Cammenga, W. Hemminger and W. Eysel, The caloric calibration of scanning calorimeters, *Thermochim. Acta.*, **247**, 129-168 (1994).

[80] L. C. Thomas, A. Boller, I. Okazaki, and B. Wunderlich, Modulated Differential Scanning Calorimetry in the Glass Transition Region, IV. Pseudo-Isothermal Analysis of the Polystyrene Glass Transition, *Thermochim. Acta*, **291**, 85-94 (1997).

[81] D. A. Ditmars, S. Ishihara, S. S. Chang, G. Bernstein and E. D. West, Enthalpy and Heat-capacity Standard Reference Material - Synthetic Sapphire (Alpha-Al_2O_3) from 10 to 2250 K, *J. S. Res. Natl. Bur. Stand.* **87**, 159-163 (1982).

[82] Y. Jin and B. Wunderlich, The Heat Capacity of *n*-Paraffins and Polyethylene, *J. Phys. Chem.*, **95**, 9000-9007 (1991).

[83] W. R. Busing, X-ray Diffraction Study of Disorder in Allied Spectra-1000 Polyethylene Fibers, *Macromolecules*, **23**, 4608-4610 (1990).

[84] Y. Takahashi and H. Tadokoro, Structural Studies of Polyethers, $(-(CH_2)_m-O-)_n$. X. Crystal Structure of Poly(ethylene oxide), *Macromolecules*, **6**, 672-675 (1973).

[85] B. Wunderlich, Macromolecular Physics, Vol. 1, Crystal Structure, Morphology, Defects, Academic Press, New York, 1973.

[86] J. Pak, A. Boller, I. Moon, M. Pyda and B. Wunderlich, Thermal Analysis of Paraffins by Calorimetry, *Thermochim. Acta*, **357/358**, 259-266 (2000).

[87] J. Pak and B. Wunderlich, Thermal Analysis of Paraffins as Model Compounds for Polyethylene. *J. Polymer Sci., Part B: Polymer Physics*, **38**, 2810-2822 (2000).

[88] M. G. Broadhurst, Extrapolation of the Orthorhombic *n*-Paraffin Melting Properties to Very Long Chain Lengths, *J. Chem. Phys*., **36**, 2578-2582 (1962).

[89] B. Wunderlich, A. Boller, I. Okazaki, K. Ishikiriyama, W. Chen, M. Pyda, J. Pak, I. Moon, and R. Androsch, Temperature-Modulated Differential Scanning Calorimetry of Reversible and Irreversible First-Order Transitions, *Thermochim. Acta*, **330**, 21-38 (1999).

[90] B. Wunderlich, The ATHAS Data Base on Heat Capacities of Polymers. *Pure and Applied Chem*., **67**, 1919-1026 (1995). For data see the internet address: *web.utk.edu/~athas/databank*.

[91] B. Wunderlich, Motion in Polyethylene. I. Temperature and Crystallinity Dependence of the Specific Heat. *J. Chem. Phys.*, **37**, 1203 (1962).

[92] C. P. Buckley, and A. J. Kovacs, Melting Behavior of Low Molecular Weight Poly(ethylene-oxide) Fractions. I. Extended Chain Crystals, *Prog. Colloid Polym. Sci.* **58**, 44-52 (1975).

[93] B. Wunderlich and C. M. Cormier, Seeding of Supercooled Polyethylene with Extended Chain Crystals. *J. Phys. Chem.*, **70**, 1844 (1966).

[94] B. Wunderlich and J. Grebowicz, Thermotropic Mesophases and Mesophase Transitions of Linear, Flexible Macromolecules (Partially preprinted in the Proc. 12th NATAS, J. C. Buck, ed. p. 291, 1983), *Adv. Polymer Sci*, **60/61**, 1 (1984).

[95] R. B. Prime and B. Wunderlich, Extended-Chain Crystals. IV. Melting under Equilibrium Conditions. *J. Polym. Sci., Part A-2,* **7**, 2073-2089 (1969).

[96] R. B. Prime, B. Wunderlich, and L. Melillo, Extended-Chain Crystals. V. Thermal Analysis and Electron Microscopy of the Melting Process in Polyethylene. *J. Polym. Sci., Part A-2*, **7**, 2091-2097 (1969).

[97] TAM32-06

[98] W. Chen, M. Dadmun, G. Zhang, A. Boller, and B. Wunderlich, Isotropization of Nematic Liquid Crystals by Temperature-Modulated DSC, *Thermochim. Acta.*, **324**, 87-94 (1998).

[99] R. Androsch, M. Pyda, H. Wang, and B. Wunderlich, A Study of Temperature-modulated Differential Scanning Calorimetry With High-resolution Infrared Thermography, *J. Thermal Analysis and Calorimetry*, **61**, 661-679 (2000).

[100] J. Pak, and B. Wunderlich, Melting and Crystallization of Polyethylene of Different Molar Mass by Calorimetry, accepted for publication, *Macromolecules*, (April 2001).

[101] J. A. Koutsky, A. G. Walton and E. Baer, Nucleation of Polymer Droplets, *J. Appl. Phys.*, **38**, 1832-1839 (1967).

[102] J. Pak and M. L. Di Lorenzo, unpublished.

[103] TAM30-36

[104] TAM4-34

[105] TAM21-57

[106] B. G. Sumpter, D. W. Noid, G. L. Liang and B. Wunderlich, Atomistic Dynamics of Macromolecular Crystals. *Adv. Polymer Sci.*, **116**, 27-72 (1994).

[107] H. Suzuki, J. Grebowicz, and B. Wunderlich, The Glass Transition of Polyoxymethylene. *British Polymer Journal*, **17**, 1 (1985).

[108] C. Schick, A. Wurm, M. Merzyakov, A. Minakov, and H. Marand, Crystallization and Melting of Polycarbonate Studied by Temperature-Modulated DSC (TMDSC) *J. Thermal Analysis and Calorimetry*, to be published (2001).

VITA

Jeongihm Pak was born on the 10th of February, 1971 in Namwon, South Korea. She was grown up in Chunchon and graduated with a B.S. in Chemistry from the Hallym University in Choonchun, South Korea. In the summer of 1996 she married with Youngsun Kim and in the fall of 1996 she began her graduate studies in the field of polymer chemistry at the University of Tennessee, Knoxville. In May of 2000, she earned a M.S. and the degree of doctor of philosophy was completed in August of 2001 under a direction of Prof. B. Wunderlich. She and her husband are expecting their first baby girl in September of 2001.